

Characterization of Proteorhodopsin 2D crystals by Electron Microscopy and Solid State Nuclear Magnetic Resonance

Dissertation zur Erlangung des Doktorgrades der
Naturwissenschaften
vorgelegt dem Fachbereich Biochemie, Chemie, Pharmazie
Institut für Biophysikalische Chemie
Johann Wolfgang Goethe Universität Frankfurt am Main
Zentrum für Biomolekulare Magnetische Resonanz Spektroskopie

von Sarika Shastri
aus Deras, Indien

Frankfurt am Main 2008

Acknowledgements

Acknowledgements

It gives me great pleasure to express my deep gratitude to my principle investigator and research guide Prof. Dr. Clemens Glaubitz without whose benevolent guidance and constant motivation, it would have not been possible to reach this stage. I thank him for giving me an excellent opportunity to work at renowned and esteemed institute. I am grateful to him for being very patient, understanding and approachable.

I assert my sincere thanks to the members of the PhD thesis committee for providing regular feedback for an improved performance in a focused manner and the project collaborators Prof. Dr. Werner Kühlbrandt, Prof. Dr. Daniel Müller and Prof. Dr. Werner Mänteke.

I feel highly indebted towards the contribution of Dr. Janet Vonck for providing precious suggestions and basic understanding related to electron microscopy at different stages of the project. I greatly appreciate help extended by Dr. Winfried Haase for freeze fracture and Mr. Deryck Mills for technical support for electron microscopy from Max Planck Institute of Biophysics, Frankfurt. Ms. Adriana Klyszejko and Ms. Gabriela Schäfer are credited for their co-operation for AFM and Spectroscopic measurements. BMBF and SFB472 are acknowledged for funding.

Special vote of thanks to Ms. Simone Kobylka and Ms. Ingrid Weber for generous assistance and care for various aspects on and off campus right from beginning until the end of the my duration in Frankfurt. A kind word of acknowledgement for Dr. Jacob Lopez, who always provided constant inputs and advice over all the varied topics under the sun. I appreciate contribution of Mr. Karsten Moers for the German translation of the summary of my work. I thank all the members of Institute of Biophysical Chemistry, Department of Solid State NMR for providing me constant help and cooperation during my tenure at the department.

In addition, I have no words of measure to express my gratitude towards my husband, Dr. Yogesh M. Shastri, who stood behind me at every step and without whose cooperation, support, motivation and sacrifice, I would not have realized my dream. I also recognize the blessings of my family, who was a constant source of inspiration across the miles. Lastly, I wish to dedicate this scientific work to my mother Late Prof. Mrs. Vidhya Mungi and my maternal uncle Late Mr. Balwant Joshi, who had introduced the concept of doctorate to me.

Summary

Summary

Proteorhodopsin (PR) originally isolated from uncultivated γ -Proteobacterium as a result of biodiversity screens, is highly abundant ocean wide. PR, a Type I retinal binding protein with 26% sequence identity, is a bacterial homologue of Bacteriorhodopsin (BR). The members within this family share about 78% of sequence identity and display a 40 nm difference in the absorption spectra. This property of the PR family members provides an excellent model system for understanding the mechanism of spectral tuning. Functionally PR is a photoactive proton pump and is suggested to exhibit a pH dependent vectorality of proton transfer. This raises questions about its potential role as pH dependent regulator. The abundance of PR in huge numbers within the cell, its widespread distribution ocean wide at different depths hints towards the involvement of PR in utilization of solar energy, energy metabolism and carbon recycling in the Sea.

Contrary to BR, which is known to be a natural 2D crystal, no such information is available for PR til date. Neither its functional mechanism nor its 3D structure has been resolved so far. This PhD project is an attempt to gain a deeper insight so as to understand structural and functional characterization of PR. The approach combines the potentials of 2D crystallography, Atomic Force Microscopy and Solid State NMR techniques for characterization of this protein.

Wide range of crystalline conditions was obtained as a result of 2D crystallization screens. This hints towards dominant protein protein interactions. Considering the high number of PR molecules reported per cell, it is likely that driven by such interactions, the protein has a native dense packing in the environment. The projection map represented low resolution of these crystals but suggested a donut shape oligomeric arrangement of protein in a hexagonal lattice with unit cell size of $87\text{\AA} \times 87\text{\AA}$. Preliminary FTIR measurements indicated that the crystalline environment does not obstruct the photocycle of PR and K as well as M intermediate states could be identified.

Single molecule force spectroscopy and atomic force microscopy on these 2D crystals was used to probe further information about the oligomeric state and nature of unfolding. The data revealed that protein predominantly exists as hexamers in crystalline as well as densely reconstituted regions but a small percentage of pentamers is also observed. The unfolding

Summary

mechanism was similar to the other relatively well-characterized members of rhodopsin family. A good correlation of the atomic force microscopy and the electron microscopy data was achieved.

Solid State NMR of the isotopically labeled 2D crystalline preparations using uniformly and selectively labeling schemes, allowed to obtain high quality SSNMR spectra with typical ^{15}N line width in the range of 0.6-1.2 ppm. The measured ^{15}N chemical shift value of the Schiff base in the 2D crystalline form was observed to be similar to the Schiff base chemical shift values for the functionally active reconstituted samples. This provides an indirect evidence for the active functionality of the protein and hence the folding. The first ^{15}N assignment has been achieved for the Tryptophan with the help of Rotational Echo Double Resonance experiments. The 2D Cross Polarization Lee Goldberg measurements reflect the dynamic state of the protein in spite of restricted mobility in the crystalline state. The behavior of lipids as measured by ^{31}P from the lipid head group showed that the lipids are not tightly bound to the protein but behave more like the lipid bilayer. The ^{13}C - ^{13}C homonuclear correlation experiments with optimized mixing time based on build up curve analysis, suggest that it is possible to observe individual resonances as seen in case of glutamic acid. The signal to noise was good enough to record a decent spectrum in a feasible period. The selective unlabeled is an efficient method for reduction in the spectral overlap. However, more efficient labeling schemes are required for further characterization. The present spectral resolution is good for individual amino acid investigation but for uniformly labeled samples, further improvement is required.

Zusammenfassung

Zusammenfassung

Proteorhodopsin (PR) wurde ursprünglich aus nicht kultivierten γ -Proteobakterium isoliert und ist in großen Mengen in den Ozeanen enthalten. PR ist wie sein homolog Bakteriorhodopsin (BR) ein TypI Retinal Bindeprotein und die Sequenzen sind zu 26% identisch. Innerhalb der PR Familie haben die Mitglieder eine Sequenzhomologie zu ungefähr 78% und zeigen einen Unterschied von 40 nm im absorptions spektrum. Diese Eigenschaft bietet ein gutes Modellsystem um zu verstehen durch welchen Mechanismus das Absorptionsspektrum moduliert wird.

PR ist ein photoaktive Protonenpumpe und es wird angenommen, dass die Richtung des Protonentransfers vom pH-wert abhängt, was auf eine Rolle als ein pH abhängiger Regulator hindeutet. Da PR sowohl in der Zelle in hoher Zahl, als auch in den Ozeanen in unterschiedlichen Tiefen weit verbreitet ist, wird angenommen, dass PR bei der Verwertung von Sonnenlicht, im Energiestoffwechsel und beim Kohlenstoffumsatz beteiligt ist.

Im Gegensatz zu BR, welches bekannterweise 2D Kristalle bildet, ist etwas vergleichbares für PR bis heute nicht bekannt. Weder der Mechanismus von PR noch seine 3D Struktur sind bisher gelöst. Die vorliegende Doktorarbeit versucht offene Punkte zum Mechanismus und zur Struktur von PR zu klären. Für die Charakterisierung werden 2D Kristallographie, "Atomic Force Microscopy" und Festkörper NMR verwendet.

Für die Bildung von 2D Kristallen konnte eine große Auswahl an Kristallisationsbedingungen ermittelt werden, was auf deutliche Protein Protein Wechselwirkungen hindeutet. Zieht man die hohe Zahl an PR Molekülen pro zelle in betracht, ist es wahrscheinlich, dass durch diese Interaktionen auch in der natürlichen Membran eine dichte Packung der Proteine auftritt. Elektronenmikroskopische Aufnahmen mit geringer Auflösung deuten auf eine ringförmige Anordnung der Proteine in einem hexagonalen Gitter mit einer Einheitszelle von $87\text{\AA} * 87\text{\AA}$. Vorläufige FTIR Messungen deuten darauf hin, dass diese Anordnung den Photozyklus nicht behindert und sowohl K als auch M Zustand konnten identifiziert werden.

Um weitere Informationen über den Oligomerisierungszustand der 2D Kristalle zu gewinnen

Zusammenfassung

wurden Einzelmolekül - und Rasterkraft Mikroskopie durchgeführt. Hierbei zeigte sich, dass das Protein in kristallinen und dicht rekonstituierten Regionen überwiegend als Hexamer vorliegt. Daneben kann zu einem geringen Anteil auch ein pentamerer Zustand beobachtet werden. Der Mechanismus der Proteinfaltung war vergleichbar zu anderen, besser untersuchten Mitgliedern der Rhodopsinfamilie. Zwischen den Daten aus der "Atomic Force Microscopy" und der Elektronenmikroskopie zeigt sich eine gute Korrelation.

Festkörper NMR an vollständig und selektiv markierten 2D Kristallen ergaben Spektren mit einer typischen ^{15}N Linienbreite von 0,6 bis 1,2 ppm. Die ^{15}N chemische Verschiebung der Schiffischen Base hat im Kristall den gleichen Wert wie funktional aktiv rekonstituierte Proben, was indirekt die Funktionalität und die korrekte Faltung bestätigt.

Die Zuordnung der ^{15}N Signale für Tryptophan wurde durch "Rotational Echo Double Resonance" Experimente vorgenommen. 2D kreuzpolarisation Lee Goldberg Messungen zeigen den dynamischen Zustand des Proteins trotz der eingeschränkten Mobilität im kristallinen Zustand. Das Verhalten der Lipide wurde mit ^{31}P messungen der Lipidkopfgruppe untersucht und zeigt, dass diese nicht fest gebunden sind, sondern sich mehr wie in einer Lipiddoppelschicht verhalten. Für ^{13}C - ^{13}C homonukleare korrelations Experimente wurde die Mischzeit durch die Analyse von Aufbaukurven optimiert. Diese Versuche deuten darauf hin, dass es möglich ist einzelne Resonanzen aufzulösen, wie im Fall des Glutamat gezeigt mit einem gutem Signal zu Rauschen Verhältnis. Selektives "unlabeling" ist eine effiziente Methode um die Ueberlappung der Signal zu reduzieren. Darüberhinaus sind für eine weitere Charakterisierung effizientere Markierungsschemata notwendig. Die bisherige spektrale Auflösung ist gut genug für die Untersuchung einzelner Aminosäuren, für vollständig markierte Proben sind weitere Verbesserungen notwendig.

Abbreviations

Abbreviations

AFM	Atomic Force Microscopy
BR	Bacteriorhodopsin
BPR	Blue Proteorhodopsin
CMC	Critical Micellar concentration
CHAPS	3-[(3-Cholamidopropyl) dimethylammonio]-1-propanesulfonate
CTAB	Cetyltrimethylammoniumbromide
CP	Cross Polarization
CPMAS	Cross Polarization Magic Angle Spinning
CW	Constant wave
DDM	Dodecyl maltoside
DTT	Dithiothreitol
DTAC	Dodecyl trimethyl ammonium chloride
DPC	Dodecylphosphocholine
DMPC	1, 2-Dimyristoyl-sn-glycero-3-phosphocholine
DOPC	1, 2-Dioleoyl-sn-Glycero-3-Phosphocholine
DP	Direct Polarization
DQF	Double Quantum Filtering
EM	Electron microscopy
EPL	<i>E.coli</i> polar lipids
FTIR	Fourier Transform Infra Red Spectroscopy
FT	Fourier Transform
GPCR	G-protein coupled receptor
GPR	Green Proteorhodopsin
HETCOR	Heteronuclear Correlation
LDAO	Lauryldimethylamino-N-oxide
LG-CP	Lee Goldberg Cross Polarization
MPD	Methyl 2-4 Pentanediol
MAS	Magic Angle Spinning
NMR	Nuclear Magnetic Resonance
OG	Octylglycoside

Abbreviations

OD	Optical density
PSB	Protonated Schiff's Base
PR	Proteorhodopsin
REDOR	Rotational Echo Double Resonance
SSNMR	Solid-State Nuclear Magnetic Resonance
SRII	Sensory Rhodopsin II
TPPM	Two pulse Phase Modulation
2D	Two dimension
3D	Three dimension

List of figures

List of figures

Chapter 1

Figure 1 : Original figure of membrane (protein) from Singer and Nicolson	23
Figure 2 : Phylogenetic analysis of PR with archeal and neurospora crassa rhodopsins	27
Figure 3: Topology plot of wild type GPR with BR	29
Figure 4: Sequence alignment of different variants of PR with BR	30
Figure 5: Homology model of wild type PR based on BR	30
Figure 6: Spectral tuning of PR family	33
Figure 7: Retinal isomerization	34
Figure 8: Photocycle models of PR	36
Figure 9: Over view of transmembranous fluxes and proton pumping in PR containing <i>E.coli</i> cells.	39
Figure 10: Sequence alignment of GPR and BPR	40
Figure 11: Sequence alignment of GPR with BR	41
Figure 12: Sequence alignment of BPR with SRII	42

Chapter 2

Figure 13: UV-Vis spectra of PR in detergent solubilized state	50
Figure 14: Sucrose density gradient for PR samples	50
Figure 15: SDS-PAGE of purified PR	52

Chapter 3

Figure 16: Principle of dialysis	58
----------------------------------	----

List of figures

Figure 17: Diffraction pattern of PR 2D crystals at different pH	64
Figure 18: EM Micrographs of PR 2D crystals	69
Figure 19: Projection Map of PR 2D crystals	70
Chapter 4	
Figure 20: CD spectra of detergent solubilized PR and PR 2D crystals	76
Figure 21: Infra Red difference spectra of PR 2D crystals at pH 8.5	80
Figure 22: Transient absorption spectra at 1541cm^{-1}	81
Chapter 5	
Figure 23: AFM of PR 2D crystals	89
Figure 24: High resolution AFM of densely packed PR oligomers	90
Figure 25: Co relation averaged AFM topographs showing hexagonal assembly of brand comparison with PR 2D crystals	91
Figure 26: Unfolding pattern of single PR embedded within membranes	93
Figure 27: Comparison of EM micrographs with AFM topographs in PR 2D crystal	95
Chapter 6	
Figure 28: MAS picture showing orientation of rotor with respect to the magnetic field	99
Figure 29: Pulse sequence of CP	101
Figure 30: ^{31}P 1D MAS spectra of DOPC in PR 2D crystal	105
Figure 31: ^{31}P 1D MAS spectra of DOPC in PR 2D crystal at 3 kHz and at different temperatures	106
Figure 32: ^{15}N 1D MAS spectra of ζ -lysine labeled PR 2D crystals	109

List of figures

Figure 33: A: ^{15}N 1D MAS spectra of Lysine and Histidine labeled PR 2D crystal	
B: ^{15}N 1D MAS spectra of U- ^{15}N labeled PR 2D crystal	110
Figure 34: Topology model of PR highlighting location of methionines	112
Figure 35: 2D ^{15}N - ^1H HETCOR and 2D ^{15}N - ^1H LG-CP spectra of ^{15}N methionines labeled PR 2D crystals	115
Figure 36: Pulse sequence of REDOR	118
Figure 37: Topology model of PR highlighting location of tryptophan	119
Figure 38: ^{15}N 1D MAS spectra of α - ϵ ^{15}N tryptophan labeled PR 2D crystals	120
Figure 39: ^{15}N 1D MAS spectra of REDOR measurements of α - ϵ ^{15}N tryptophan labeled PR 2D crystals with clear assignments	123
Figure 40: ^{15}N 1D MAS spectra of REDOR measurements of α - ϵ ^{15}N tryptophan labeled PR 2D crystals	124
Figure 41: Topology model of PR highlighting location of cysteines	126
Figure 42: ^{13}C 1D MAS spectra of cysteine labeled PR 2D crystal	127
Figure 43: Topology model of PR highlighting location of histidine	128
Figure 44: ^{13}C 1D MAS spectra of histidine labeled PR 2D crystal	129
Figure 45: 1D CPMAS and 1D DPMAS Temperature scan of U- ^{13}C labeled PR 2D crystal	131
Figure 46: Picture depicting differential labeling pattern with 1-3 ^{13}C Glycerol and 2- ^{13}C Glycerol labeled sample	133
Figure 47: 1D CPMAS spectra of ^{13}C labeled sample with different labeling schemes	134

List of figures

Figure 48: Pulse sequence of DARR	137
Figure 49: 2D DARR spectra of ^{13}C labeled sample with 2- ^{13}C Glycerol and spin diluted labeling scheme	138
Figure 50: CP buildup curve of ^{13}C labeled sample for optimization of DARR mixing time	139
Figure 51: 2D ^{13}C - ^{13}C DARR for U ^{13}C PR 2D crystals with 125 msec mixing time	140
Figure 52: Section of 2D ^{13}C - ^{13}C DARR for U ^{13}C PR 2D crystals depicting the alanine region	141
Figure 53: Section of 2D ^{13}C - ^{13}C DARR for U ^{13}C PR 2D crystals depicting the isoleucine region	142
Figure 54: Section of 2D ^{13}C - ^{13}C DARR for U ^{13}C PR 2D crystals depicting the threonine and serine region	142
Figure 55: Section of 2D ^{13}C - ^{13}C DARR for U ^{13}C PR 2D crystals depicting the glutamic acid region	143
Figure 56: 2D ^{13}C - ^{13}C DARR for U ^{13}C PR 2D crystals with selective unlabeled with 125 msec mixing time	144
Figure 57: 2D ^{13}C - ^{13}C DARR for U ^{13}C PR 2D crystals with selective unlabeled and U ^{13}C PR 2D crystals depicting aliphatic regions	145

Appendix

Figure 58: Topology plot of DGK	148
Figure 59: Principle of sitting drop method of crystallization	149

List of figures

Figure 60: 3D crystals of DGK	150
Figure 61: Specific activity of DGK under different conditions with glycerol	153
Figure 62: Specific activity of DGK under different conditions without glycerol	154
Figure 63: Freeze fracture picture of DGK reconstitution conditions	155

List of tables

List of tables

Table 1: Composition of Defined Medium	47
Table 2: Composition of resolving gel	51
Table 3: Composition of Stacking gel	51
Table 4: Composition of Minimal Medium	55
Table 5: List of labeled/unlabeled amino acids for NMR samples	56
Table 6: Summary of 2D crystallization screening conditions for PR	66
Table 7: List of identified FTIR band position for PR 2D crystals	81
Table 8: Details of Tryptophan residues in wild type PR sequence	119
Table 9: Summary of Tryptophan Assignments	125
Table 10: Summary of 3D crystallization screens for DGK	151
Table 11: Summary of 2D crystallization screens for DGK	152

Contents

Contents

ACKNOWLEDGEMENTS	2
SUMMARY	3
ZUSAMMENFASSUNG	5
ABBREVIATIONS	7
LIST OF FIGURES	9
LIST OF TABLES	14
CHAPTER 1-INTRODUCTION	22
1.1 Membrane proteins and challenges.....	22
1.2 Biophysical approach for membrane proteins	23
<i>1.3 What are Pumps and channels?</i>	25
<i>1.4 What is Rhodopsin?</i>	26
<i>1.5 What is Proteorhodopsin?</i>	28
1.5.1 Distribution of genes and sequence information	31
1.5.2 Spectroscopic properties	31
1.5.2.1 Spectral tuning	32
1.5.2.2 Absorption maxima.....	33
1.5.2.3 Retinal isomerization	33
1.5.2.4 Photocycle.....	34
1.5.3 Functional aspects.....	37
1.5.3.1 Influence of pH	37

Contents

1.5.3.2 Light activated proton pump.....	38
1.5.3.3 Energy production and photo effect.....	38
1.5.4 Homology model	40
1.6 Aims of thesis	43
CHAPTER 2 : MATERIALS AND METHODS	45
2.1 Materials	45
2.1.1 General materials	45
2.1.2 Equipment.....	45
2.1.3 Software.....	46
2.2 Methods.....	46
2.2.1 Expression and purification	46
2.2.1.1 Host organism	46
2.2.1.2 Culture maintenance	46
2.2.1.3 Expression.....	46
2.2.1.4 Membrane preparation and solubilization	48
2.2.1.5 Protein purification	49
2.2.1.6 Protein estimation	49
2.2.1.7 Protein purity	50
2.2.1.8 DNA sequence	52
2.2.1.9 Protein sequence	52
2.2.1.10 Preparation of lipid stock.....	53
2.2.1.11 General sample preparation	53
2.2.1.12 Preparation of samples for EM	54
2.2.1.13 Electron microscopy and image processing.....	54
2.2.1.14 Preparation of samples for NMR measurements	54
2.2.1.15 Specifically labeled samples.....	54
2.2.1.16 REDOR samples	55
2.2.1.17 Uniformly labeled samples	55
2.2.1.18 Selectively unlabeled samples	55

Contents

CHAPTER 3 : RECONSTITUTION AND 2D ELECTRON MICROSCOPY	57
3.1 Motivation.....	57
3.2 Background.....	57
3.3 Approach.....	58
3.4 Theory and image processing	59
3.5 Results and Discussion	60
3.5.1 Biochemical analysis and crystallization screens	60
3.5.1.1 Effect of detergent.....	60
3.5.1.2 Effect of additives	62
3.5.1.3 Effect of buffer.....	62
3.5.1.4 Effect of pH.....	63
3.5.1.5 Effect of dialysis duration.....	64
3.5.1.6 Effect of lipid	64
3.5.1.7 Effect of protein concentration	65
3.5.1.8 Other parameters.....	66
3.5.2 EM analysis.....	68
3.5.3 Conclusions.....	72
3.5.4 Perspective	72
CHAPTER 4 : FUNCTIONAL CHARACTERIZATION OF PR 2D CRYSTALS.....	74
4.1 Stability of PR 2D crystals: CD spectroscopy	74
4.1.1 Motivation.....	74
4.1.2 Approach.....	74
4.1.3 Sample preparation	75
4.1.5 Conclusion	77
4.2 Functionality of PR 2D crystals PR: FTIR time resolved spectroscopy.....	77
4.2.1 Motivation.....	77

Contents

4.2.2 Background	78
4.2.3 Sample preparation	78
4.2.4 Results and Discussion	78
4.2.5 Conclusions.....	81
4.3 Functionality of PR 2D crystals PR : SSNMR	82
CHAPTER 5 : ASSEMBLY OF PR: AN AFM STUDY	84
5.1 Scope.....	84
5.2 Approach.....	84
5.3 Advantages for membrane proteins	85
5.4 Motivation.....	86
5.5 High-resolution AFM imaging	86
5.6 Single-molecule force spectroscopy	87
5.7 Results and Discussion	88
5.7.1 Comparison of PR AFM data with BR.....	88
5.7.2 Oligomerization	89
5.7.3 Assembly.....	90
5.7.4 (Un)folding pattern with SMFS and F-D spectra	91
5.7.4.1 Comparison of PR unfolding pattern with BR.....	92
5.8 Comparison of BR and PR from Electron Microscopy	94
5.9 Conclusion	94
5.10 Functional implication	96
CHAPTER 6 : SOLID STATE NMR CHARACTERIZATION OF PR 2D CRYSTALS	97

Contents

6.1 Motivation.....	97
6.2 Background.....	98
6.3 Basic SSNMR Methods.....	99
6.3.1 Magic angle spinning (MAS).....	99
6.3.2 Decoupling.....	99
6.3.3 Cross polarization (CP).....	100
6.3.4 Recoupling.....	101
6.4 Investigation of lipids in the 2D crystalline samples with ^{31}P measurements from the lipid head groups.....	102
6.4.1 Motivation.....	102
6.4.2 Importance of lipids.....	102
6.4.3 Advantages of ^{31}P for lipid investigation.....	103
6.4.4 Results and Discussion.....	103
6.4.5 Conclusion.....	105
6.5 Schiff Base characterization with MAS NMR on ^{15}N - ζ -Lys labeled PR.....	107
6.5.1 Motivation.....	107
6.5.2 Results and Discussion.....	107
6.6 ^{15}N characterization of Methionines.....	110
6.6.1 Motivation.....	110
6.6.2 Approach.....	111
6.6.3 ^{15}N - ^1H Heteronuclear experiment.....	111
6.6.3.1 HETCOR experimental parameters.....	112
6.6.4 ^{15}N - ^1H LG-CP experiment.....	112
6.6.4.1 ^{15}N - ^1H LG-CP experimental parameters.....	113
6.6.5 Results and Discussion.....	113
6.6.6 Conclusions.....	116
6.7 ^{15}N Tryptophan assignments with Rotational Echo double Resonance (REDOR).....	116
6.7.1 Motivation.....	116

Contents

6.7.2 Approach.....	117
6.7.3 Results and Discussion	119
6.7.4 Conclusion	123
6.8 Selective ^{13}C characterization of PR 2D crystals.....	125
6.8.1 U ^{13}C Cysteine	125
6.8.1.1 Motivation.....	125
6.8.1.2 Conclusion	126
6.8.2 U ^{13}C Histidine.....	128
6.8.2.1 Motivation.....	128
6.8.2.2 Conclusion	128
6.9 Uniform ^{13}C characterization of PR 2D crystals.....	129
6.9.1 Uniformly labeled ^{13}C samples.....	129
6.9.1.1 Motivation.....	130
6.9.2 Approach.....	130
6.9.3 Temperature scan.....	130
6.9.1.4 Conclusion	132
6.10 ^{13}C labeled samples with different labeling schemes	132
6.10.1 Motivation.....	132
6.10.1.1 2- ^{13}C Glycerol labeled samples	132
6.10.1.2 Selectively unlabeled U- ^{13}C Glucose labeled sample.....	135
6.10.1.3 ^{13}C - ^{13}C 2D Homonuclear correlation measurements on U- ^{13}C labeled samples	135
6.10.1.3.1 Motivation.....	135
6.10.1.3.2 Approach.....	136
6.10.2 Results and Discussion	137
6.10.2.1 U- ^{13}C uniformly labeled samples.....	137
6.10.2.2 ^{13}C spin diluted sample	143
6.10.3 Conclusions.....	145
APPENDIX.....	147

Contents

Abbreviations.....	147
Motivation.....	147
Diacyl glycerol kinase.....	148
3D crystallization.....	149
Principle of sitting drop crystallization.....	149
Results.....	150
2D crystallization.....	151
Results.....	152
Conclusions.....	155
Material and Methods.....	156
DGK expression.....	156
Solubilization and purification.....	156
Reconstitution.....	157
Activity assay.....	157
REFERENCES.....	159
CURRICULUM VITAE.....	171

Chapter 1-Introduction

1.1 Membrane proteins and challenges

Biological cell membranes provide an interface between the internal cellular and outer extracellular environment. These membranes have basic hydrophobic phospholipid bilayer matrix and associated with it are the proteins, which interact with the external environment and thus help the cell to communicate with the exterior. Based on the extent of embedding of these proteins in the bilayer, they are broadly classified into integral membrane proteins or peripheral proteins. Peripheral membrane proteins are primarily linked to the membrane by specific interactions; however, the integral membrane proteins form the integral part of the membrane by spanning through the membrane with their hydrophobic domains, which are known as trans-membranous regions. Polar side chains dominate these trans-membranous regions and Van der Waals interactions coupled with entropy driven parameters play an important role in stabilizing interactions within the hydrocarbon core region of the bilayer. Integral membrane proteins, which lie within the bilayer, are classified into two general types: β -barrels and bundles of α -helices. The folding mechanism and natural abundance for β -barrels and helix bundles is very different and β -barrel proteins are much less common as compared to α -helical proteins [1].

Most accepted mechanism for the folding of the α helical proteins is a two stage model [2]. Where in the first stage the membrane protein is inserted across the bilayer and its topology is established. In the second stage, the tertiary and quaternary structures are built. The second stage involves assembly and reorientation of the trans-membranous segments established in the first phase. In addition the SecY membrane component in bacteria and Sec 61 translocon complexes in eukaryotes, or protein-conducting channels, work in concert with bound ribosomes to insert proteins into membranes during the first step of membrane protein assembly [3].

The integral membrane proteins, because of their diversity of structure and dynamics are associated with variety of functions and are classified accordingly. For example, these membrane proteins facilitate functions like enzymes, transporters, linkers, signal transduction, receptors, recognition and adhesion sites etc. Membranes also provide barrier to the diffusion process. Since these proteins have a spectrum of functions to perform, they provide a vast field for

Chapter 1-Introduction

pharmacological targets.

For better understanding of the structure function relationship of these membrane proteins it is necessary to have the three dimensional structure of the protein, which poses several challenges.

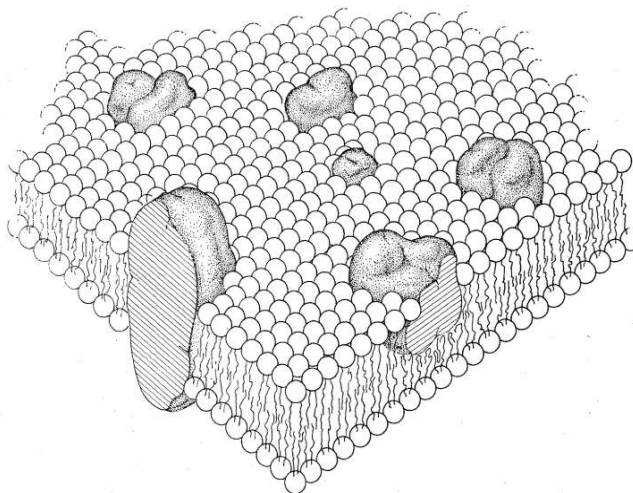


Figure 1 : Original figure from Singer and Nicolson (1972) depicting membrane cross section with integral proteins in the phospholipid bilayer mosaic. Phospholipids are represented as spheres with tails, integral membrane proteins as embedded shaded, globular objects. Some transmembranous protein span entire membrane on left.

1.2 Biophysical approach for membrane proteins

Biophysics is multifaceted area of science. It usually deals with structure and dynamics of molecules, the influence of environment, energy transformation and transfer, thermodynamics and modeling of the biomolecules. It also provides an explanation to the physical phenomenon of biological systems, which occur at the molecular level and works to understand structures of individual molecules as well as interactions between molecules as complex mechanisms. The main area of interest is to understand membranes and membrane protein. In recent years there is increasing number of structures from the membrane proteins, which is possible not only because of better understanding of the protein and crystallization techniques but also because of new generation instrumentation and infrastructure. There is a wide choice of biophysical techniques available for understanding the structural and functional relationship of these cell membranes and membrane proteins. X-Ray Crystallography, NMR and Cryo EM are the common techniques for membrane protein structure determination. All these techniques have a potential of structure elucidation but at the same time have own set of limitations for biological (membrane) protein

Chapter 1-Introduction

samples. Although the preferred choice is 3D Crystallography but considering the application of the relevant technique, only selected ones are discussed.

X-Ray crystallography has a prerequisite of a well diffracting 3D crystal. This is major hurdle for amphipatic membrane proteins, which have a tendency to aggregate in aqueous environment to shield their hydrophobic regions. Most of the crystallization conditions depend on reducing the solubility or alternatively increasing the super saturation in the aqueous environment. Aggregation and thus denaturation of the membrane protein is much faster than the crystallization process. Even if aggregation and denaturation is overcome, the major obstacle is the good quality diffraction from the membrane protein crystal and the properties of these complexes do not favor the formation of well-ordered lattice to yield a good diffraction pattern for structural studies.

High-resolution structural data can be studied by electron microscopy. The major break through with electron microscopy is the high resolution 2D structure of BR [4-6], light harvesting complex [7], tubulin [8] and aquaporin [9] with resolution of 3.0 Å, 3.4 Å, 3.7 Å and 1.9 Å respectively. The technique is also widely used for several other retinal proteins. E.g. A 3D density map of bovine rhodopsin was determined by electron cryo microscopy of 2D crystals with $p22_1 2_1$ symmetry to a resolution of 3.5 Å [10]. The 3D structure of invertebrate rhodopsin (squid rhodopsin) as studied by cryo-electron microscopy of 2D crystals provided the first 3D structural comparison between invertebrate and vertebrate G-protein-coupled receptors [11]. Another example of GPCR is of frog rhodopsin with 6 Å resolution which was studied with this technique [12]. A huge number of new structures of reaction intermediates have been published with X-Ray crystallography using trapping approaches, but there were also studies using electron microscopy [13-15]. The technique is also widely used to detect the conformational changes in the 2D crystals [16-20]. All the approaches are based on same principle, which involve formation of 2D arrays by induction of either lipid-protein or protein-protein interaction. There are proposed theories for the 2D crystallization and can occur in various stages. It can occur by assimilation of microcrystal or reordering of protein after reconstitution in the lipid bilayer. However, the approach involves obtaining of the 2D crystals through various means. E.g. with the aid of biobeads [21, 22] or dialysis [23-25] and there after application of image processing

Chapter 1-Introduction

[26]. However, for reasons of reproducibility dialysis is the most conventional method. The major limitations include obtaining a well diffracting 2D crystal and 3D reconstruction of the images.

NMR spectroscopy is unique among the other 3D structure determination methods for proteins and nucleic acids at atomic resolution. This method is of utmost importance in context to the proteins, in the sense that it does not require crystalline protein. This property becomes indispensable for membrane proteins, which are difficult to crystallize due to the large detergent protein micelle. NMR applications include investigations of dynamic features of the molecular structures as well as studies of structural, thermodynamic and kinetic aspects of interactions between proteins and other solution components, which may be either ligands or drug targets. Solution state NMR is finding increasing application for the structure calculation of (membrane) proteins. Although there is no upper limit for the size of protein but in practice it is limited by the size of the protein detergent complex, which hinders the fast tumbling rates to average out anisotropic chemical shifts and couplings.

SSNMR, still in its budding stage, in principle can be applied to large protein detergent or protein lipid complexes [27] and has the potential to observe the anisotropic interactions, which reflect the structure as well as dynamics of protein [28]. It is an ideal choice because it does not require the biological sample to be either in a soluble or in a crystalline state. These orientation dependent anisotropic interactions for the protein are very complex and to overcome this problem various modifications like Magic Angle Spinning and sample alignment have been introduced [29]. Theoretically, there is no upper molecular weight limit that can be studied by SSNMR unlike solution state NMR that is restricted by the size of the complex for fast isotropic tumbling. These modified approaches need specialized instrumentation like special probes, pulse sequences etc. along with optimal biochemical contribution.

1.3 What are Pumps and channels?

Integral membrane proteins that transport substances across the membrane are categorized broadly into pumps or as channels. There exist some basic structural differences and requirements for proteins to act either as pump or channel, which are usually dependent on the

Chapter 1-Introduction

function of the protein. Broadly they can be covered under the name of transporters, which provide means to the ions and many molecules that cannot freely pass through the hydrophobic membrane but are crucial for biological systems and so aid their movement in and out of the cell. Channels allow the movement of charged species down the gradient without the expense of energy. They require a membrane spanning domain through which the substances generally ions can diffuse and a gate to control the entry and exit of the ions which operates as per the requirement. However, there are some channels, which are always open based on the biological function. Usually the rate of ion diffusion is of the order of 10-100 million ions per second [30]. Pumps facilitate the building of the electrochemical gradient by selective opening and closing of two gates at the expense of energy. There is usually some holding time of ions in the pump to have significant gradient of ions across the membrane. The diffusion rate of ions for a pump is roughly about 100 times per second as in case of sodium-potassium pump primary transporter [31].

In a lipid bilayer, these gates physically comprise of some selected amino acids in and near the trans-membranous domain. Usually charged amino acids with their side chains, which are sensitive to the micro environmental conditions contribute to such category. These residues show some conformation changes in response to the surroundings and can regulate the diffusion of ions through the trans-membranous domain.

1.4 What is Rhodopsin?

One such well characterized family of proteins is Rhodopsin, which has provided basis for detailed understanding of structure and function relationship [32]. Based on hydropathy plots, the family has characteristic seven trans-membranous helices that form an internal binding pocket, where the chromophore 'retinal' is attached. This association leads to the formation of a light absorbing pigment known as Rhodopsin. Upon photo excitation, a conformation change occurs in the retinal, covalently bound through the Schiff base to a lysine located in the seventh helix. This initiates a cascade of electrochemical reactions known as photocycle. Primary function of such proteins is light driven transport of ions in microorganisms and photo induced signal transduction for vision perception in case of higher organisms.

Broadly, the rhodopsin family members are classified into two-types. The Type I rhodopsin class

Chapter 1-Introduction

functions as light driven ion transporters (BR and halorhodopsin) phototaxis receptors (sensory rhodopsin I and II) or has unknown functions (e.g. fungal rhodopsins) [4, 33-35]. These proteins are characterized by very short interhelical loop region. They are also found in some halophilic archaea and γ -proteobacteria, some fungi and green alga [36].

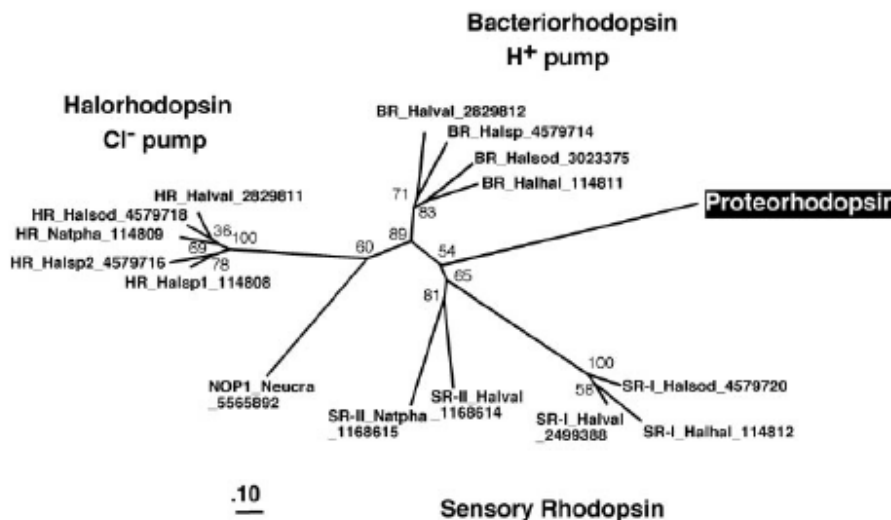


Figure 2 : Phylogenetic analysis of PR with archeal (BR, HR and SR prefixes) and neurospora crassa rhodopsins. The picture is taken from [37].

The Type II rhodopsin acts as a photo sensory pigments and exist as visual rhodopsin, located in the retinal layer of eyes in the animal kingdom and exist as retinochrome found in human or mouse brain [38]. All type II rhodopsins are so far reported in higher eukaryotes [32]. This category features relatively larger hydrophilic domain and comprises of visual pigments, which act as photosensitive receptors in higher eukaryotes e.g. rods, and cones pigments in humans. These two different rhodopsin types show no significant sequence similarity but have identical topologies.

Similar topology with seven transmembranous domains is exhibited by GPCRs, which comprise a large family of integral membrane proteins. These proteins found only in eukaryotes, can sense presence of certain biochemical molecules outside the cell and activate inside a cascade of signal transduction pathways leading to cellular responses. They are involved with several vital

Chapter 1-Introduction

functions like smell, vision, transmission of nerve impulses etc. and form drug targets for over half of modern pharmacological targets. The first 3D crystal structure of a mammalian GPCR known as bovine rhodopsin (1F88) was solved in the year 2000 [39]. With this crystal structure, it was observed that although the seven transmembranous helices are conserved, the relative orientation of the helices differ significantly from that of BR. The first structure of a human GPCR was solved in the year 2007 (2R4R, 2R4S) [40] which was followed immediately by a higher resolution structure of the same receptor (2RH1) [41, 42]. This GPCR structure of human β_2 -adrenergic receptor showed high similarity to the bovine rhodopsin in terms of the relative orientation of the seven trans-membrane helices. However, the conformation of the second extracellular loop was entirely different between the two structures.

1.5 What is Proteorhodopsin?

One major discovery in past decade was that of PR, which is a bacterial homologue of BR and belongs to Type I retinal family. PR genes were first identified as an outcome of the cloning and the sequencing of large genomic fragments of the seawater from an uncultured marine γ -proteobacterium cluster known as “SAR 86” [37]. PRs are believed to exhibit wide distribution worldwide and posses phylogenetic diversity [43-47]. PRs are estimated to be present in 13% of all phototrophic marine bacteria [48]. About 10% of Bacteria and Archea in the oceanic photonic zone have PR photosystem [48, 49] and occupy 20% of the inner membrane surface area [50]. Initially PRs were believed to belong to the uncultivated strains γ and α -proteobacteria [43, 45, 46, 51]. Until recently, when it was reported that SAR11 strain HTCC1062 '*Pelagibacter ubique*' can be cultivated, which expresses a PR gene when cultured in autoclaved seawater and in its natural environment, the ocean [50]. PR genes have now been also identified for the genomes of cultured oceanic members of *Flavobacteriaceae* [52] and SAR92 clade from γ -proteobacterium [53]. Over a brief period several PR variants numbering in hundreds [47] have been identified in the marine plankton.

The PR gene encodes a 249 amino acid long polypeptide and possesses a molecular weight of 27kDa [37]. The hydropathy plots indicate seven trans-membranous domains, which is a typical feature of rhodopsin family. The amino acid residues, which form the binding pocket in case of archeal rhodopsins, are also conserved in PR. The topology plot of wild type PR modeled on BR

Chapter 1-Introduction

showing the important residues is shown in figure 3. The major residues include Asp97, the proton acceptor and Schiff base counter ion (homologous to Asp 85 in BR), a part of counter ion, Asp227(Asp212 in BR) which is close to the Schiff base and C13=C14 bond of the chromophore. Glu108 is homologous to the internal proton donor Asp96 for BR and reprotonates the Schiff base during M to N transition in PR [54, 55]. The most conserved residue in the chromophore binding site across all archeal retinal proteins and all PRs is Asp227, homologous to Asp212 and the chromophore retinal is bound to the protein via a Schiff base to Lys231 homologous to Lys216 in BR. The sequence alignment of PRs with BR is shown in figure 4. For better understanding, the homology model of PR based on BR is also given in figure 5.

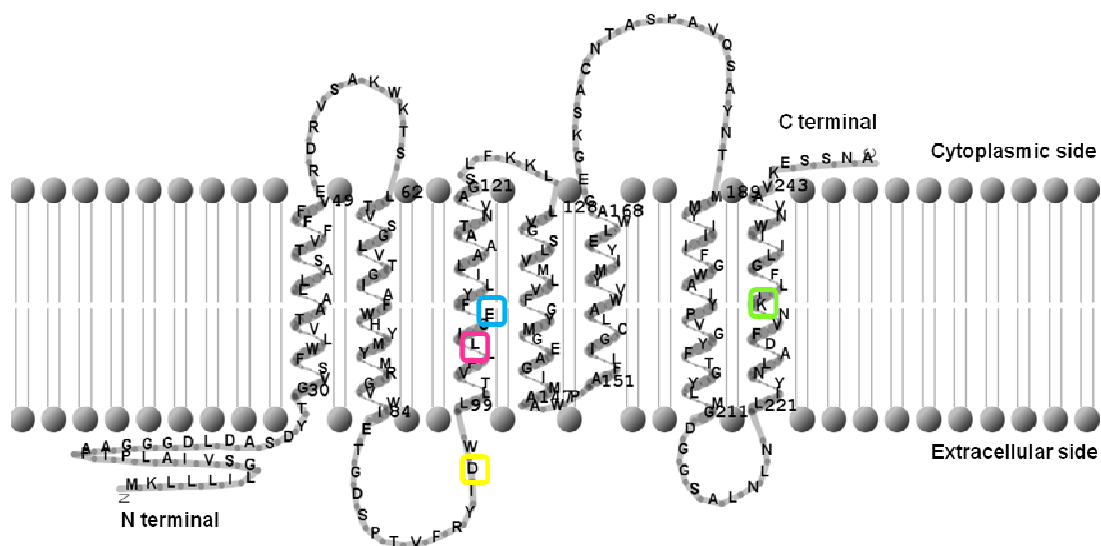


Figure 3 : The topology plot for wild type GPR [56] with BR (1C3W) as a template. The picture shows the C terminus towards the cytoplasmic side and N terminus facing the extracellular side. The Lys231 is squared in green, proton acceptor Asp97 in yellow, spectral tuning switch Leu105 in pink and proton donor Glu108.

Chapter 1-Introduction

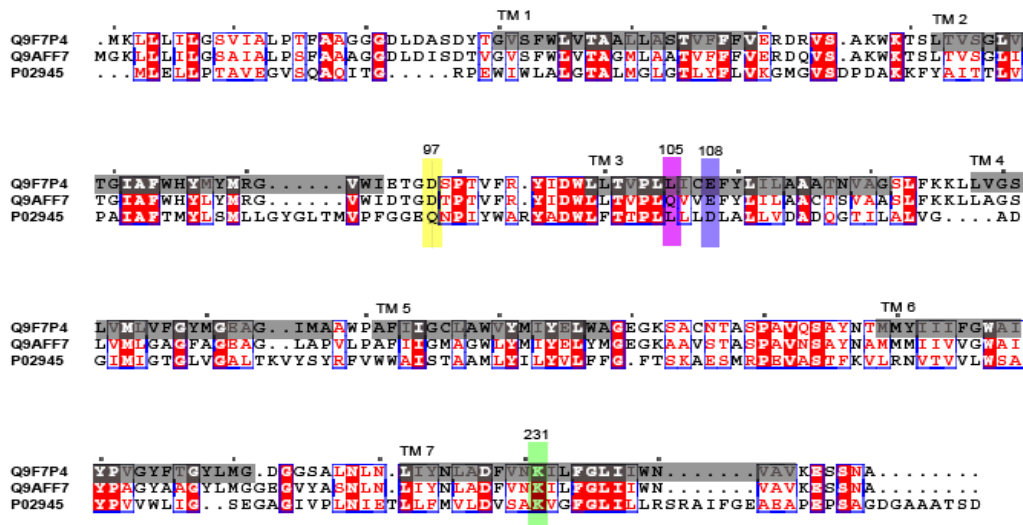


Figure 4 : Sequence alignment results for 2 different variants of PR with BR. GPR (Q9F7P4), BPR (Q9AFF7) and BR (P02945) were used for alignment. The important residues in GPR are highlighted. Proton acceptor (yellow), spectral tuning switch (purple), proton donor (blue) and lysine Schiff base (green). Grey regions represent the helical regions of GPR.

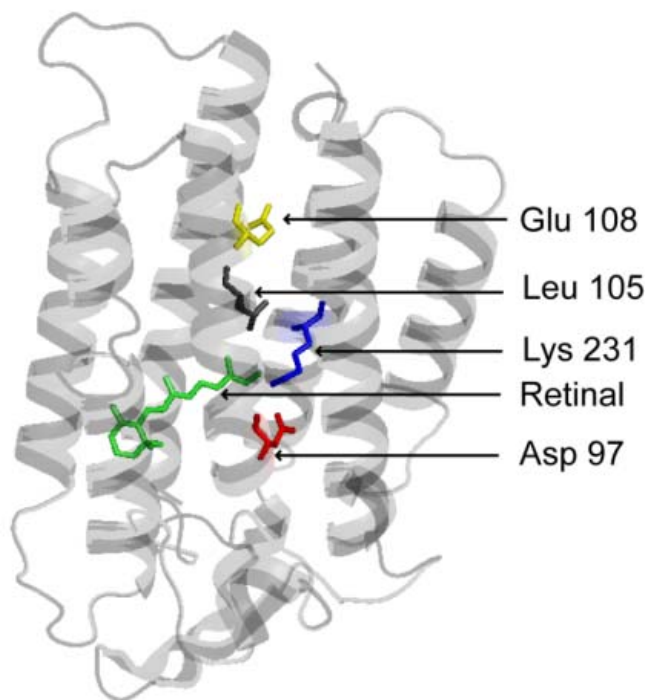


Figure 5 : Homology model of PR based on BR (1C3W). Chromophore retinal and essential residues E108 (primary proton donor), D97 (primary proton acceptor), K231 (Schiff base) and L105 (responsible for colour tuning) are highlighted. This picture is an taken from [57].

Chapter 1-Introduction

1.5.1 Distribution of genes and sequence information

Various evidences suggest the relatively frequent transfer of PR between different lineages and common lateral transfer of PR genes [58]. In this context, identification of the exact origin, based entirely on the sequence is challenging. An extended survey and study involving large insert clones has reported that vast majority of the clones originate from α or γ -Proteobacterium. Full genome sequencing of the isolates and the shotgun sequencing have hinted towards encoding of PR by *bacteroidetes* [47] and Oceanic *Vibrio* and *photobacterium* species also have some strains possessing PR. Similar gene sequences are reported for eukaryotic *P.Lunula* and in marine group II *Euryarchaeotes* [49]. PR photo system, encoded by a single gene is capable of gene duplication and diversification. The different strains of PR as an outcome of such phenomenon are favored by positive selection for their survival and propagation in the photic zone. Reports have documented the presence of genes necessary for biosynthesis of retinal downstream of PR. This supports the fact that for functional relevance, the target cell should have the desired capability of retinal production. This kind of arrangement of genes provides a bioenergetic favor and contributes to the widespread acquisition of PR [48]. A strong selection pressure plays an important role for preservation of these photoactive systems and aids in wide distribution. The light absorbing rhodopsins were initially restricted to Archea and Eukarya but discovery of PR in bacteria extends the representation in all the three domains of life.

1.5.2 Spectroscopic properties

PCR based gene surveys have helped identify different PR variants, which are spectroscopically tuned to absorb different wavelengths of light. The PRs isolated from the surface waters e.g. Monterey Bay show absorption maxima at 520 nm and are referred to as green absorbing proteorhodopsin (GPR). Whereas PR from greater depths e.g. Central North Pacific are named as Blue proteorhodopsin (BPR) and absorb maximally at 480 nm [37, 43, 51, 59]. The distribution of these PRs has shown to be stratified with depth. These two PR families detected in the Mediterranean Sea and the Sargossa Sea did not show any geographic isolation. However, season based variations were observed. This was explained on the basis of stratification of nutrients and salinity, penetration of light, variations in temperature with respect to the season [60]. In addition to this, the contribution from dissolved organic matter may have control over the abundance of PR [61]. The topology of these two groups is similar, however there exists no

Chapter 1-Introduction

significant similarities in their sequence which might suggest different origin [32].

1.5.2.1 Spectral tuning

The four different *H.salinarium* rhodospin display similar variation in color and share <50% sequence similarity. However, PR family could prove potential for studying the spectral tuning in the big rhodospin family because these two groups differ in about 40 nm in their absorption maxima but have a substantial 78% identical amino acid sequence. The tuning is suggested to be optimized to match the light that reaches the dwelling level of bacteria [59].

Based on the theoretical structural models some of the potential but reliable amino acid residues responsible for the spectral difference are identified in these two groups. These are residues 68 (Isoleucine in BPR and Valine in GPR) and 105 (Glutamine in BPR and Leucine in GPR) and can be seen in figure 4. Mutation studies on these two residues indicate that the mutation at position 68 has trivial effect on the spectroscopic properties. However, mutation at 105 position can completely interconvert the spectral properties. The Glutamine to Leucine mutation between GPR and BPR thus proved to be spectral tuning switch. This residue is also in close vicinity to the protonated Schiff base nitrogen. The mutation of the corresponding residue in case of BR and human rhodopsin is known to affect the spectral properties [62, 63]. The observed spectral changes are explained based on altered hydrogen bonding, which repositions the quaternary charged complex and in turn results in the spectroscopic differences [51, 59]. This absorption is also explained based on the fact that both Methionines and Leucine have non-polar side chains. However, there is only limited information available for such Methionines containing subgroup. Spectral tuning properties are unique within the SAR11 family where GPR and BPR share about 86% of amino acid (Pelagibacter GPR and Sargasso sea EAI06928 BPR) [60]. This value is higher than 78% as reported for earlier SAR86 group [59].

The only histidine, His75 is cited to play an important role in the spectral tuning properties of PR especially GPR. It is known that the protein exhibits shifting of the absorption spectra with the change in the pH. At acidic pH, it is red shifted whereas at basic pH it is blue shifted. It is suggested that under physiological pH 6, this Histidine is unprotonated and as the pH turns basic the protonation and reprotonation takes place. The spectral properties of PR in intact cells have

Chapter 1-Introduction

also been studied. Most of the functional spectral diversity is anticipated to be because of difference in polarity or structure of single amino acid residue the retinal binding pocket [64].

1.5.2.2 Absorption maxima

The expression of PR in *E.coli*, in the absence of host organism (SAR86) results into a stable protein, which exhibits photocyclity, is a reflection of its correctly folded state [65]. The verification for the binding of PR with the retinal comes from the generation of 520 nm pigment in the membranes containing PR apoprotein and only in presence of retinal. Furthermore, the half bandwidth of ~100 nm, a signature of retinylidene protein is also observed. Normally retinal in an unbound form gives a λ_{\max} =370 nm. However, in case where it is bound through the Schiff base to the Lysine 231, the λ_{\max} is red shifted to a new wavelength of 520 nm. The absorption spectra of PR variants can be seen in figure 6.

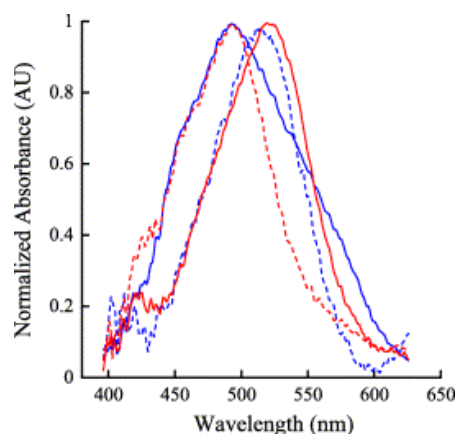


Figure 6 : Spectral tuning of the PR family. Absorbance spectra of PR variants show the importance of position L105 (Q107) to PR spectral properties. The absorbance spectrum of Bac31A8 PR (solid red line) is similar to the absorbance spectrum of Q107L Hot75m1 PR (dashed blue line). The absorbance spectrum of Hot75m1 PR (solid blue line) is similar to the spectrum of L105QBac31A8 PR (dashed red line). The picture is an taken from [64].

1.5.2.3 Retinal isomerization

Retinal extraction experiments at alkaline pH of 9 indicate that the light adapted state consists of 40% 13 *cis* and 60% all *trans* retinal. However, this ratio changes to 20% 13- *cis* and 80% all *trans* in the dark-adapted state. At acidic pH of 6, there was no difference between the light and the dark-adapted state. This ratio was found to be 20% 13 *cis* and 80% all *trans* state. This

Chapter 1-Introduction

behavior is temperature dependent and resembles the values from sensory rhodopsin [66]. Both light and dark-adapted states display similar absorption maxima but the extinction coefficient for light adapted proteins is 10% reduced as compared to the light adapted state [67]. The recent SSNMR data on GPR shows that the chromophore exists in mainly all-*trans* configuration in the ground state [68].

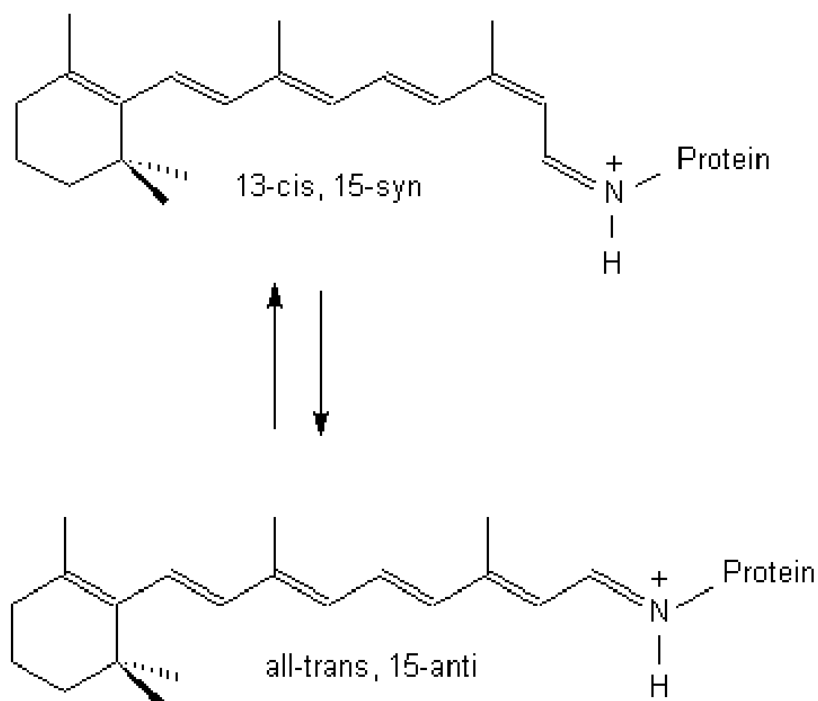


Figure 7 : Retinal isomerization from *13 cis* to *all trans* and vice versa.

1.5.2.4 Photocycle

The rhodopsins have a characteristic cyclic photochemical cascade of reactions known as photocycle. In case of transport rhodopsins like BR and halorhodopsin, the typical time required for photocycle is <20 ms. However for sensory rhodopsin it 10 times longer [33]. The photocycle of GPR has resemblance to the BR photocycle and the photo kinetics are also comparable ~20 ms [69]. The difference in the kinetics of the photocycle is indicative of the functionality of the PR. The slower photocycle reflects involvement in the efficient light detection and a faster photocycle refers to efficient pumping action. The nature of photocycles in GPR and BPR is similar to BR, but the intermediates are still unclear and unspecified [54, 69-71]. It is known that

Chapter 1-Introduction

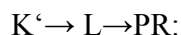
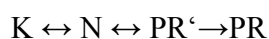
the photocycle of BPR is 10 times slower than that of GPR [59, 69].

Different models have been suggested based on the multiphasic decay of the kinetic signal which indicate the existence of a spectrally silent intermediates for PR [72] and the different suggestive models are given below.

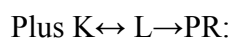
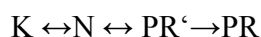
1. Model with sequential reactions:



2. Models with two parallel photocycles, such as:



3. Or model with a branch:



Unlike BR, the photocycle of PR is suggested to be pH dependent. The characteristic features of PR photocycle were determined by time resolved absorption and Fourier Transform Infrared spectroscopy [67]. The PR in the reconstituted form exhibits short photocycle of 20 msec, which has typical M and O intermediates, where decay of O is the rate-limiting step. The absorption spectrum with varying pH indicates that the pKa of the proton acceptor Asp97 is 7.68. Although there is a lot of resemblance of the photocycles between PR and BR, there also exist some evident differences. E.g. for PR L like intermediate whose existence is still unclear was not detected and pH >7 shows presence of M like and O like intermediate upon photo illumination. However, at pH 5 no traces of M like intermediate could be found. Acidic and basic pH kinetics show different visible intermediates and time scales, only the K intermediate shows little pH dependency and the protonation state of Asp97 varies. At lower pH, PR starts to lose retinal, which leads to precipitation.

Chapter 1-Introduction

Other studies based on the transient spectra at pH 9.5, show the existence of three spectrally different intermediates, K, M, and N, named in analogy with the BR photo intermediates. Model analysis based on time-dependent absorption kinetic signals at four wavelengths suggested the existence of two more spectrally silent intermediates and lead to a sequential reaction scheme with five intermediates, K, M₁, M₂, N, and PR', before decay to the initial state PR. An L-like intermediate was not observed, probably for kinetic reasons [73].

The photocycle kinetics of GPR and BPR are significantly different. This reflects influence of lower light penetration to the lower levels in the sea. It also infers the adaptability of the PR to the available light in its natural niche. For better comparison of the functional discrimination of the residues that from the binding pocket across the different Type I family, the concept of super pocket was introduced. This super pocket sequence was extracted from the full-length sequence based on well-defined criteria and comprised of 26 residues. In case of PR, the binding super pockets were separated into two groups.

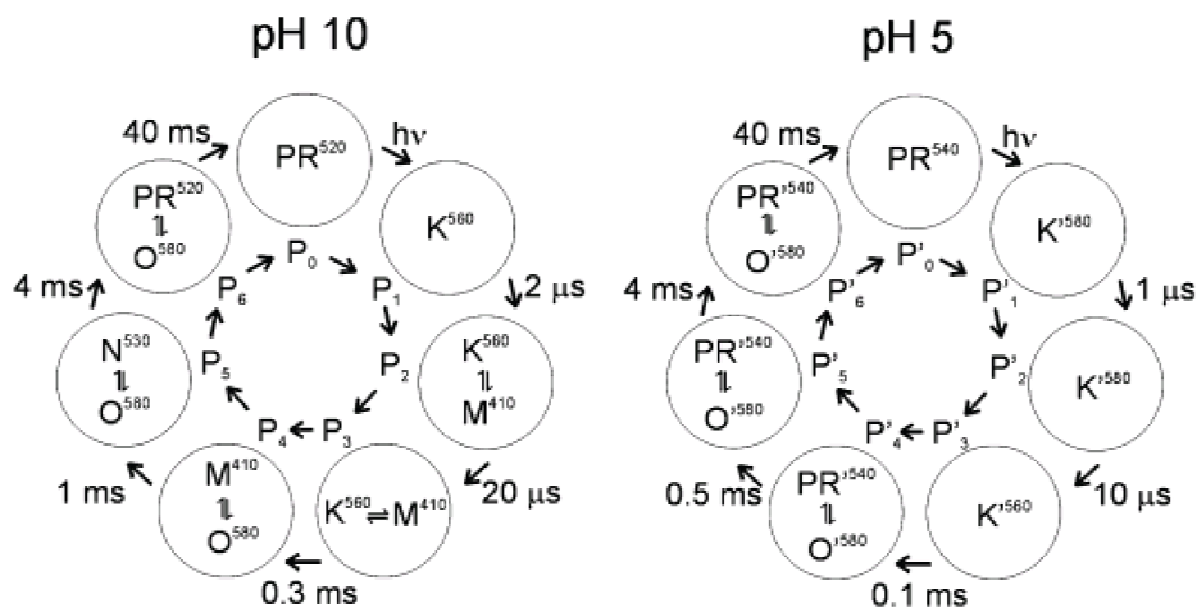


Figure 8 : Photocycle models of PR alkaline (pH 10) and PR acidic (pH 5).The picture is an taken from [67]. The different spectroscopic intermediates with characteristic wavelengths are denoted.

Group A with Met residue equivalent to 105 GPR where as larger group B with wide array of residue types at this position. The mutation L105Q in GPR vs. Q105L in BPR completely exchanges the absorption spectra of the two pigments and affects the photocycle of the mutated

Chapter 1-Introduction

protein [69]. Various evidences suggest that BPR behaves more like a light sensor than a proton pump based on its longer photocycle. Biochemical analysis established its association with retinal when over expressed heterologously in *E.coli*. Based on biophysical analysis, GPR functions as an ion pump rather than resembling a sensory rhodopsin [59] and its photocycle is comparable to that of BR.

The early steps in the photocycle of PR were analyzed by ultrafast pump/probe spectroscopy. The results obtained for the rate of retinal isomerization at alkaline and acidic pH values showed that at pH 9, the functionally important primary proton acceptor (Asp97, pKa = 7.7) is negatively charged and consequently, a reaction cycle analogous to the BR is observed. The excited electronic state of PR displays a pronounced biphasic decay with different time constants. However, at pH 6 where Asp97 is protonated a similar biphasic decay is observed, but it is significantly slower. This indicates that in PR the charge distribution within the chromophore binding pocket is a major determinant for the rate and the efficiency of the primary reaction [74].

1.5.3 Functional aspects

1.5.3.1 Influence of pH

The pH dependent spectral shift is reported for over 20 natural PR variants [64]. The values of absorption maxima span from 536-569 nm for acidic forms of PR but for basic forms there are two groups. First between 488-493 nm for BPR and the other group between 518-526 nm for GPR. pKa of the titratable group which is responsible for the spectral shift is calculated to be 8.2 for intact cells and 8.4 for purified protein. The values for all, over 20 PR variants covered a range from 7.1 to 8.5 [64]. It is shown that Asp97Asn mutant did not exhibit the pH sensitive shifting pattern [54].

The pH of natural oceanic environment lies between 7.5 and 8.1 [75]. In this pH range, which is close to the pKa of the proton acceptor majority of the PR will be in functionally inactive state, which would mean mere wastage of light energy. In order to make the most efficient use, probably PR expressing cells utilize this pKa for the regulatory function. This is questionable in the light of PR known to be a photoactive proton pump. There also exists a possibility of having local pH maintenance, which is basic for active PR functioning [64]. However, until date the

Chapter 1-Introduction

reason for PR to have pKa values in the ambient range remains unanswered. In contrast, the pKa value of BR is many units below the natural environment, which makes it an efficient proton pump [76, 77].

1.5.3.2 Light activated proton pump

Gene and Protein sequence analysis in combination with laser flash induced photolysis have provided proof for PR to be a light activated proton pump. The deprotonated form of PR is the functionally active form, which pumps the protons from inside of the cell to the outside [54, 67, 71, 78]. Time resolved FTIR spectroscopy suggests that in the protonated state of the Asp97, the direction of proton pumping can be inverted and this change is pH dependent [67].

Studies on oriented membrane fragments and reconstituted PR, show proton transport at high pH but not at low pH [78]. During the course of proton pumping, the light energy is finally used to produce ATP via intermediate conversions. Suspensions of *E.coli* cells expressing PR produced transient pH decrease when exposed to light, providing further support to conclude that this PR is a light-driven proton pump [50].

1.5.3.3 Energy production and photo effect

The rough estimation of the PR containing bacteria in the ocean accounts to 10^{28} which makes them the most widespread organisms [47, 79]. These huge numbers propose an important question: *Why is PR present in such high number in bacteria naturally and what is the biological significance?*

Initial experiments showed that PR functions as the proton pump which includes light mediated transport of protons. Therefore, it was logical to measure proton motive force (pmf), which is electrochemical potential of protons across the membrane and is maintained by bacteria under aerobic conditions by oxidative phosphorylation. Bacteria use this pmf for several biological activities such as propelling the flagella [80] and ATP synthesis [81] and it is shown that BR uses this proton pump to produce ATP [82]. Similar hypothesis was applied to PR. It was observed that when cellular respiration of PR expressing *E.coli* cells was hampered using either

Chapter 1-Introduction

respiratory poison or by oxygen depletion, the host cells could create pmf. When cells were illuminated with light of same wavelength as their absorption maxima, the derived pmf could propel the cell flagella [83]. This supported the theory that photoactive proton pumping of PR can generate cellular energy but under defined conditions. It was shown that the cells expressing PR in presence of retinal could also titrate azide concentration in contrast to the cells possessing either only PR gene or only retinal. The laboratory cultivated *P.ubique* demonstrated comparative growth rates under illuminated and unilluminated conditions. When a *Flavobacterium* MED154 was used for similar photo experiments but with natural seawater, there were observed differences. The cells under unilluminated conditions picked up growth, when exposed to light. This simple experiment displayed the positive influence of light on the PR encoding cells. The mRNA upregulation analysis complements the fact that PR has phototrophic function in bacteria [52]. The phototrophic mode of energy production suggests that the absorption maxima could be tuned to optimize the available light.

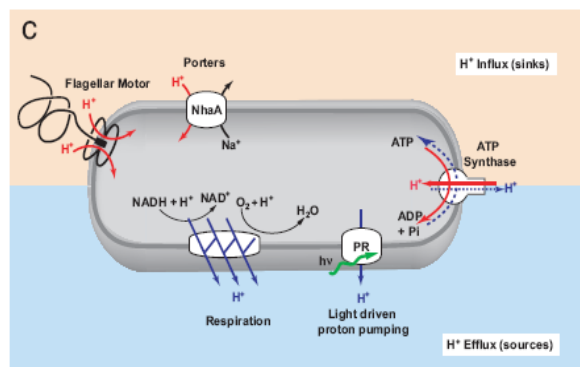


Figure 9 : Over view of transmembranous fluxes and proton pumping in PR containing *E.coli* cells. The picture is an taken from [83].

Based on information available for haloarcheal BR [84, 85], it was postulated that the light activated PR, induces pmf. This induced pmf could drive ATP synthesis as proton reenter the cell through the ATP synthase complex. This hypothesis based on photophosphorylation in PR containing *E.coli* cells was tested with luciferase based assay on PR containing and PR deficient *E.coli* cells. The light induced changes in ATP levels were measured and increased ATP levels were observed after few minutes of illumination only in the PR containing cells. This also

Chapter 1-Introduction

indicates that the possibility of utilization of light energy for biochemical energy conversion [86].

The wide distribution of PR in the marine environment along with capability of spectral tuning could support a potential photoheterotrophic mode of survival and suggest a probable role in the carbon and energy cycling in the photonic zone in the ocean. This inference provides an answer as to why PR exists in such huge numbers and is favored by nature.

1.5.4 Homology model

The PR family members show high homology amongst themselves (up to 99%) as shown in figure 10 as compared to sequence homology to BR, which is ~22%, with Archeal sensory rhodopsin ~14%, and with Halorhodopsins up to 24% [64].

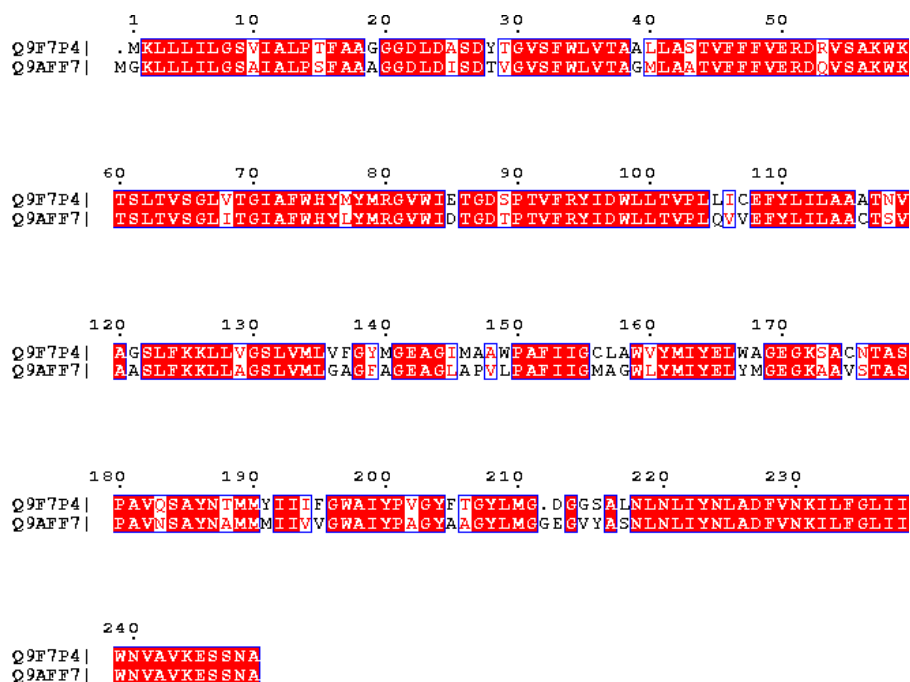


Figure 10 : Sequence alignment for GPR (Q9F7P4) and BPR (Q9AFF7).

For molecular dynamics simulation, GPR models based on BR (1C3W) template show increased stability with low energies in contrast to the models based on SR II (1H68) [87]. The BR based

Chapter 1-Introduction

model provides more realistic 3D homology on account of potential energy calculations. Another reason for the favored homology with BR is the collapse of the model based on SRII with 2 ns dynamic simulation. The reason of the collapse being, formation of strong salt bridge between the chromophore, retinal and the Asp227 [88]. The BR based model also supports in explanation of spectroscopic and pH dependent properties of GPR and at the same time provides feasible picture of the binding pocket and an overall structural stability. The sequence alignment of GPR with BR is shown in figure 11.

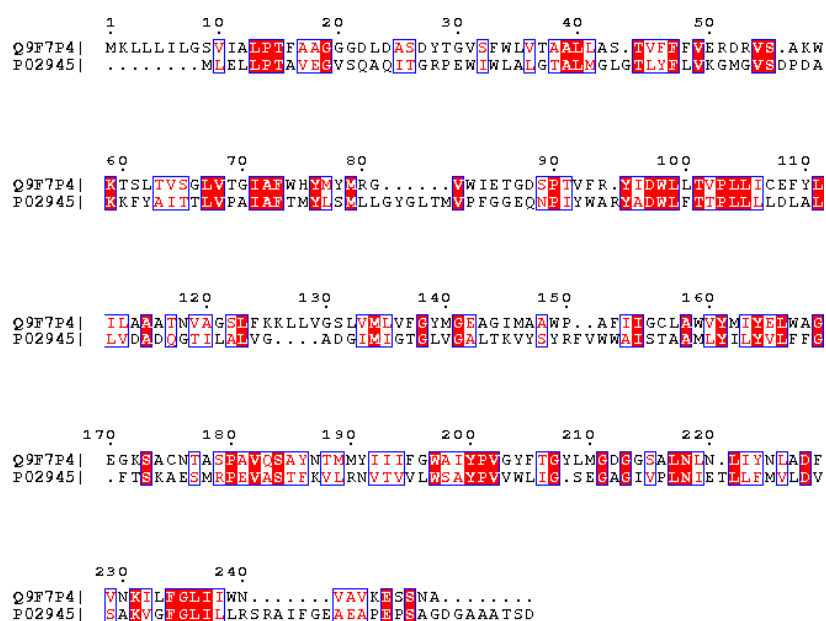


Figure 11 : Sequence alignment of GPR (Q9F7P4) with BR (P02945).

The BPR is unique to have the most blue shifted absorption wavelength amongst all the retinal proteins (after sensory rhodopsin II) and pronounced pH dependence as compared to other retinal proteins. In contrast to the GPR, for BPR it is SRII, which serves as better homology template based on optical spectroscopy, homology modeling and molecular orbital theory [65]. At alkaline pHs BPR spectroscopic properties are similar to SRII and they resemble BR more at acidic pH. The fact that the BPR resembles more to SRII than to BR, but the experimental data indicates it to be a proton pump, this contradiction argues about the possible functionality of PR as a photo sensor.

Based on the overall minimized energy calculations and overall stability to the long-term

Chapter 1-Introduction

molecular dynamics SRII has proved to be more preferred homology model for BPR. The BR based models failed similar to the GPR, due to the collapse after 2 ns dynamics because of strong salt bridge formation between chromophore and Asp229. Finally, BR based model turned out to be unrealistic and unstable as observed by molecular orbital calculations. The BR based model generated high transition energy, which in turn led to very high ordering, and was responsible for the salt bridge. Over all, there exists a contradiction about the functionality of the BPR as it functions as a slow proton pump when compared to as BR. Above all, its homology model resembles SRII, which is a photo sensor [65]. Although there exists a considerable sequence identity among naturally occurring PR genes, the origin of taxonomic lineage still cannot be predicted [45]. The sequence alignment of BPR with SRII is shown in figure 12.

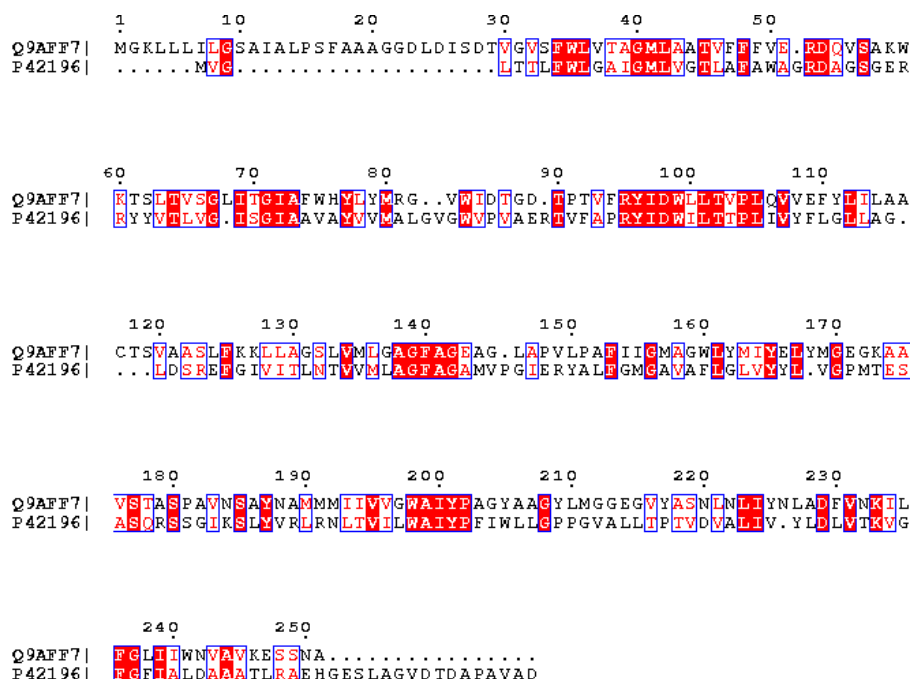


Figure 12 : Sequence alignment of BPR (Q9AFF7) and SRII (P42196).

Structural model of PR along with multiple sequence alignment indicates that majority of active residues are conserved between PR and Archeal BR. The phylogenetic comparison of PR with Archeal rhodopsin suggests that PR forms an independent branch. However there are indications that PR resembles sensory rhodopsin [89].

PR can be successfully expressed in *E. coli* with exogenous addition of retinal unlike BR [90,

Chapter 1-Introduction

91]. The heterologous expression of PR in *E.coli* can question about the location pattern when over expressed. For this, the immunofluorescence staining using antibodies reactive to *Myc* tag provided the best answer. These studies have shown that at lower expression levels PR is abundant in the cells, while at higher expression levels there is an indication of self association [64]. However, this staining pattern for higher expression levels is unlike BR [6].

1.6 Aims of thesis

High-resolution structures are available for type I rhodopsin which include BR, halorhodopsin and sensory rhodopsin II. However, similar information is lacking for PR. The discovery of this novel gene has opened range of questions, which open up a wide area of investigation. A spectrum of approaches have helped to understand better about the distribution of PR, and variability which included techniques like PCR surveys [46, 51], directed sequencing of BAC of fosmid clones [43, 45, 46, 48, 49], whole genome sequencing [50] and random shotgun sequencing of environmental DNA [92]. However, biophysical approaches have also been just touched upon.

The rhodopsins were known to exist in the microbial world as 'BR' found in some Archea and in animals as sensory rhodopsin. However, PR is newly discovered which inhabits marine bacterioplankton, is relatively less characterized. The structure and function information is unexplored. In the absence of 3D structures, there are many open questions, which need to be addressed. For this PhD thesis main focus has been on wild type GPR, in order to answer few of such questions with different biophysical approaches:

- With *Electron Microscopy*, attempts have been made to find the best crystalline conditions. The dual purpose being to achieve structural insights into the crystalline state of protein with the help of projection map on one hand and on the other aiming for high resolution and improved sensitivity for SSNMR.
- *Atomic Force Microscopy* has been used to reveal the oligomerization state of the protein in the crystalline form and *Single Molecule Force Spectroscopy* to reveal the (un)folding patterns of the membrane protein from the native environment.

Chapter 1-Introduction

- Correlation and comparison of the data from electron microscopy with atomic force microscopy has been attempted to derive conclusive structural information especially about the oligomeric state of PR in 2D crystals.
- With *FTIR spectroscopy*, the functionally active state of the protein in the 2D crystalline form is investigated whereas *Circular Dichorism* revealed the stability pattern of the protein within the crystalline arrangement.
- SSNMR characterized the ^{13}C and ^{15}N line shapes and achieved the first ^{15}N Tryptophan assignments with the help of Rotational Echo Double Resonance. The ^1H - ^{15}N CPLG measurements have demonstrated the dynamic aspects of the protein although in restricted mobility arrangement. ^{31}P SSNMR measurements on the 2D crystals were used to characterize the lipids and finally the ^{13}C - ^{13}C DARR homonuclear correlation experiment with 125 msec mixing time showed the possibility of resolving individual amino acid as demonstrated by the Glutamic acid chemical shifts.

Chapter 2 : Materials and Methods

2.1 Materials

2.1.1 General materials

Most of the routine chemicals were acquired from Sigma but sources of special materials are listed here. The nickel-nitrilotriacetic acid (Ni-NTA) resin used for protein purification was obtained from Qiagen (Hilden, Germany); dialysis tubing with 12-14 kDa was obtained from Spectrum Laboratories Inc. (Breda, Netherlands); protein standard for gels were obtained from Applichem (Darmstadt, Germany). lipids such as 1,2-Dioleoyl-*sn*-Glycero-3-Phosphocholine (DOPC); 1,2-Dimyristoyl-*sn*-Glycero-3-Phosphocholine (DMPC); 1-Palmitoyl-2-Oleoyl-*sn*-Glycero-3-Phosphocholine (POPC); 1-Palmitoyl-2-Oleoyl-*sn*-Glycero-3-[Phospho-*rac*-(1-glycerol)] (POPG); Archeal lipid, E. coli Polar Lipid Extract were obtained from Avanti Polar Lipids (Alabaster, USA). Detergents like n-Dodecyl- β -D maltoside (DDM) was purchased from Applichem GmbH (Darmstadt, Germany) and n- β octyl-D-glucopyranoside (OG) was obtained from Glycon Biochemicals (Luckenwalde, Germany). SM-2 Biobeads were obtained from BioRAD (München, Germany).

2.1.2 Equipment

For estimation of protein concentration, an ultraviolet (UV) and visible Jasco V-550 spectrophotometer (Jasco, Gross-Umstadt, Germany) was used. For preparative ultracentrifugation an Optima™ LE-80K ultracentrifuge from Beckman Coulter (Fullerton, USA) was used with Ti70 rotor. Bruker style 4 mm zirconium rotor, KEL-F caps and bottom inserts were obtained from RototecSpintec (Biebesheim, Germany). Experiments were measured using 4 mm MAS DVT probeheads. 4 mm Bruker style zirconium rotors were sealed by HR MAS inserts. For long-term measurements silicon rubber discs were placed between the top insert and the cap to avoid dehydration. The probeheads were obtained from Bruker Biospin (Rheinstetten, Germany). 400 MHz, 600 MHz and 850 MHz spectrometers, used for NMR measurements were purchased from Bruker (Karlsruhe, Germany). Philips CM120 electron microscope with an accelerating voltage of 120 kV was used for screening. Freeze-fracture replicas were produced in the freeze-fracture unit BAF400T (Bal-TEC Inc., Principality of Liechtenstein) and were analysed in an EM208S electron microscope (FEI Company). The CD

Chapter 2-Materials and Methods

spectra were acquired on Jasco 720 CD Spectrometer and FTIR data was collected on IFS66 spectrometer.

Individual experimental settings specific to each experiment shall be indicated in the figure legends and specific pulse sequence used for acquiring data shall be described.

2.1.3 Software

Acquisition and analysis software used for NMR includes Topspin 1.3 Topspin 2.0 and XWIN-NMR Version 3.5 all from Bruker Biospin (Rheinstetten, Germany), Sparky 3 from Goddard and Kneller at the University of California (San Francisco, USA). Typical chemical shifts of amino acids were obtained from the Biological Magnetic Resonance Bank (BMRB) webpage. Topology models were generated using TMPres2D [56]. The electron micrographs were processed with MRC program package [93].

2.2 Methods

2.2.1 Expression and purification

2.2.1.1 Host organism

For over expression of PR, the *E.coli* expression system was used. The host organism used was *E. coli* C41 (DE3) strain with PR expression gene encoded in the pET27 (b+) vector. The protein had Kanamycin as resistance marker and HSV and 6x His tags on the C terminal end. The plasmid was a generous gift from M.Engelhard from Dortmund, Germany.

2.2.1.2 Culture maintenance

The cryo stock of a log phase culture was prepared by shock freezing in liquid nitrogen in final concentration of 40% glycerol. These culture aliquots were stored at -80°C. A loopful of these aliquots was used for inoculation in the fresh medium. Repeated freeze thawing was however avoided.

2.2.1.3 Expression

Chapter 2-Materials and Methods

Depending on the intended use, the expression of wild type PR was done in different media. E.g. LB medium for crystallization screens, defined medium for specific labeling or minimal medium for uniform labeling.

Typically, preculture was inoculated in Luria Bertani (LB) medium overnight at 37°C at 200 rpm. Next day about 10-15 ml of actively growing cells were added to 1 litre of autoclaved medium (LB/ defined medium/minimal medium) with 50 µg/ml kanamycin. The cells were collected when an OD₅₇₈ of 0.8 was reached. After spinning down, cells were resuspended in fresh medium. In case of labeled preparations, fresh medium containing labeled amino acids was introduced at this stage. After 15 min of incubation, 1 mM IPTG and 0.7 mM of all-trans retinal dissolved in ethanol were added. Over expression was achieved by a further incubation at 37°C for 3–4 h and was visually observed by a pink color change of the cells. The cells were harvested by centrifugation at 6,000 rpm at 4°C for 10 mins.

While making specifically labeled sample e.g. Tryptophan labeling for REDOR measurements, defined media with labeled amino acid was used. The composition of defined medium is given below.

Table:1 Composition of Defined medium for selective labeling

Components	Amount for 1 Liter
Alanine	0.50 g
Arginine	0.40 g
Aspartic Acid	0.40 g
Cystine	0.05 g
Glutamine	0.40 g
Glumatic Acid	0.65 g
Glycine	0.55 g
Histidine	0.10 g
Isoleucine	0.23 g
Leucine	0.23 g
Lysine hydrochloride	0.42 g
Methionine	0.25 g
Phenylalanine	0.13 g
Proline	0.10 g
Serine	2.10 g
Threonine	0.23 g
Tyrosine	0.17 g
Valine	0.23 g

Chapter 2-Materials and Methods

Others	
Adenine	0.50 g
Guanosine	0.65 g
Thymine	0.20 g
Uracil	0.50 g
Cytosine	0.20 g
Sodium acetate	1.50 g
Succinic acid	1.50 g
NH ₄ Cl	0.50 g
NaOH	0.85 g
K ₂ HPO ₄	10.50 g

After autoclaving add:

Components	Volume for 1 liter
40% Glucose	50 ml
1M MgSO ₄	4 ml
0.01M FeCl ₃	1 ml
Trace elements	10 ml
Antibiotic (100 µg/ml)	1 ml

Composition of trace elements

Component	Amount for 10 ml of trace elements
CaCl ₂ *2 H ₂ O	2 mg
ZnSO ₄ *7 H ₂ O	2 mg
MnSO ₄ *H ₂ O	2 mg
L-Tryptophan	50 mg
Thiamine (B1)	50 mg
Niacin	50 mg
Biotin	1 mg

Add the required amount after filter sterilization to the medium

The final pH of the solution is around 7.2

2.2.1.4 Membrane preparation and solubilization

Cells were harvested and disrupted with a cell disrupter (Constant cell system, UK) at 1-2 kbar. To remove the contamination from earlier usage the cell disrupter was washed thoroughly with about 300 ml of water then with 300 ml of 0.1 M NaOH and then again equal amount of water / buffer. The homogeneous cell pellet in MES buffer pH 6, was then subjected to the disrupter. The membrane fraction was collected by centrifugation at 45,000 g at 4°C for 30 mins.

Chapter 2-Materials and Methods

Membranes were solubilized in solubilization buffer (1.5% -D-Dodecyl maltoside (DDM), 300 mM NaCl, 50 mM MES, 5 mM Imidazole, pH 6.0 for 48 hours minutes at 4°C. The insoluble fraction was removed by ultracentrifugation at 45,000 g for 15 mins at 4°C.

2.2.1.5 Protein purification

The NiNTA was equilibrated with equilibration buffer (300 mM NaCl, 50 mM MES, pH 6.0) with at least 10 volumes of the column in a disposable syringe. After equilibration, the disposable syringe was inverted over a glass beaker and with the help of airflow and the NiNTA was transferred to the beaker. The supernatant (slightly red in color) after ultra centrifugation was incubated with this NiNTA for at least 2 hours at 4°C. After incubation (most likely the NiNTA beads turn red), the NiNTA column was again packed, followed by slow washing step with about 100 ml of washing buffer (Triton X -100= 200 µl / 200 ml), 300 mM NaCl, 50 mM MES, 50 mM Imidazole, pH 6.0). The detergent concentration in wash buffer was lower than CMC. The protein was finally eluted in a elution buffer (Triton X -100 = 200 mg/ 100ml), 300 mM NaCl, 50 mM MES, 200 mM Imidazole, pH 7.5).

2.2.1.6 Protein estimation

The quantitative estimation of protein was carried out using UV-Vis Spectroscopy. UV-Vis absorption spectra in the range of 250 nm up to 600 nm wavelength were acquired. The total protein content was determined from the two different peaks. The retinylidene peak was observed at 520 nm, which was further used for calculation of protein concentration whereas total protein content was estimated from the peak at 280 nm. The relative purity of protein preparation was estimated by the ratio of $Abs_{280\text{ nm}} / Abs_{520\text{ nm}}$. For a decently pure protein preparation it was between 1.6 -2.2. The absorption value at 520 nm was used to calculate the amount of PR in mg/ml quantities. Usually 1:10 dilution of protein was used and referenced against the elution buffer.

$$(Abs_{520\text{nm}} * \text{dilution factor}) / (1.6 * 0.3) = \text{concentration of protein mg/ml}$$

Extinction coefficient of PR =1.6

Thickness of quartz cuvette=0.3 mm

Chapter 2-Materials and Methods

The typical yield of protein was 2-3 mg/lit from LB medium, 15-18 mg/lit for defined medium and 10 g/lit for minimal medium.

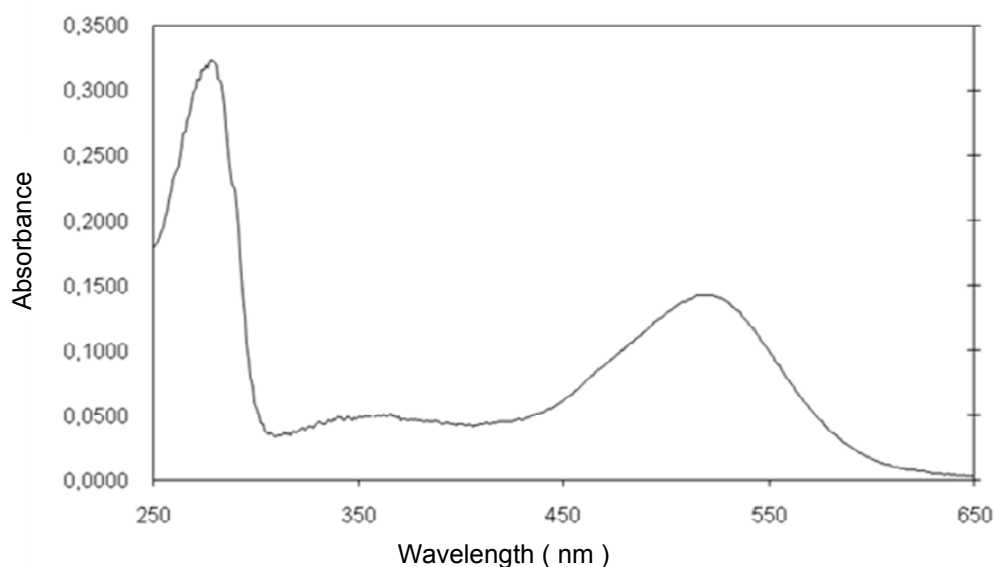
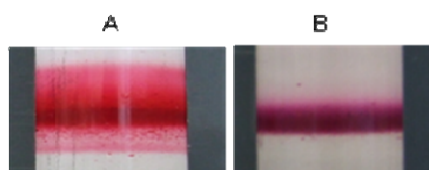


Figure 13 : UV-Vis spectra in the range of 250-600 nm for the Triton X-100 solubilized wild type GPR with typical retinylidene peak of ~100 nm at 520 nm and total protein content at 280 nm.

2.2.1.7 Protein purity

The purified protein was evaluated for the purity of preparation by using SDS PAGE, where a single band of monomer at 27 kDa was clearly observed after coomarsie staining. For further verification, the protein was run on Superdex 200 column. However, it was performed only for initial standardization. The purity of protein as judged by SDS PAGE was over 95%, was adequate for setting up the 2D crystallization trials, and hence gel filtration was not a routine for every preparation.

NOTE: The homogeneity of the reconstituted sample was further checked on 60-80% sucrose gradient. For an ideal preparation a single sharp band was obtained.



Chapter 2-Materials and Methods

Figure 14 : Evaluation of homogeneity of reconstitution on sucrose gradient A. diffused band of inhomogeneous sample and B single sharp band of homogenous reconstituted sample.

Table 2: Resolving gel composition

	Ingredients	1 gel
1	Gel buffer + Glycerol	2 ml
2	40% Acrylamide	1 ml
3	Water	1,5 ml
4	APS	7.5 μ l
5	TEMED	7.5 μ l

Table 3: Stacking gel composition

	Ingredients	1 gel
1	Gel buffer	300 μ l
2	40% Acrylamide	1 ml
3	Water	1,5 ml
4	APS	7.5 μ l
5	TEMED	7.5 μ l

Chapter 2-Materials and Methods

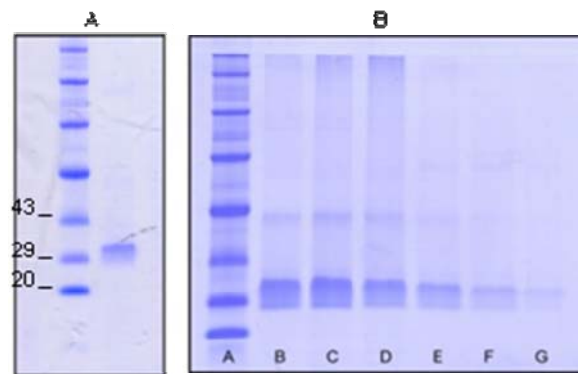


Figure 15 : A: SDS PAGE of purified PR after single step NiNTA purification showing a single monomeric band. B Major fractions from analytical Gel filtration of detergent solubilized PR. Gel filtration was carried out using Superdex 200.

2.2.1.8 DNA sequence

```
AATAATTTTGTTTAACTTTAAGAAGGAGATATACATATGAAATTACTGATATTAGGTAGTGTTATT
GCACTTCCTACATTTGCTGCAGGTGGTGGTGACCTTGATGCTAGTGATTACACTGGTGTTCCTTTTTGGT
TAGTTACTGCTGCTTTATTAGCATCTACTGTATTTTTCTTTGTTGAAAGAGATAGAGTTTCTGCAAAATG
GAAAACATCATTAACGTATCTGGTCTTGTTACTGGTATTGCTTTCTGGCATTACATGTACATGAGAGG
GGTATGGATTGAAACTGGTGATTTCGCCAACTGATTTAGATACATTGATTGGTTACTAACAGTTCCTCT
ATTAATATGTGAATTCTACTTAATTCTTGCTGCTGCAACTAATGTTGCTGGATCATTATTTAAGAAATT
ACTAGTTGGTTCCTTGTTATGCTTGTGTTTGGTTACATGGGTGAAGCAGGAATCATGGCTGCATGGCC
TGCATTCATTATTGGGTGTTTAGCTTGGGTATACATGATTTATGAATTATGGGCTGGAGAAGGAAAATC
TGCATGTAATACTGCAAGTCCTGCTGTGCAATCAGCTTACAACACAATGATGTATATTATCATCTTTGG
TTGGGCGATTTATCCTGTAGGTTATTTACAGGTTACCTGATGGGTGACGGTGGATCAGCTCTTAACTT
AAACCTTATCTATAACCTTGCTGACTTTGTTAACAAGATTCTATTTGGTTTAATTATATGGAATGTTGCT
GTTAAAGAATCTTCTAATGCTCTCGAGATCAAACGGGCTAGCCAGCCAGAACTCGCCCCGGAAGACCC
CGAGGATGTCGAGCACCACCACCACCACCCTGAGATCCGGCTGCTAACAAGCCC GAAAGGAAGCTG
AGTTGGCTGCTGCCACCGCTGA.
```

The DNA sequence was then translated 5'3' in frame 1 to get the desired PR sequence arrangement using ExPASy. ExPASy stands for (Expert Protein Analysis System) [proteomics](#) server of the [Swiss Institute of Bioinformatics](#) (SIB).

2.2.1.9 Protein sequence

The protein sequence of the wild type GPR as obtained after sequencing is given below :

Chapter 2-Materials and Methods

NNFV Stop L Stop EGDIH **MKLLILGSVIALPTFA** **AGGGDL D ASDYT**
GVSEFWLVTAALLASTVFFFVERDRVSAKWKTS **LTVSGLVGTGI**
AFWHYMYMRGVWIE **TGDSPTVFRYIDWLLTVPLLICEFYLI**
LAAATNVAGSLFKKLLVGS **LVMLVFGYMGEAGIMAAWP** **AFI**
IGCLAWVYMIYELWAGEGKSACNTASPAVQSA **YNTMMYIIF**
GWAIYPVGYFTGYLMG **DGGSALNLIYNLAD** **FVNKILFGLII**
WNVAV **KESNALEIKRAS** **QPELAPEDPE** **DVE** **HHHHHH** Stop DPA
ANKARKEAELAAATA

In all there are 280 amino acids including the following

- 1) **Signal sequence : MKLLILGSVIALPTFA**
- 2) **HSV TAG : QPELAPEDPE**
- 3) 6x **His tag: HHHHHH**
- 4) Additional residues

2.2.1.10 Preparation of lipid stock

Lipids were obtained from Avanti Lipids as stocks in chloroform or powder. Desired amount of Lipid was dried under inert gas (Nitrogen) and if required traces of chloroform were further removed in vacuum for 2 hours. Lipid was resuspended in 2% of OG solution to a final concentration of 5 mg/ml, sonicated until a clear solution was obtained. This stock of solubilized lipid was stored in small volume aliquot at -20°C .

2.2.1.11 General sample preparation

DOPC was solubilized in 2% OG and PR was reconstituted at a very low lipid to protein ratio of ~ 0.25 (w/w). The protein was diluted to 1 mg/ml with the dialysis buffer. The protein and lipid mixture was allowed to equilibrate at RT for about 1 h and then transferred to presoaked dialysis tube (12-14 kDa cut-off) with clamps. Typical crystalline preparations involved slow detergent removal by dialysis with the aid of dialysis tubes against excess of dialysis buffer (50 mM Tricine, 100 mM NaCl, 10 mM MgCl_2 , 3 mM NaN_3 , 5 mM DTT, pH 8.5, 7.5% MPD). The dialysis buffer was changed every day and the crystalline samples were obtained after 7 days. These samples were then used either for electron microscopy or for NMR measurements.

Chapter 2-Materials and Methods

2.2.1.12 Preparation of samples for EM

For EM screening the expression was done using readymade Luria Bertani medium (Carl roth GmbH art no:X968.3) and purification was carried out as described earlier. After reconstitution, about 5 μ l of samples were put out on the carbon coated copper grids (400 mesh) and allowed to incubate at room temperature for 2 min. The grids were placed upside down on 2% uranylacetate (pH 4.5) and held for 30 sec to remove excess of sample. The grid was finally air-dried.

Additionally freeze-fracture replicas produced in the freeze-fracture unit BAF400T (Bal-TEC Inc., Principality of Liechtenstein) were analysed in an EM208S electron microscope (FEI Company).

2.2.1.13 Electron microscopy and image processing

Grids were examined in a Philips CM120 electron microscope with an accelerating voltage of 120 kV at a magnification of 45,000 \times or 60,000 \times . Images were collected on a 2K \times 2K slow-scan CCD camera (Gatan Inc.).

The crystal images were processed using the MRC program package [94]. A Fourier transform of crystalline area was calculated. The diffraction spots were indexed and the unit cell parameters were calculated. A filtered image of the 2D crystal was created by extracting the phase and the amplitude information from the diffraction spots. Then the image was subjected to lattice unbending by cross correlation of the image with a small central part of the filtered image as a reference and subsequent interpolation of the image to the ideal lattice from the reference. The amplitude and phases from the Fourier transform of the unbent image could be used to calculate the projection map.

2.2.1.14 Preparation of samples for NMR measurements

The reconstituted samples after the dialysis duration were pelleted down in an eppendorf at 25,000 rpm at 4°C for 30 mins in an ultracentrifuge. The pellet was subjected to 8-10 subsequent washes with fresh dialysis buffer without the salts, DTT and MPD. Finally it was packed in 4 mm rotor with a top and bottom insert. The samples were stored at 4°C until measured.

2.2.1.15 Specifically labeled samples

Chapter 2-Materials and Methods

For specific labeling of the amino acid, defined medium was used for expression. The amino acid, which needed to be labeled, was replaced with the appropriate label. The expression and purification was done in the same manner as described earlier. The ^{15}N ζ lysine, ^{15}N Tryptophan, ^{13}C Cysteine, ^{13}C Histidine samples were prepared in this way.

2.2.1.16 REDOR samples

For REDOR measurements, doubly labeled samples were prepared using the defined media, where ^{15}N Tryptophan label was used for (i) position along with and ^{13}C label for the appropriate (i-1) residue.

2.2.1.17 Uniformly labeled samples

For preparation of uniformly labeled samples minimal media was used, whose composition is given below. The ^{13}C labeled glucose (2 gm/lit) and ^{15}N labeled $(\text{NH}_4)_2\text{SO}_4$ (0.3 gm/lit) were introduced at the time of Induction.

Table 4: Composition of minimal media

Components	Amount for 1 liter
K_2HPO_4	10.5 g
KH_2PO_4	4.5 g
10% MgSO_4	1 ml
40%Glucose	10 ml
$(\text{NH}_4)_2\text{SO}_4$	0.5 g
Thiamine (2.5mg/ml)	1 ml

2.2.1.18 Selectively unlabeled samples

For preparation of selectively unlabeled samples, first the amino acids, which need to be unlabeled, are identified. The expression is carried out as in case of uniformly labeled samples in the minimal medium, except that the identified amino acids are added to the medium in addition to the normal components of the minimal medium in the same amounts as shown for defined medium.

Chapter 2-Materials and Methods

Table 5: List of labeled/unlabeled amino acids for NMR samples

Amino Acids labeled	Amino Acids unlabeled
Arginine	Alanine
Aspartic acid	Glycine
Asparagine	Isoleucine
Cysteine	Leucine
Glutamine	Phenylalanine
Glutamic acid	Serine
Histidine	Threonine
Lysine	Valine
Proline	Tyrosine
Tryptophan	

Chapter 3 : Reconstitution and 2D Electron Microscopy

3.1 Motivation

Our 2D crystallization screen was initially motivated by the similarities between BR and PR, and the fact that BR is arranged in 2D arrays within the *Halobacterium salinarium* membrane [93]. However, nothing is known about the arrangement of PR protobacterial membranes. The first goal was therefore to find suitable 2D crystallization conditions. The projection map of well diffracting 2D crystals would help in understanding the structural details of the protein in the membrane and at the same time could also be used for detailed mechanistic studies by SSNMR as natural 2D crystals of BR (purple membrane) did yield very well resolved spectra [95]. Major benefits of 2D crystals for SSNMR study are high sample concentration and homogeneity. Furthermore, it is assumed that crystal packing would reduce internal molecular motions, which might interfere with coherent averaging by magic angle sample spinning. In view of advantages conferred by 2D crystals, the trials were attempted.

3.2 Background

The simplest definition of 2D crystals is arrangement of single layers of ordered membrane protein molecules in two planes. Broadly the membrane protein 2D crystals are classified into Type I crystals and Type II comprise of soluble proteins. The need of 2D crystals for membrane proteins arise because of the following reasons:

- The orderly arrangement of the protein has a preferred identical orientation.
- The Fourier transformation of 2D crystal is discrete and the structural information is contained in the form of defined reflection or “spots” because the Fourier transform of the 2D crystal is the FT of the molecules sampled at positions of reciprocal lattice points. This explains the reason for the discreteness.
- The amplitude and phase of each reflection is calculated from the FT of the images.
- If appropriate crystalline condition is screened then various intermediates can also be crystallized with similar conditions.

However, like any other technique there are some limitations associated with the 2D crystallization trials.

Chapter 3-Reconstitution and 2D Electron Microscopy

- Obtaining a 2D crystal is a matter of luck and can take very long time with or without success.
- Significant amount of time can be invested in improving the quality of 2D crystal.
- The crystalline arrangement of the protein is achieved in vesicles, membranes or tubes. In all these cases, each image provides only single view of the molecule. Nevertheless, in order to reconstruct the overall view of the protein arrangement in the crystalline packing the tilted data from random orientations needs to be collected. This gives the biggest challenge.
- From biochemical point of view, although the protein is reconstituted into the membrane but may not be active. This is because the crystalline packing offers limited flexibility, which might be required for the functionality of the protein.

3.3 Approach

1. *Reconstitution*: The most traditional but still the most widely used approach as it has produced the maximum number of crystalline samples. The setup utilizes small amounts of known concentration of detergent solubilized protein and detergent solubilized lipid is added to it in molar protein to lipid ratio in the range of 0.1-10. After incubation of this mixture at RT or on ice, the detergent is removed either quickly by adding hydrophobic biobeads or slowly by dialysis. Various screens can be set up depending upon varying parameters like temperature, pH, concentration, additives, lipids etc.

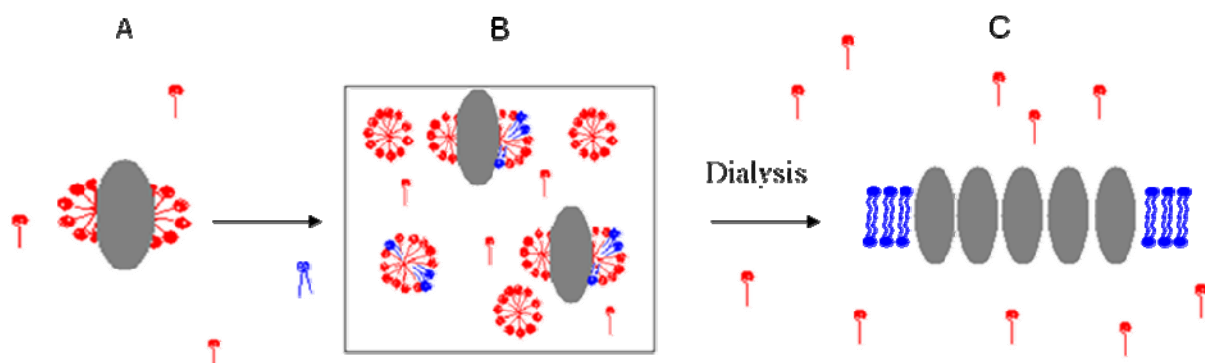


Figure 16 : Principle of dialysis A: detergent (red) solubilized membrane protein (grey). B: Mixture of detergent solubilized membrane protein with lipids (blue) in the dialysis bag. C: After definite time duration for dialysis the detergent molecules replaced by lipids and protein attains a crystalline conformation.

Chapter 3-Reconstitution and 2D Electron Microscopy

2. *In situ Approach*: This approach is used for those proteins, which constitute the dominant fraction of the entire membrane protein fraction. The underlined principle is to raise the concentration of desired protein above the critical threshold required for the lattice formation by extracting excess of bulk lipids from the membranes. The choice of detergent for lipid extraction should be such that it does not dissolve the membrane protein. Typically, a membrane suspension of known concentration is prepared and extraction of lipid is done by incubation with detergents for hours at different temperatures. The detergent is removed mostly by dialysis. This method is least disruptive as protein always resides in its membrane. However, this preparation is prone to contamination with non crystalline membrane material and hence the unit cell may vary from batch to batch.
3. *Surface Crystallization*: Especially suited for membrane proteins, which have a natural tendency to form arrays at interface between the 2 phases. The phases referred to are air-water or carbon water interface. This type of approach can also be extended to the substrate induced 2D crystallization. It requires less time and may yield large crystalline arrays with very little protein requirement. If carbon-water interface is chosen then it can directly be done on carbon-coated grid and can be observed directly. However, there may exist a possibility of inhomogeneity in larger patches. Additives used for inducing the crystallization may contribute to the background noise.

3.4 Theory and image processing

The electron microscopy technique is well suited for studying the 2D crystals. The major credit for development and refinement this technique for the study of membrane proteins goes to Henderson et al [4, 96]. Recent developments of electron crystallography using a combination of electron diffraction and electron imaging has made structure determination of biomolecules reach atomic resolution.

Electron microscopy is based on strong scattering power of electrons. The atomic scattering intensities are 100,000 times larger than the X-Rays and because of these strong interactions, it is possible to obtain a high quality diffraction pattern from very small samples which permit the

Chapter 3-Reconstitution and 2D Electron Microscopy

usage of very thin samples such as biomembranes, which have a thickness of one or two molecules. The electrons are scattered by the shielded coulomb potential and as a result, the density maps in electron microscopy represent the coulomb potential. The electrons can be focused to produce a high-resolution image.

Fourier transformation of the electron microscopic image shows a diffraction pattern from which the reciprocal vectors are determined. A filtered image is created by using the information from the diffraction spots, which originate from the periodic structure from which the intensities and phases on the reciprocal lattice points are used for back transform. The signal to noise ratio of the primary data from two-dimensional crystals is initially low because of lattice imperfections and beam damage. For the purpose of increasing the signal to noise ratio, the data is usually filtered in digital format (filtering) and lattice imperfections are computationally corrected (unbending). This results in an image, which shows the average over multiple unit cells. The optical diffraction pattern thus obtained from the crystalline arrays contains information about the symmetry and the quality of the specimen.

After image processing for the crystal improvement, a projection map is calculated. For the acquisition of high-resolution data on biomolecules the samples are usually studied in the frozen-hydrated state (electron cryo-microscopy), which resembles the natural hydration state of the proteins. The cryo conditions also prevent the radiation damage to the sample.

3.5 Results and Discussion

3.5.1 Biochemical analysis and crystallization screens

There are many parameters, which need to be optimized to obtain a perfectly well ordered and highly diffracting 2D crystal. However, considering the feasibility of the screening, these parameters need to be prioritized. Multiple parameters were tested simultaneously and most important parameters are discussed under different headings.

3.5.1.1 Effect of detergent

By definition, detergents are amphipatic molecules which have a polar head group region and a

Chapter 3-Reconstitution and 2D Electron Microscopy

non polar side chain. The purpose of detergent is to cover the hydrophobic residues of the helical region, which span the membrane such that it is properly folded and is functional outside the membrane. Detergent is expected to ape the physical properties of lipid bilayer in anticipation that the structural properties of the protein will be restored. In case of membrane proteins, the detergents orient in such a manner that the hydrophobic tail region surrounds the hydrophobic region of the protein and the polar head groups interact with the aqueous external environment in a thermodynamically stable conformation. These detergents are characterized by the critical miceller concentration, aggregation number, head groups, side chains and degree of saturation or unsaturation of the bonds in the side chain. Based on the charge carried the head group these detergents behave differently and have different impact on the membrane protein which is briefly discussed.

In short, *Ionic detergents* have a net charge, which can be positive, or negative. Ionic detergents are more sensitive to pH, ionic strength, and the nature of the counter ion, and can interfere with charge-based analytical methods. E.g. SDS.

Non-ionic detergents consist of uncharged hydrophilic head group are non-denaturing, but are less effective at disrupting protein aggregation. They have mild properties, which are strong enough for breaking lipid–lipid interactions and lipid–protein interactions but are not capable of disrupting the protein-protein interactions. Such detergents preserve the native conformational state of membrane protein. E.g. OG.

Zwitterionic detergents possess intermediate properties, which can efficiently disrupt protein aggregation, offer slow denaturing and net-zero charge. E.g. CHAPS.

Considering all these aspects, different detergent screens were set. The detergents were evaluated based on the stability of the protein monitored by the UV-Vis spectra and the ease of detergent removal with dialysis. For this LDAO, C₁₂H₈, Hecameg, Triton-X, CHAPS, DPC, DDM, CTAB, Sodium Cholate, DTAC and combination of detergents was analyzed. These detergents were known to have BR in functional state hence were shortlisted. It was observed that PR was definitely more stable in Triton-X 100, DDM and OG, which belong to the class of non ionic detergents. Once the protein was stable, considering the effect of the CMC on the duration of the dialysis, the detergent screen was further expanded to the use of different combinations of

Chapter 3-Reconstitution and 2D Electron Microscopy

detergents for protein elution and lipid solubilization. The best combination was achieved with PR eluted in non-ionic Triton X-100 (CMC of 0.25–0.3 mM) and lipid solubilization in OG (CMC of 20–25 mM) [97].

NOTE: The detergent screen was also evaluated for the ease of removal from the system. It was found that the presence of extra detergent in the system causes loss of resolution in SSNMR spectra. In order to regain the resolution additional washing steps with dialysis buffer were introduced.

3.5.1.2 Effect of additives

Amphiphiles are generally used in 2D and 3D crystallization. They aid in crystallization by various mechanisms. Some are believed to reduce the size of the protein detergent micelle and provide assistance in increasing the interaction between the extramembranous segments [98]. Another hypothesis says that they make the detergent micellar collar more flexible, which in turn helps in crystal growth [99] and in the absence of lipids cover the transmembranous part. Some small additives can directly act on the extra membranous part of the protein as seen in Ca⁺⁺ATPase. The use of additives is more frequent in case of 3D crystallography; however, for 2D it is still not a routine yet. The list of common additives used for crystallization screens is also available [100, 101].

In case of PR, MPD, which is an amphiphile and has nonpolar character, enhanced the growth of 2D crystals. Several different concentrations were tested and the best was found with 7.5% concentration in the dialysis buffer. It is known that MPD binds to the hydrophobic sites and prefers leucine side chains. Binding of MPD involves amino acid residues in the helical or β sheet regions. MPD binding to protein is penetrative and leads to displacement of the water molecules in the grooves and cavities on the protein surface, which in turn reduces the solvent accessible areas and has implications on the solubility of the protein. MPD, normally expected to be a strong denaturant but in this case it promotes stabilization of protein by preferential hydration, which is due to binding of MPD molecules to the hydrophobic surface.

3.5.1.3 Effect of buffer

The buffer, which is used to dialyze out the detergent from the reconstitution mixture, plays a

Chapter 3-Reconstitution and 2D Electron Microscopy

key role for crystallization. This is because the buffer has salt, additives, temperature and specific pH and most important it interacts directly with the protein and alters the solubility. After screening different divalent salts e.g. MgCl_2 , NiCl_2 , CoCl_2 , BaCl_2 , MgCl_2 , CaCl_2 and monovalent salts e.g. KCl , LiCl , NaCl , in different combinations and concentrations, the best condition was obtained in combination with 100 mM NaCl and 10 mM MgCl_2 .

NOTE: The concentration of salts in the dialysis buffer was optimized considering the requirements for the NMR measurements. The NMR samples with high concentration of salt are known to have arching problems. In order to avoid this problem the concentration of salts was restricted to minimum required.

3.5.1.4 Effect of pH

Protein has a net charge and the buffer has a specific pH. This implies that there will be alteration of interactions, which may influence the crystallization. The effect of pH on the solubility will be much stronger at low ionic concentration of the buffer. Apart from this, PR has shown a pH dependent vectorality for the pumping of protons [67]. Since pH has important role in the functioning of PR, a pH range of 4-10 was screened. The quality of crystals improved slightly towards the alkaline pH, while it deteriorated at acidic pH 4. The lowest pH value for the crystal formation was pH 6 and the best crystals were obtained at pH 10.

Reconstitution under acidic condition (pH 6) led to diffused, low order diffraction spots, compared to those obtained under physiological condition (pH 7). At alkaline pH (up to 11), the quality of crystals improved slightly (figure 17 B). The pH of seawater is around 7.2–8.5 which means that most PR molecules in a marine bacterium under native conditions are pumping protons from inside the cell to the outside. As the pKa of the proton acceptor is ~ 7.2 , PR is either inactive or transports protons in opposite direction at acidic pH, which could lead to a heterogeneous mixture of the molecules in different conformational states, leading to the diffused diffraction spots.

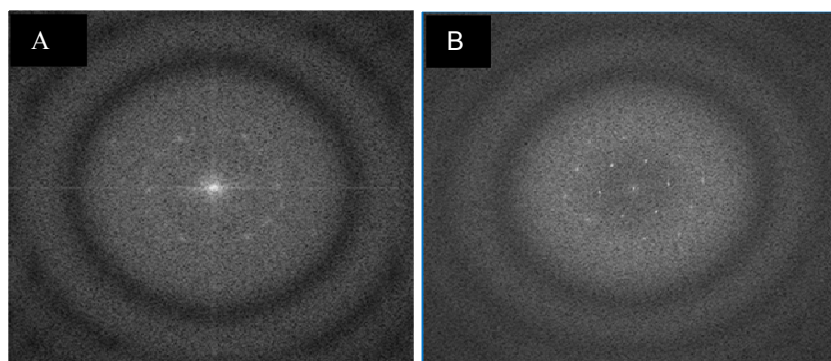


Figure 17 : Diffraction pattern of PR 2D crystals at different pH. A: Diffused spots and one order diffraction pattern at pH6 B: Two orders of diffraction pattern at pH10

NOTE: The projection map as shown in figure 19 was calculated with the sample reconstituted at pH 10. However, to be close to the physiological range the SSNMR samples were prepared at pH 8.5.

3.5.1.5 Effect of dialysis duration

It was observed that when above stated combination of detergent is used and the samples are analyzed with EM after 7 days and 14 days, no significant improvement in the quality was observed. Hence, a manageable dialysis time of typically one week with regular buffer changes was used.

3.5.1.6 Effect of lipid

Lipids are amphiphiles with a hydrophilic head group and two saturated or unsaturated hydrophobic chains. Lipids play an important role in providing the membrane protein a native environment for proper folding and functioning. During reconstitution, the lipids gradually replace the detergent belt around the hydrophobic region of membrane protein. The lipids also have characteristic head groups and side chains, which determine the inherent properties of lipid *per se*. Hence, for crystallization it is one of the most important parameter for screening.

In addition, the importance of lipids have been reported to have considerable impact on the stabilization of the crystal structure of BR [102]. Most likely, crystallization can be favored by

Chapter 3-Reconstitution and 2D Electron Microscopy

using native lipid environment as in case of BR, Photosystem II, Ca⁺⁺-ATPase, Na⁺ and K⁺-ATPase, Rhodopsins and Light harvesting complex II. In some cases, combination of lipids have also proved to be essential [103]. DMPC has a significant success associated with it. It was found to be successful for Photosystem I/II, aquaporin, porin, and mixture of DMPC with other lipid for e.g. lactose permease. For crystallization, it is important to consider the hydrophilic and hydrophobic balance of the protein. The lipid to protein ratio is known to have been influenced with this parameter [23].

The dependence of BR assembly on the membrane lipid content have been investigated earlier by conventional kinetics, equilibrium methods [104, 105] and neutron diffraction [106]. The reports support the fact that the change of lipids during reconstitution affects the membrane protein assembly of BR. Lipid environment may be influential in deciding the oligomeric state of the protein. The contribution of the head group moieties for the stabilization of the BR trimers is also well documented [4, 107].

In context to the importance of lipids for crystallization, a series of lipids were screened based on different chain lengths and head groups. These included POPC, POPG, Soy PC, DOPC, Archeal Lipids, E.coli Lipids, Egg PC and DMPC. Different combinations and different ratios of these lipids were tested. It was observed that the crystals of comparable diffraction pattern as shown in figure 17 B were obtained with almost all the lipids except for DMPC. The inability of crystallization with DMPC could be explained based on its short side chain. The best diffraction was obtained with DOPC as shown in figure 17 B and hence was standardized. The Protein to Lipid ratio range for obtaining crystals was 1:0.25 - 0.16 (w/w). A low lipid to protein ratio of about 0.20 (w/w) was essential for the formation of homogenous 2D crystalline samples. Increasing the amount of lipids to more than ~0.25 (w/w) led to formation of isolated crystalline patches that apparently prevented further growth of these areas.

3.5.1.7 Effect of protein concentration

It is important to begin the crystallization with the protein of substantial purity. In case of PR, the purity was over 95% as judged by SDS PAGE, which was a good starting point. The concentration of protein in the crystallization setup was usually 1 mg/ml. However a complete

Chapter 3-Reconstitution and 2D Electron Microscopy

range from 100 µg/ml up to 5 mg/ml was screened but no significant effect of protein concentration was observed.

3.5.1.8 Other parameters

Reducing agents: Different reducing agents and combination in different concentration were also experimented with β-mercaptoethanol, DTT and isopropanol in order to reduce the disulphide bonds. No significant difference was observed.

Temperature: An entire temperature range from 4°C up to 60°C was screened with different modifications like ramp. The temperature screening did not help much and finally room temperature of 20°C± 2°C was chosen for routine crystallization.

The different parameters, which were varied, and the range of testing conditions have been summarized in the following table. However, it should be noted that multiple combinations of these parameters were tested at a given time.

Table 6: Brief summary of conditions screened for 2D crystallization of PR

Type of screen	Range screened	Comments / best condition
Protein:Lipid Ratio (w/w)	1:5, 1:2.5, 1:1.25, 1:0.83, 1:0.41, 1:0.166, 1:0.083	First diffraction pattern with 1: 0.83 and the best with 1:1.20
Monovalent salts	Sodium chloride, Potassium chloride, Lithium chloride	Lithium Chloride no crystals
Monovalent salt concentration (mM)	50, 100, 250, 500, 750, 1000	100 mM
Divalent salts	Manganese chloride(MnCl ₂), Calcium chloride (CaCl ₂), Nickel chloride(NiCl ₂), Cobalt chloride (CoCl ₂), Magnesium chloride (MgCl ₂), Barium chloride (BaCl ₂)	Magnesium chloride (MgCl ₂)

Chapter 3-Reconstitution and 2D Electron Microscopy

Divalent salt concentration (mM)	5, 10, 25, 50, 100, 250,	10 mM
Combination of Sodium chloride and Magnesium chloride (mM/mM)	1000/10, 800/10, 600/10, 400/10, 200/10, 100/10 1000/20, 800/20, 600/20, 400/20, 200/20, 100/20	100/10
pH	4, 5, 6, 7, 8, 9, 10	No crystal under pH 6, Diffused crystals at pH 6, Best crystals at pH 10
Temperature (°C)	4, 20, RT, 25, 30, 37, 60, ramp	First crystals at 37 later RT was used.
Buffers	Citrate, MES, Tris HCl, Tricine, Phosphate, Hepes,	No effect (except for pH)
Buffer range (mM)	10, 20, 50, 100,	No effect
Detergent removal	biobeads and dialysis	biobeads used for initial reconstitution screening
Incubation with biobeads (h)	2, 4, 6, 10	4- 6
Dialysis duration (days)	3, 5, 7, 10, 15, 20, 25, 30	10-12 days was optimum
Protein concentration (mg/ml)	0.100, 0.25, 0.5, 0.75. 1, 2, 3, 4, 5	No effect
Lipids	DOPC, POPC, POPG, EPL, Archeal, lipids, Soy PC, POPE, DMPC,	DMPC gave no crystal
Detergents for lipid solubilization	Triton X-100, DDM, OG	Crystals of comparable quality
Detergents for protein elution	CHAPS, CHAPSO, Triton X-100, DDM, OG, CTAB, LDAO,	Protein was stable in Triton X-100, DDM, OG as

Chapter 3-Reconstitution and 2D Electron Microscopy

	Hecameg, DTAC, Sodium choleate, C ₁₂ H ₈ ,	observed by UV Vis spectra
Reducing agents and concentration (mM)	DTT(2,4) β-mercaptoethanol, (2,4), Isopropanol (1.5%, 2.5%, 5%)	No effect
Additives	Glycerol, MPD	MPD better than glycerol
Concentration of additives (MPD %)	2.5, 5, 7.5, 10, 12.5,15 ,17.5, 20	7.5%

In all over 1000 conditions were screened in order to obtain well diffracting 2D crystals, which were suited for cryo electron microscopy analysis. The first diffraction pattern was observed in the condition number 24 (Condition number 24: Protein concentration in elution buffer = 1mg/ml, protein to lipid (w/w) ratio of 1: 0.83, detergent removal with biobeads (ratio of biobeads to detergent = 40:1), incubation time = 2 h, temperature = 37°C and lipid used was *E.coli* polar extract. Further screening gave a better diffraction pattern in condition number 142 (protein to lipid (w/w) ratio =1:0.2 , lipids used were *E.coli* polar extract, temperature = 37°C, dialysis duration 5 days and dialysis buffer consisted of 250 mM Sodium chloride in Hepes buffer at pH7). These conditions which later remained constant throughout the rest of the screening conditions.

Based on high reproducibility and reliability of the reconstitution approach, the 2D crystals of PR were attempted with dialysis. In addition, the sample preparation is discussed earlier in chapter 2. Unfortunately, highly ordered 2D crystalline sheets or vesicles which would be ideal for 2D crystallography were not obtained under any conditions tested. Interestingly, the pH of the reconstitution buffer and the detergent used for solubilization of lipid and for the elution of protein played a crucial role for the quality of the diffraction pattern. The use of appropriate detergents for membrane protein stabilization and crystallization played a crucial role and has been discussed extensively [108].

3.5.2 EM analysis

Chapter 3-Reconstitution and 2D Electron Microscopy

The best 2D crystals were obtained using synthetic lipids (DOPC) at pH 10 using an initial lipid to protein ratio of ~ 0.25 (w/w) as described in figure 18.

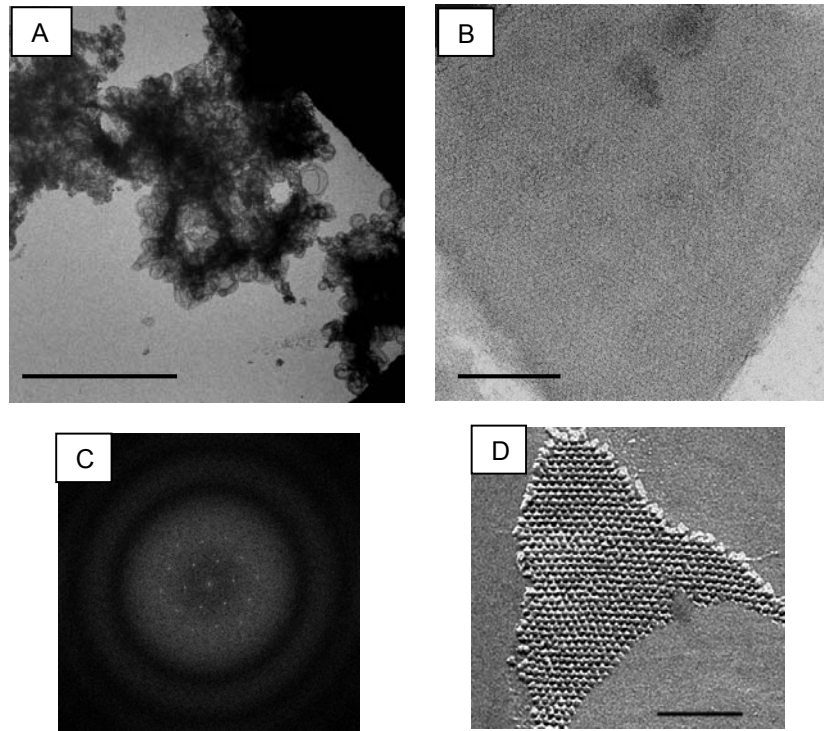


Figure 18 : EM Micrographs of PR 2D crystals. A : Overview of the PR 2D crystalline preparation (bar 1mm). B : Best 2D crystals of PR were obtained in DOPC at pH 10. C : Fourier transformation of (B) shows two orders of diffraction spots. D : Freeze-fracture EM image depicts the 2D crystalline arrangement of PR samples.

The conditions under which these crystals were prepared include following parameters. Protein to lipid ratio (w/w) of 1:0.25, PR eluted in 0.02% Triton X-100, DOPC solubilized in 2% OG, protein concentration of 1 mg/ml, dialysis buffer containing 100 mM NaCl, 10 mM MgCl₂, 7.5% MPD, 5 mM DTT, 3mM NaN₃, 50 mM Tricin buffer with pH adjusted to 10).

Figure 18 A shows the overview of the crystalline proteoliposomes. The size of the crystalline vesicles was in the order of 0.5 μm as seen in figure 18 B and the best diffraction pattern is shown in figure 18 C. The crystalline arrangement of PR becomes especially clear using freeze-fracture electron microscopy (figure 18 D).

Chapter 3-Reconstitution and 2D Electron Microscopy

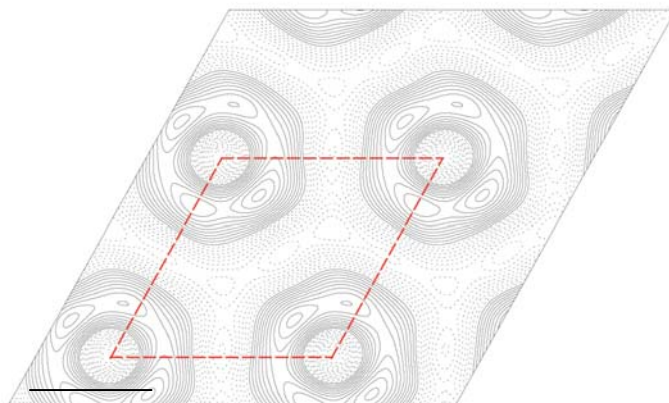


Figure 19 : Projection map in negative stain has been calculated at a resolution of 37 Å. The parts of the protein protruding out of the membrane correspond to high density regions (solid contours) in the map. The unit cell dimensions are 87 Å×87 Å. Two by two unit cells are shown. PR oligomerizes into a donut shaped ring-shaped assembly. The scalebar is ~50 Å and is indicated in black solid line.

A projection map as shown in figure 19 was calculated from a negatively stained sample. Because the negative stain does not penetrate in the membrane, the projection map only depicts parts of the protein sticking out of the membrane. As can be seen in the Fourier transform (figure 18 C), the protein has a hexagonal packing as in the case of BR. However, the resolution of 37 Å does not allow distinguishing between 3-fold or 6-fold symmetry. A comparison with the well resolved structure of BR could indicate a trimeric arrangement [4] but a higher oligomer would be possible as well. The calculated size of the unit cell of 87 Å×87 Å is too large for an individual PR molecule and supports this assumption. The protomers assemble into a ring like structure with an average diameter of 42 Å. The role of electrostatic interactions in guiding the assembly of PR towards 2D and 3D arrays has been recently described by Liang et al [109]. Their conclusions about a hexagonal lattice arrangement are consistent with presented electron microscopy data.

In search of the best crystallization conditions, a systematic variation of parameters was carried out as described in detail in the biochemical analysis. All together over thousand conditions were tested initially with biobeads and then with dialysis and checked for sample homogeneity by density gradient centrifugation and for formation of 2D crystals by electron microscopy. This

Chapter 3-Reconstitution and 2D Electron Microscopy

systematic screen resulted finally in more than 900 successful crystallization conditions with comparable sample quality but low diffraction. This means that the success rate of obtaining at least low diffracting 2D crystals is relatively high. The formation of any ordered protein arrangements within the membrane could be driven by entropy, protein–protein or protein–lipid interactions. In case of PR, the same low-resolution 2D crystals were obtained under a wide range of conditions, which would hint towards dominating protein–protein interactions. It could also indicate, that PR might form protein patches in the native membrane.

One reason for the limited crystal growth is undesired obstruction or discontinuity in the crystalline plane of growth. The formation of small patches of crystals can also be discussed in light of the recent AFM data. For obtaining best projection map, the ideal requirement is well-separated and single sheet of well-ordered 2D crystalline patch. The AFM data as discussed in chapter – 4, indicates the formation of hexamers in majority of the densely reconstituted region and the crystalline patch. With electron microscopy, only the crystalline patches could be observed with the corresponding diffraction pattern and in the absence of diffraction pattern, the rest would be unnoticed.

However, with the aid of AFM small proportion (<10%) of pentamers is also observed since it is possible to select the crystalline patch individually. This means that the sample possess inherent inhomogeneity, which obstructs the growth of crystalline patches. To determine the proportion of 2D crystalline to the non-crystalline region with electron microscopy is very challenging and attempts to separate these two inhomogeneous fractions with sucrose gradient were unsuccessful because the density of both the regions was similar. This hindered the separation of purely crystalline patches and further calculation of projection map for EM analysis.

Another possible explanation for obtaining plenty but small crystalline patches is simultaneous presence of multiple nucleation sites and dislocation of lattice. Various nucleation sites initiated the 2D crystal formation, which grew to small crystalline region from a densely reconstituted region. However, before these small crystalline patches could fuse to yield a larger patch, the continuity was probably broken due to presence of pentamers. With multiple nucleation sites, the crystal has a tendency to grow very fast but is limited to smaller size. Experiments to slow down

Chapter 3-Reconstitution and 2D Electron Microscopy

the crystallization to get bigger patches, using low temperatures and different detergents failed. Under such conditions, the PR molecule has limited growth. The growth of crystalline patches has been reported for BR using special detergents [110]. Similar attempts to grow these small crystalline patches with the aid of specific detergent were also unfruitful.

3.5.3 Conclusions

In conclusion, it is possible to crystallize PR under wide variety of conditions. The poorly diffracting low quality 2D crystals were highly reproducible. The pH of the dialysis buffer and detergent for solubilization of lipid and the protein played a crucial role. The interesting aspect of the 2D crystal of PR was the ability to crystallize under wide range of different conditions and produce similar quality of diffraction pattern. The most likely explanation could be that the protein has the tendency to associate or adhere by itself. Such a case is suggestive of strong protein protein interaction. The high number of PR molecules per cells, relatively bigger unit cell size of the 2D crystals and the donut shaped assembly of the PR molecules as observed with the projection map hint towards the higher oligomeric state of the protein.

3.5.4 Perspective

In case of PR obtaining the 2D crystals was relatively faster than its improvement. At this stage it is not conclusive, whether the inherent inhomogeneity of the crystalline sample or the quality of crystals in itself is the reason for the limited growth and poor diffraction quality of the crystal. The improvement of the crystal would definitely be advantageous for better resolution of the projection map, which will enrich the structural information but at the same time could also prove beneficial for the better correlation with the AFM and the SSNMR data. There are increased chances of all these techniques to prove complimentary to each other to get an improved overview of PR.

Probable ways of improving the crystal in the light of the recent oligomerization information would be to have the homogenous population to begin with. MALDI data on the detergent solubilized protein hinted towards the monomeric state of the protein (data not shown) but the state of art techniques like LILBID and analytical centrifugation could help in knowing the

Chapter 3-Reconstitution and 2D Electron Microscopy

oligomeric state prior to crystallization. This would also indicate the presence of any other impurities if present and might interfere with the crystallization process.

In case of PR, the same low-resolution 2D crystals were obtained under a wide range of conditions, which hints towards dominating protein–protein interactions. It could also indicate, that PR might form protein patches in the native membrane. It would be worthwhile to check for the different growth conditions if they have any impact on the natural assembly of the protein.

Chapter 4 : Functional Characterization of PR 2D crystals

Circular dichroism is a well known spectroscopic technique for determination of folded state of the protein, conformational state of the protein under different conditions and for determination of involvement of protein-protein interaction for the related conformation change of the protein. In this chapter, the focus is on CD spectroscopy measurements, which were carried out for accessing the thermal stability of PR 2D crystals and comparison with detergent solubilized state.

The second part of the chapter deals with Fourier Transform Infra Red Spectroscopy, which has been extensively used to probe into the photocycle of BR, where the characteristic structural changes and photointermediates are determined with the help of typical FTIR bands in the difference spectra. In this section, attempts for the presence of the photocycle and then later for identification of different photointermediates of the PR photocycle have been discussed.

4.1 Stability of PR 2D crystals: CD spectroscopy

4.1.1 Motivation

Reconstitution of the membrane protein in lipids outside the natural environment always questions the correct folding of the protein. In context to this, the purpose of studying the 2D crystals with CD spectroscopy is to determine the difference or compare the differences in the protein folding behavior in detergent solubilized and 2D crystalline form and help in further functional characterization of the protein.

4.1.2 Approach

CD spectroscopy is used routinely for the characterization of the folded state of the protein, its secondary or tertiary structure. It also finds its application to observe the patterns obtained from different members of a family of proteins or groups. Application of CD to study the effect of temperature, pH, reversibility of folding, effect of denaturants, protein protein interactions is also well known.

Circular dichroism is defined as the difference in the absorbance of left circularly polarized light

Chapter 4-Functional characterization of PR 2D crystals

(LCPL) and right circularly polarized light (RCPL).

$$CD = Abs(LCPL) - Abs(RCPL).$$

CD is generally reported in units of absorbance molar ellipticity units (mAU) or ellipticity (mdeg or m°), which are a thousandth of a degree. For any molecule to be “CD active”, a molecule must be structurally asymmetric and exhibit absorbance. In case of protein samples, asymmetry results from chiral molecules such as the peptide backbone of proteins, a non-chiral molecule covalently attached to a chiral molecule (aromatic amino acid side chains), or a non-chiral molecule in an asymmetric environment (e.g., a chromophore bound to a protein). Proteins are CD active (all amino acids except glycine contain a chiral carbon, thus are asymmetrical), and the resulting CD signals are sensitive to protein secondary and tertiary structure. Secondary structure can be determined by CD spectroscopy in the "far-uv" spectral region (190-250 nm). At these wavelengths, the chromophore is the peptide bond, and the signal arises when it is located in a regular, folded environment.

CD signals for pure alpha helix, beta sheet, and random coil structures each give rise to a characteristic shape and magnitude of CD spectrum. For obtaining the information regarding the secondary structure and the stability of the protein with respect to the temperature, the CD spectra were carried out at Institute for Biophysics, in collaboration with Prof. Mantele and measurements were done by Ms. Gabriela Schäfer.

4.1.3 Sample preparation

The CD spectra from 2D crystalline preparation was obtained at a concentration of 1 mg/ml and this liquid sample was used for CD measurements. The CaF₂ cuvettes with 4-5 μ l sample and a path length of \sim 60 μ m were used. For comparison, spectra of the detergent solubilized protein were also measured. The temperature range of 20°C up to 90°C was analyzed for stability and the melting point measurements. The temperature was manually adjusted using the water bath. Data was collected in the range of 185 nm - 260 nm. The typical CD spectrum from the crystalline as well as the detergent solubilized protein is shown below in figure 20 A and B.

The detergent sample shows a typical alpha helix pattern in figure 20 A. Whereas the CD spectra from the crystalline preparations in figure 20 B indicate presence of additional interactions. It was difficult to acquire the data for the crystalline preparations due to light

Chapter 4-Functional characterization of PR 2D crystals

scattering. But the typical α helical dip is observed which changes continuously with the increase in the temperature. At a first glance, it might appear that the extent of minima at around 210 or 209 nm for the crystalline preparation is different but this is because of high sample concentration. The diluted samples from the crystalline preparations showed identical minima as that of detergent solubilized samples. However, it should be noted that no correction for light scattering was made. A good measure to determine the relative α helical content is to fit the CD spectra with the existing values for the helical content from the available database. The majority of the proteins in the available databases are soluble proteins, a very small fraction comprises of the membrane protein and almost none for the membrane protein 2D crystals.

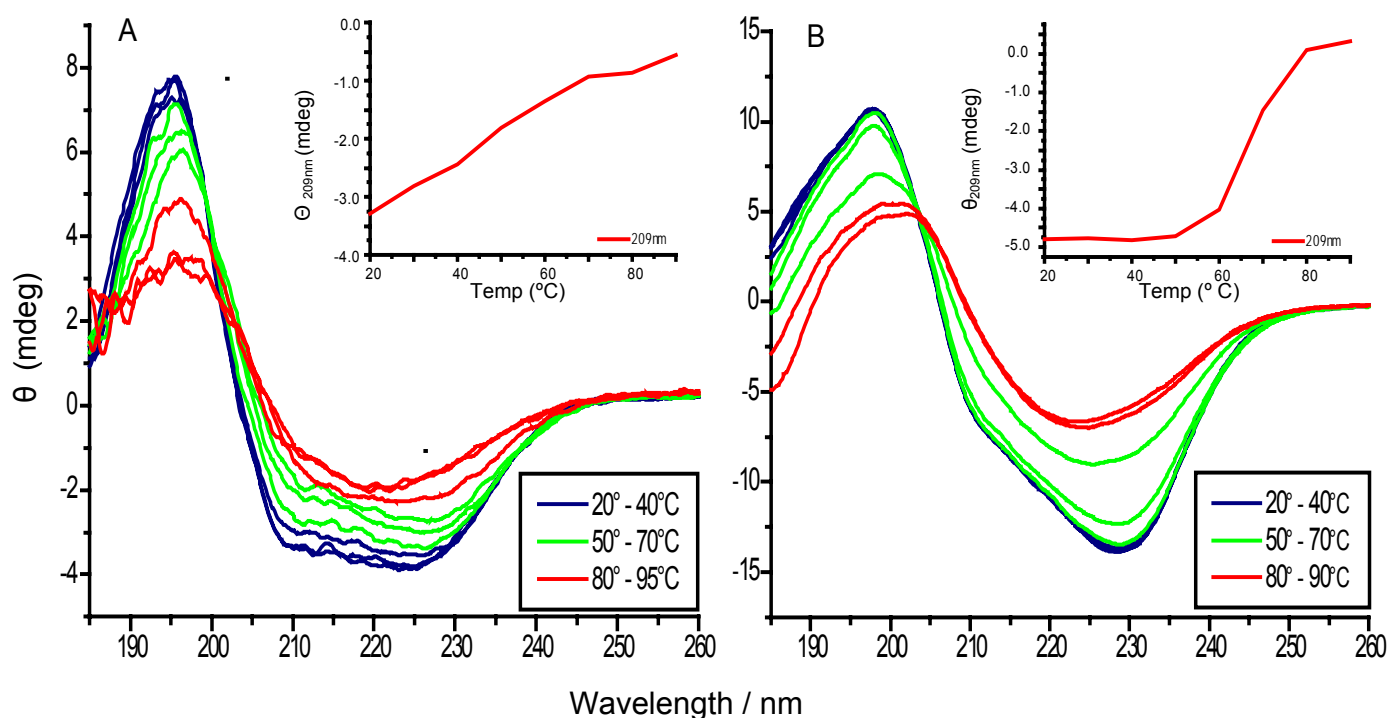


Figure 20 A : Circular Dichroism spectra of detergent solubilized PR at different temperatures showing the typical α -helical pattern, inset: transient absorption at 209 nm. B Circular Dichroism spectra of PR 2D crystals at different temperatures, inset: transient absorption at 209 nm. These spectra were collected at Institute for Physics by Ms.Gabriela Schäfer.

The typical range to obtain a good fit is to have the data points between 175 nm and 230 nm. However, it was observed that the 2D crystals caused light scattering in the lower wavelength

Chapter 4-Functional characterization of PR 2D crystals

region. Hence, it was not possible to obtain the exact value for the α -helical content for the PR 2D crystals.

The transient absorption curve is plotted with values for 209 nm for both the sample preparations. This data clearly shows transition of states with increasing temperature. However, the mode of transition is different. In case of detergent solubilized PR, the slope is gradual but for 2D crystals, it is steeper. Both spectra show two different forms at different temperatures. In case of detergent solubilized protein, there is a gradual degradation of the protein with slight increase in the temperature. This can be attributed to the increasing solubility of the detergent with increasing temperature, which makes the local environment less stable. However, 2D crystals are stable up to 50°C and then cooperatively start to dissimilate. This change of state can be due to the sudden disruption of a more stable local environment for the protein in 2D form.

4.1.5 Conclusion

The CD spectra in the detergent solubilized form and 2D crystalline form suggests similar folding pattern, which resembles the helical pattern as shown in figure 20 Nevertheless, the transient absorption spectra indicate a more stable conformation for the protein in 2D crystals. The crystals are stable upto 50°C and the melting point for the PR 2D crystals can be calculated to be around 70°. This stability information is very important from long term NMR measurements point of view. The stability of protein at these temperature ensures that the protein is in proper conformation state while the NMR measurements are recorded

4.2 Functionality of PR 2D crystals PR: FTIR time resolved spectroscopy.

4.2.1 Motivation

Crystallization of protein in 2D always questions the functional state of the protein in the relatively restricted environment. In this context, the purpose of applying FTIR on the 2D crystals is to determine the functional state of the protein. In case the protein is functional, it should be possible to observe the photocycle with repeated cycles of photo excitation and relaxation. PR is a retinal protein; hence, it is important to identify the different photo states of the photocycle, if the protein enters the photocycle and if there exists any photocycle.

Chapter 4-Functional characterization of PR 2D crystals

4.2.2 Background

Microbial rhodopsin comprises a family of photoactive seven trans membranous helical retinal proteins, which is found in diverse microorganisms [32, 37, 111]. The most well studied member of this family is BR and a homologue of archeal rhodopsin is PR. The cascade of cyclic reactions, which follow the retinal photo isomerization, is known as the “photocycle” and is characterized by presence of distinct and spectroscopically identifiable intermediates and has been discussed in chapter 1. The pH dependent color changes are attributed to the protonation state of the counter ion of the retinal Schiff base. For BR, such changes were linked to the protonation state of Asp85 [112]. The corresponding residue for Asp85 in PR is Asp97, whose protonation state can be followed by pH dependent FTIR difference spectroscopy for identification of the photocycle intermediates. These measurements were carried out at Institute for Biophysics, in collaboration with of Prof. Mantele and measurements were done by Ms. Gabriela Schäfer.

4.2.3 Sample preparation

Prior to the measurement, the dialysis buffer was exchanged to a simple phosphate buffer with the pH 8.5 and concentrated using centrifugation. 5 μ l of this solution was dried with stream of N₂ on a CaF₂ window with a shallow groove. A second window was placed on top and a final sample thickness of 10 μ m was achieved. The consistency of the sample was similar to highly concentrated liquid sample. This window then was placed in a temperature controlled sample holder inside an IFS66v/s FTIR spectrometer. A series of 50 Rapid Scan spectra were collected and averaged to obtain a better signal to noise ratio. The measurements were performed at 4°C mainly to slow down the photocycle to obtain better resolution especially in the fast decaying steps of photocycle (K intermediate step). The interference due to formation of ice crystals can also be avoided while measuring at 4°C.

4.2.4 Results and Discussion

The protonation state of Asp97 in the 2D crystalline state at pH 8.5, (which is above the pK_a of the proton acceptor) was followed by rapid scan infrared difference spectroscopy as shown in figure 21. The time resolution obtained for rapid scan measurements depends on the velocity of

Chapter 4-Functional characterization of PR 2D crystals

the moving mirror and the number of scans averaged per measurement. For these measurements, the fastest time resolution achieved was 76 msec. The largest negative band observed at $\sim 1541\text{ cm}^{-1}$ and positive band at $\sim 1523\text{ cm}^{-1}$ can be assigned to the C=C stretching vibration of the retinal in the alkaline pH [113]. The negative band at 1541 cm^{-1} shows the depopulation of the ground state and the positive band at 1523 cm^{-1} represents an arising K intermediate. The positive band at 1200 cm^{-1} and negative bands at position 1235 cm^{-1} and 1250 cm^{-1} show the 13 *cis* isomerisation of the retinal and arise from C-C stretching vibrations. The bands $\sim 1300\text{ cm}^{-1}$ / 1400 cm^{-1} can be due to the stretching of N-H and C-H. The C=N stretching vibration of Schiff base of PR comes at $\sim 1651\text{ cm}^{-1}$. The positive band at $\sim 1189\text{ cm}^{-1}$ can be assigned to C₁₄-C₁₅ stretch of retinal in K state. Thus, it is after photo excitation, that the 13 *cis* state of retinal is observed. The band pattern in this range is also useful for tracking the right isomerization of the retinal. Basically this band arises from the photoproduct of the 13 *cis* portion of retinal [114] and can be observed in acidic as well as alkaline form of PR [67]. Occurrence of the characteristic peaks in the figure print region of retinal after photo excitation indicate presence of K state in the 2D crystalline form.

Further the C=C stretching of the retinal in the M state is difficult to detect with infrared spectroscopy owing to its small dipole moment. The presence of M state for PR is marked by appearance of positive band in the range of 1700 cm^{-1} in the reconstituted sample. This is observed at 1755 cm^{-1} and is assigned to the C=O stretching vibration from Asp97. In case of the 2D crystalline samples, the similar band at 1755 cm^{-1} is observed and is attributed to the protonation of Asp97 [67].

After the successful assignment of the retinal band further following the retinal C=C band at 1540 cm^{-1} , it can be observed, that the protein exhibits the M intermediate as observed by transient absorption spectroscopy. The major peaks identified are listed in the following table.

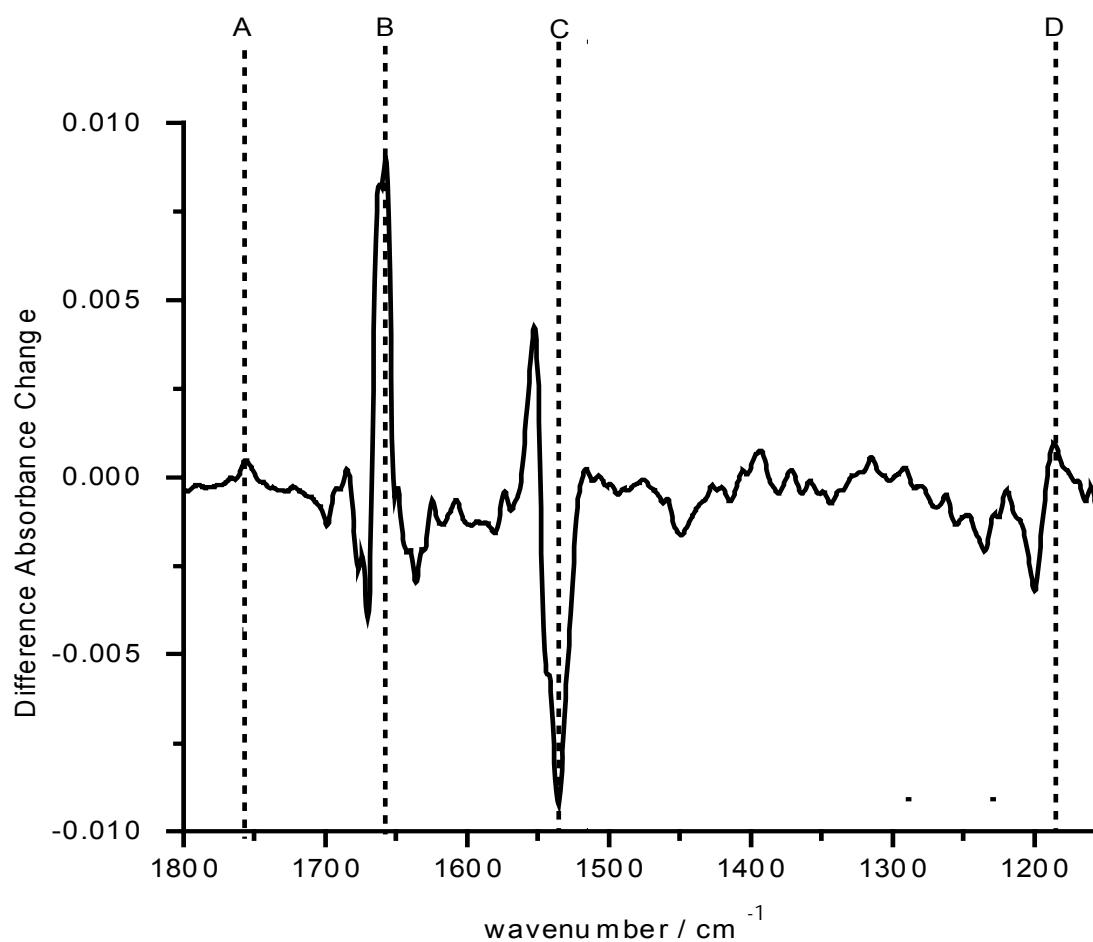


Figure 21 : Infrared light and dark difference spectra of PR2D crystals after 75 msec of excitation at pH 8.5. The spectra show vibration bands in the Aspartate region photo excitation at 532 nm BigSky Ultra Nd:YAG laser. The bands around 1200 cm⁻¹ indicate that the 13 *cis* isomerization of the retinal has occurred and a positive band at 1755 cm⁻¹ shows the presence of M state. The bands around 1200 cm⁻¹ indicate that the 13 *cis* isomerization of the retinal has occurred and a disappearing band at 1523 cm⁻¹ shows the decline of the K state. This spectrum was acquired by Ms. Gabriela Schaefer at Institute of Physics, Frankfurt.

The measurements indicate the retinal band at 1540 cm⁻¹ undergoes photo kinetics upon excitation and relaxes to the initial normal base line. It should be noted that that the negative band at 1540 cm⁻¹ is the ground state depopulation and the ground state is therefore repopulated as shown in figure 22. Comparable spectra could be obtained after repeated photo excitation and relaxation, which indicate that the photocycle is iterative and is not hindered. This is an indication of active protein state in the 2D crystalline form

Chapter 4-Functional characterization of PR 2D crystals

Table 7: List of identified FTIR band position for PR 2D crystals

label	Band position (positive)	Band position (negative)	Indication
	~1523	~1541	C=C stretching vibration of retinal at alkaline pH
C		~1541	Depopulation of ground state
	~1523		Arising K state
	~1200	~1235/~1250	C-C stretching vibration indicating 13-cis isomerization
B	~1651		C=N stretching vibration of Schiff base
D	~1189		C ₁₄ -C ₁₅ stretch of retinal in K state
A	~1755		C=O stretching vibration of Aspartate 97

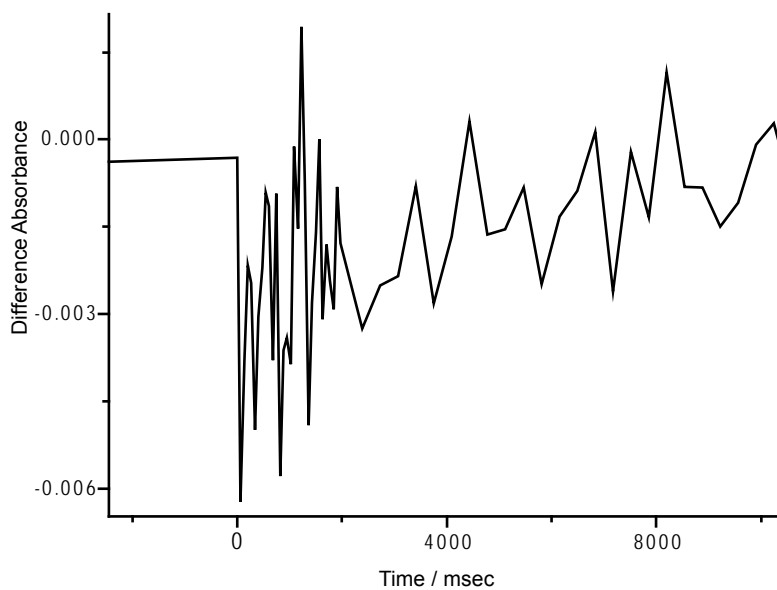


Figure 22 : Transient absorption of the ground state depopulation at 1541cm^{-1} and its re population after the photocycle. This spectrum was acquired by Ms. Gabriela Schaefer at Institute of Physics, Frankfurt.

4.2.5 Conclusions

Chapter 4-Functional characterization of PR 2D crystals

Based on the preliminary FTIR measurements, it is obvious that the PR in 2D crystalline form does enter the photocycle and K and M intermediates could be identified. The identification of the N and O intermediate is difficult, due to an ongoing discussion about the band positions and shape of a true N or O spectra. Furthermore, the low time resolution of the rapid scan technique leads to the observation of mixed states, which cannot easily be decomposed into the true spectra. Since the difference bands of the photoproduct disappear over time, and the baseline is recovered, the protein crystals undergo photocycle. This concludes that the 2D crystalline packing does not affect the functionality of the PR but as expected slight changes in the time constants of the photocycle are visible due to the rigid environment in the 2D crystals.

The activity of PR in vivo has been as shown before by monitoring single cells of *E. coli* and their observed response to light due to the proton motive force (pmf) that bacteria use as the energy source to power the rotary flagellar motor which enables them to swim [83]. Suspensions of *E. coli* membranes containing PR were also observed with laser flash-induced absorbance changes to determine the activity of the protein. Light-mediated proton translocation was determined by measuring pH changes in a cell suspension exposed to light, where the net outward transport of protons was observed only in PR containing *E. coli* cells and only in the presence of retinal and light [37]. Time resolved FTIR spectroscopy has been used to study the photo intermediates of PR which are involved in fast transient proton release in reconstituted state [115]. The light induced proton currents in the PR reconstituted samples were also measured in a compound membrane system where proteoliposomes were adsorbed to planar lipid bilayers [67].

Considering the sparse amount of lipids in the 2D crystalline preparations, it was difficult to adsorb the proteoliposomes to the planar lipid bilayers and hence the spectroscopic analysis for identification of intermediates was opted to show the functionality of the protein.

4.3 Functionality of PR 2D crystals PR : SSNMR

An indirect evidence of active functionality was also judged by measuring the chemical shift values for the ^{15}N - ζ -labeled lysine samples. It was observed that the chemical shift values for such labeled lysine had similar chemical shift values as for the fully functional reconstituted

Chapter 4-Functional characterization of PR 2D crystals

sample. This suggested that the local chemical environment of the Schiff base lysine for both sample preparations is similar and may have similar active functionality.

The details of these experiments are described in Chapter 6.

Chapter 5 : Assembly of PR: An AFM study

5.1 Scope

AFM has emerged as a powerful tool for biologists in terms of providing the ability to study biological samples in their native environment and has the capability to illustrate the topographical features at sub molecular level [116, 117]. It shows a unique way for characterization of structure function relationship of the native membrane proteins. AFM provides sub nanometer resolution of the substructures as well as associated conformational changes, oligomerization state, dynamics and assembly.

SMFS (single molecule force spectroscopy) permits detection of inter as well as intra molecular interactions. This method is able to unearth the interactions which are primarily involved in the stabilization of secondary structure [118]. It represents a multifunctional tool that finds its application in the oligomeric state and conformational change determination for better understanding of structural and functional characteristics of the protein. The unique technique helps simultaneous monitoring of the varied parameters, which aid in the determination of flexibility or rigidity of the protein. It can be used to determine the folding and the unfolding pathways of the membrane proteins and finds its application in studying the association patterns of membrane proteins, which lead to higher oligomerization states. Time dependent SMFS can also probe into the kinetics of these processes [119, 120].

This work was done in collaboration with Prof. Daniel Mueller and Adriana L. Klyszejko from Biotechnology Center, University of Technology, Dresden, Germany. The results of this study have been published in Journal of Molecular Biology (2008) 376, 35–41.

5.2 Approach

Different kind of information can be obtained with AFM technique depending upon the mode of operation:

Contact mode: This mode is especially used to study membrane proteins where the probing tip is gently touched at the surface of the protein with a constant force while scanning. These probing tips are known as cantilevers with very small force constants (~0.1 N/m).

Chapter 5-Assembly of PR : An AFM study

Tapping and oscillating mode: Usually this mode is used to record the topography of a weakly immobilized specimen and where the tip undergoes a vertical oscillation.

For the purpose of high-resolution structural data collection, AFM is the mode of choice in contact mode. The effective forces contributing to the deformation of the specimen may be overall sum of force applied to the stylus, the electrostatic repulsion and Van der Waal attraction between the two surfaces. This feature has been extensively discussed in aqueous environment [121]. However higher forces may prove to be of an additional benefit of studying the hidden feature in a protein as in case of AB loop in BR [122]. These weak Van der Waals and electrostatic forces can be minimized by optimizing the pH and ionic concentration of the buffer. The force distance curves between the tip and the sample under different buffer conditions determine the best imaging conditions. While recording the AFM data the vibrations in the microscope should be considerably minimized. To increase the chances of adsorption for the crystalline patches significantly, various buffer related parameters need to be optimized. E.g incubation time between the application of the sample and the washing step, concentration of ions in the buffer etc.

5.3 Advantages for membrane proteins

Like all techniques, AFM too has its own advantages and disadvantages. The benefit of working with AFM is very high signal to noise ratio which enables every single protein to be observed [123]. It does not require any specific labeling but analyzes the samples under normal buffer conditions. This applies not only to the field of polymers and inorganic crystals but has profound application in the field of biology and the specimens are widely diverse. These range from fibers, DNA, cells, viruses and bacteria. The information obtained in terms of lateral and vertical resolution with high signal to noise of the topographs make significant contribution to understanding of the single biomolecules. The AFM probe interacts directly with the protein surface and measures the electrostatic potential, detects current (pA) and this contribution in any case cannot be overlooked when trying to acquire high-resolution structural information from membrane proteins in their native environment. This technique can be applied on reconstituted as well as 2D crystalline samples. The biggest advantage with 2D crystal is of flat surface of the crystalline patches, which provide an excellent specimen quality for the AFM measurements. But to avoid any structural damage to the biological sample, utmost care should taken to reduce the

applied friction forces between tip and the sample.

5.4 Motivation

The structure and function relationship of BR and its homologs, the light-driven chloride pump halorhodopsin [124] and sensory rhodopsin [125], have been studied at molecular resolution. However, for PR the structural information is limited. Like the other members of this family, by virtue of being a membrane protein, PR is expected to possess additional stability due to the inter as well as intra molecular interactions [126].

PR is relatively new and the structural aspects need to be explored. The electron microscopy data reveals a donut shaped assembly of PR molecules and a bigger unit cell size. The bigger unit cell size of PR, which is $87\text{\AA} \times 87\text{\AA}$, when compared to BR unit cell size of $64\text{\AA} \times 64\text{\AA}$, suggests an oligomeric state of the protein. However, the poor resolution of the 2D crystals limited further detailed information especially about the oligomeric state by electron microscopy. Hence, in order to probe into the oligomeric state of the protein single image AFM analysis was attempted. In contrast to this, detailed information is available for other retinal proteins e.g rhodospin and in particular BR under optimum conditions for the assembly, conformation changes, oligomerization and dynamic aspects of these proteins [127-129]. This becomes relevant when observing the 2D crystals of our protein, which is in crystalline arrangement and may exhibit similar behavior of oligomerization, stability and (un) folding pattern. The major aim of this study was to observe if the protein exhibits similar structural oligomerization patterns as other retinal proteins such as BR or are there striking differences ?

5.5 High-resolution AFM imaging

Reconstituted proteorhodopsin membranes were adsorbed onto freshly cleaved mica in buffer solution (300 mM KCl, 10 mM MgCl_2 , 20 mM Tris-HCl, pH 8.0). After this, the sample was washed with imaging buffer (150 mM KCl, 10 mM MgCl_2 , 20 mM Tris-HCl, pH 8.5) to remove weakly attached membranes. The AFM used was a Nanoscope III (Digital Instruments, Santa Barbara, California) equipped with a J-scanner ($\approx 100 \mu\text{m}$) and oxide sharpened Si_3N_4 stylus on a cantilever with a nominal spring constant of $\approx 0.1 \text{ N/m}$ (OMCLTR-400-PS, Olympus, Tokyo,

Chapter 5-Assembly of PR : An AFM study

Japan). Contact mode AFM imaging performed by electrostatically dampening the forces applied locally between the AFM stylus and protein membrane to ≈ 50 pN [130]. Such low forces prevented possible deformations of the protein by the scanning AFM stylus [131]. Topographs recorded in trace and retrace scanning directions showed no significant differences confirming that the scanning process of the AFM did not disturb the protein surface. All measurements were carried out at room temperature.

5.6 Single-molecule force spectroscopy

The motivation for single molecule force spectroscopy was to determine the (un)folding pattern of the PR helices from the crystalline arrangement. This is typically performed with the aid of force distance spectra (F-D curve). To calculate the F-D spectra, a single protein is tethered between the tip of the micromachined AFM cantilever and a supporting surface. The tip-surface separation is then continuously increased using a piezoelectric actuator while the forces applied to the molecule by the cantilever are detected with an accuracy of a few pN. The continuous extension of an individual protein molecule results in subsequent unfolding of the protein domains. Plotting force against tip-surface separation produces a characteristic force-distance (F-D) curve from which the unfolding force as well as the unfolding pathway of a single protein domain is derived [132, 133].

To mechanically unfold individual PR using SMFS, the protein membrane was first imaged by AFM. Then the AFM stylus was brought into contact with the membrane protein surface. Applying a constant force of ≈ 1 - 1.5 nN for ≈ 1 s ensured that one terminal end of the protein attached to the stylus via nonspecific interactions [130, 134, 135]. Separation of stylus and membrane stretched this molecular bridge and exerted a force at the protein leading to its unfolding. The F-D spectra recorded during the unfolding process showed characteristic patterns similar to those previously assigned to the unfolding of one BR molecule [128, 130] or to the unfolding of one halorhodopsin molecule [134] by pulling from the C-terminal end. The first 20 nm of the F-D traces exhibited higher noise compared to the remaining trace due to non-specific AFM stylus-sample interactions [128, 130]. Thus, force peaks lying within this region are masked by noise and show higher deviations compared to the peaks detected at separations

Chapter 5-Assembly of PR : An AFM study

above 20 nm. SMFS was conducted in buffer solution (150 mM KCl, 20 mM Tris-HCl, pH7.8) at a pulling velocity of 87 nm/s.

5.7 Results and Discussion

Although the given resolution was not sufficient to differentiate between the cytoplasmic and extracellular sides of the PR in the 2D crystals, but AFM imaging of reconstituted PR membranes in buffer solution showed two different packing regions. One was crystalline (*) and the other densely packed (**) region as shown in figure 23. At high-resolution the surface of the 2D PR crystals revealed donut-like structures arranged in a hexagonal lattice of 8.8 ± 0.7 nm (ave \pm SD; $n=30$) side length. These donut-like structures exhibited protrusions extending 0.9 ± 0.3 nm ($n=50$) above the lipid surface. In contrast to BR, the total area covered by the unit cell of the hexagonal proteorhodopsin lattice corresponds is 33.53 nm² which is twice that of BR. This indicated higher chance of adjusting six PR molecules in a unit cell.

5.7.1 Comparison of PR AFM data with BR

For BR, AFM studies under optimum conditions the diameter of the crystalline patches varied between 0.5-0.15 μ m. In the extracellular side, a typical feature of protrusions extending up to 0.5 nm was observed for which the major contribution is the β sheet between the trans-membrane domain B and C. On the cytoplasmic side, the flexible EF loop provided the force dependent conformational changes. These EF loops were observed as sharp protrusions of ~ 0.8 nm in height with 100 pN force applied on the AFM stylus. However, when the force applied increased 3 times, this feature becomes less conspicuous. The AB loops become more visible with an applied force of 300 pN and reveal to have a height of ~ 0.6 nm. The hexagonal lattice of BR trimers in native purple membrane patches shows a side length of ≈ 6.2 nm [4] with single BR molecule protruding between ≈ 0.5 and 0.8 nm from the lipid bilayer [131]. The area covered by the hexagonal unit cell of the purple membrane lattice is 16.64 nm² which accommodated three BR molecules [57]. These results are further discussed under different sub headings.

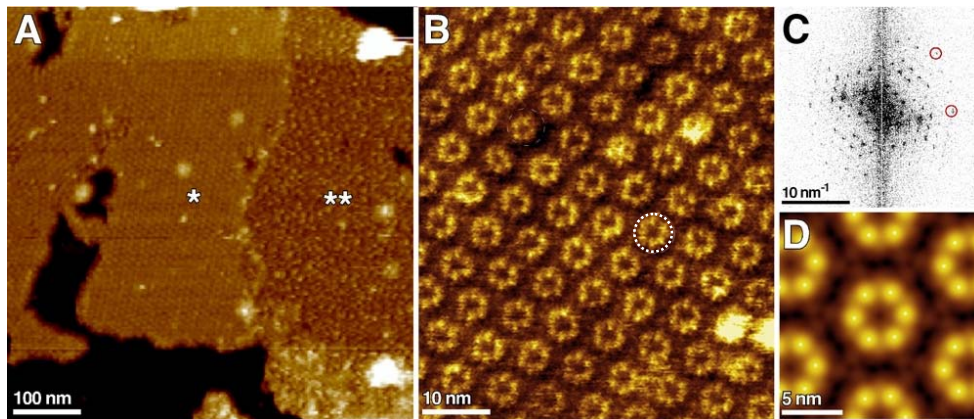


Figure 23 : AFM of 2D crystals and densely packed PR membranes. A, Survey showing crystalline (*) and densely packed (**) patches of PR embedded in the lipid (DOPC) bilayer. The lipid bilayer protruded 4.5 ± 0.5 nm ($n=10$) from the support, the crystals 7.1 ± 0.5 nm ($n=10$) and the densely packed proteorhodopsins 6.3 ± 0.5 nm ($n=10$). B, High-resolution topography showing the hexagonal lattice ($a = 8.8 \pm 0.7$ nm) of donut shaped oligomers formed by PR. C, Calculated diffraction pattern of (B) documents spots (red circles) suggesting a lateral resolution of ≈ 1.5 nm. D, Correlation average of (B). The symmetrized average showed a 9% deviation from six-fold symmetry. AFM topographs recorded in buffer solution exhibit a full gray level corresponding to vertical scale of 20 nm (A) and 2 nm (B and D).

This data was collected by Adriana L. Klyszejko in Prof. Daniel Mueller lab at biotechnology Center, University of Technology, Dresden, Germany and figure is taken from [136].

Note: When compared with the electron microscopy data, the size of the unit cell correlates very well. However, with electron microscopy the distinction between the crystalline part and the non-crystalline part was not achieved. The probable reason is that only the crystalline areas would provide the diffraction pattern and in the absence of diffraction pattern from the non-crystalline part, this region would be unnoticed.

5.7.2 Oligomerization

Approximate calculation suggests ≈ 24.000 PR molecules per SAR86 cell [59]. When in a densely packed crystalline lattice, as in case of BR, this would refer to a circular flat circular patch of 600 nm in diameter occupying a major portion of a cell surface. This implies that with half packing density of PR the area covered would be twice the area of the cell membrane. Hence, the larger unit size of the PR donuts pose a question on the oligomeric state of the protein. In this case may point towards trimers, tetramers, pentamers or hexamers.

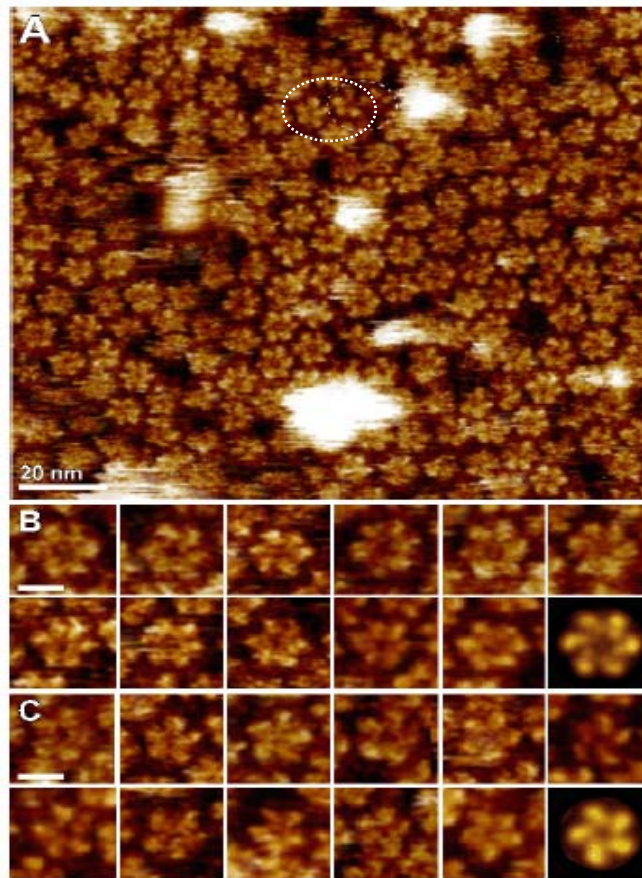


Figure 24: High-resolution AFM of densely packed proteorhodopsin oligomers. A, PR molecules could assemble into different oligomeric forms. Galleries show individual hexameric (B) and pentameric (C) proteorhodopsin oligomers. The last oligomers shown with black background represent correlation averages. Scale bars in (B) and (C) correspond to 5 nm. AFM topographs recorded in buffer solution exhibit a full gray level corresponding to vertical scale of 2 nm.

The data was collected at Technische Universität Dresden, Center of Biotechnology in collaboration with Dr. Daniel Müller by Adriana L. Klyszejko and figure is taken from [136].

5.7.3 Assembly

The oligomeric dimensions of BR trimers and PR in 2D crystalline form exhibited a hexagonal lattice. The superimposition of BR molecules indicated a tangential assembly. However, for hexameric PR in the crystalline state, the PR molecules did not have sufficient space to accommodate in the tangential manner. The unique way to place these 6 PR molecules in the

Chapter 5-Assembly of PR : An AFM study

lattice is to arrange them in a radially symmetric fashion. Averaging of several topographs indicated that all the molecules in the lattice were equal with respect to each other. It means that it is cooperative process, either all of them pointing towards inside or outside. However, the resolution was insufficient to determine the direction of the arrangement.

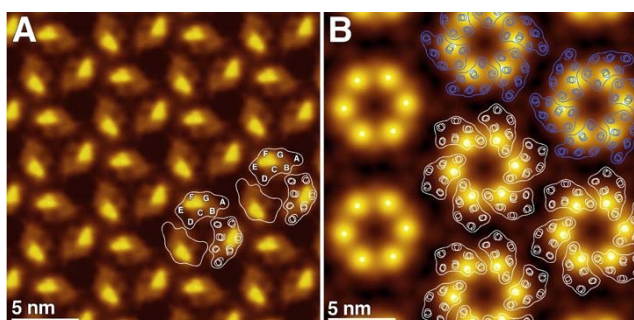


Figure 25 : Correlation averaged AFM topographs showing the hexagonal assembly of BR trimers of native purple membrane (A) and of reconstituted proteorhodopsin hexamers (B). A, Cytoplasmic purple membrane surface: The highest protrusion of each bacteriorhodopsin molecule corresponds to the polypeptide loop connecting transmembrane α -helices E and F[131]. The outlined BR shapes were adapted from sections close to the cytoplasmic surface of BR trimers obtained from electron crystallographic analyses[4]. B, Crystallized proteorhodopsin hexamers: Assuming each of the six protrusions to represent one proteorhodopsin molecule, the proton pumps must be assembled radially to fit into the oligomer. Outlines in white and blue show two of many possible orientations of the PR molecules. Averaged topographs exhibit a full gray level corresponding to vertical scale of 2 nm.

This data was collected by Adriana L. Klyszejko in Prof. Daniel Mueller lab at biotechnology Center, University of Technology, Dresden, Germany and figure is taken from [136].

5.7.4 (Un)folding pattern with SMFS and F-D spectra

The proper folding of the membrane protein is important for the protein to be functionally active. This is governed by intermolecular interactions which are responsible for appropriate folding and are decisive in the functional and structural properties of the membrane protein [137]. The mechanical unfolding of the membrane protein was conventionally approached by varying the physical parameters of temperature or chemical parameters like detergents [138, 139]. The stability of the protein may depend on either monomeric interaction or oligomeric interaction or on both. This constitutes an important area for further investigation and is subject to study.

Chapter 5-Assembly of PR : An AFM study

BR in purple membrane and PR in 2D crystalline form represent a relatively stable conformation in the membrane. However the stability of any membrane protein is determined by overall interaction of the protein with the lipid bilayer as well as the inter and intra molecular interactions [126]. The nature of molecular interactions, which are responsible for providing the stability to the structural components within a protein can be measured by force spectra. The force spectra are a plot of the applied force and the distance and are correlated to the extraction of individual protein from the membrane. Each curve requires a detailed analysis for measuring the probability of unfolding for an individual structural element and the amount of unfolding force. The individual peaks of the single force extension curves is generally fit with worm like chain model. The force spectrum may be correlated to the actual unfolding of individual residues in a membrane protein. F-D spectra contain information about the unfolding process and the last peak shows the completion of the extraction procedure.

The forces that stabilize or destabilize the stable conformation include those, which are involved in positioning the membrane protein and interactions, which stabilize the secondary structure. However, it is known that the intra molecular forces have higher contribution as compared to the intermolecular forces to maintain the functional and structural integrity of membrane protein

5.7.4.1 Comparison of PR unfolding pattern with BR

For PR, application of moderate force ($\sim 1\text{nN}$) for 1sec for calculation of the force distance curves indicated unfolding pattern was similar. Considering the number of amino acids that comprise the PR sequence, the stretched polypeptide chain lengths of 88, 148 and 219 matches with the pair wise unfolding of the helices. This strongly indicates a similar secondary structure with transmembranous region.

In case of BR it was concluded that length and position of polypeptide chains responsible for unfolding pattern within the BR molecule remain unaffected irrespective of the oligomeric state of the protein. However, the mechanical stability and strength of the molecular interactions of structural segments were dependent on BR assembly. The mechanical stability of the unfolding pattern of the paired helices E (5th) and D (4th) was maximum and minimum for monomeric arrangement. Amongst the members of the retinal family, the probability of transmembranous

Chapter 5-Assembly of PR : An AFM study

helix to unfold in a paired manner was found to be highest for BR [127]. The unfolding in a paired fashion has been reported earlier [128, 132, 134, 140].

The unfolding pattern of BR, as studied by force distance spectra in SMFS suggests that the unfolding is very characteristic [128]. The helices G (7th) and F(6th) along with E (5th) and D (4th) always unfold pair wise and helices B (2nd) and C (3rd) occasionally fold in sequential manner. An average of several different unfolding spectra indicated 4 pronounced peaks in descending order [132]. Previous studies on BR and halorhodopsin indicated a sequential mode of unfolding of the transmembranous helices of the loops [128, 134, 135].

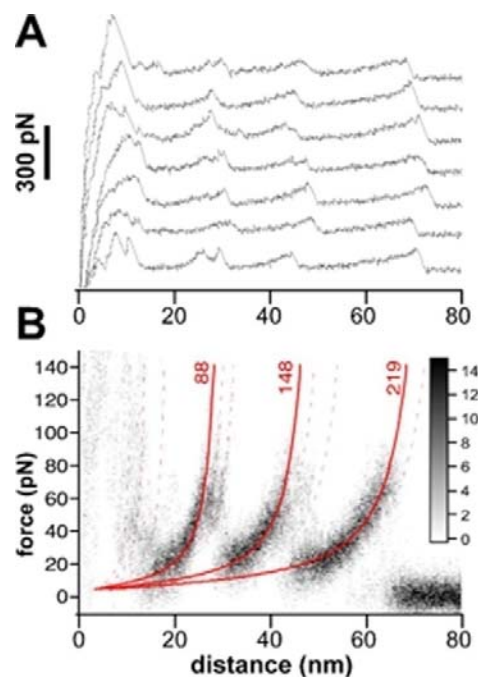


Figure 26 : Unfolding pattern of single PR embedded within membranes. A, Individual F-D curves each one recorded upon unfolding a single proteorhodopsin molecule by SMFS Force -Distance curve exhibit a maximum length of ≈ 70 nm. B, Superimposition of 30 F-D spectra enhances common patterns. Red curves are fits using the worm-like-chain (WLC) model. The three main peaks detected at pulling distances correspond to stretched polypeptide lengths of 88, 148 and 219 amino acids. These distances denote that the unfolding intermediates of PR structure match exactly with those measured for BR.

The data was collected at Technische Universität Dresden, Center of Biotechnology in collaboration with Dr. Daniel Muller by Adriana L. Klyszejnko and figure is an taken from [136].

5.8 Comparison of BR and PR from Electron Microscopy

Under native conditions BR assembles into trimers which are in turn arranged into 2D hexagonal lattice [141]. Recrystallization of BR in presence of detergent yield 2D crystals with $p22_12_1$ symmetry and show dimeric arrangement and an orthorhombic lattice[142]. BR forms highly ordered 2D crystals naturally in the native membrane of *H. salinarium*. BR has trigonal lattice ($a=b=6.2$ nm, $\gamma=60^\circ$) [141]. The retinal lies in the intra membranous cavity formed by 7 trans membranous helices generally denoted by A to G. The main portion that protrude out of the membrane are the loops connecting the trans-membranous A and B as well as E and F on the cytoplasmic side and between B and C inter helical loop on the extracellular side. The latter forms a twisted anti parallel β sheet and is more stable than the flexible EF loop [143].

In case of PR, comparison with the well resolved structure of BR, could indicate a trimeric arrangement [4] and suggest the bigger size of the unit cell. This indicates a possibility of a higher oligomer. The protein has a hexagonal packing as in the case of BR. However, the resolution of 37 \AA does not allow distinguishing between 3-fold or 6-fold symmetry. The calculated size of the unit cell of $87 \text{ \AA} \times 87 \text{ \AA}$ is too large for an individual PR molecule and supports this assumption. The protomers assemble into a ring like structure with an average diameter of 42 \AA . The formation of any ordered protein arrangements within the membrane is driven by entropy, protein-protein or protein-lipid interactions. In case of PR, the same low-resolution 2D crystals were obtained under a wide range of conditions, which would hint towards dominating protein-protein interactions. It could also indicate, that PR might form protein patches in the native membrane.

5.9 Conclusion

This study provides important conclusions about the oligomeric state and the unfolding pattern of PR in the crystalline arrangement. The major conclusions from this study are listed as below.

- The sample is actually a mixture of small 2D crystalline patches as well as non crystalline but densely packed areas.
- The protein in the 2D crystalline area exhibits hexameric oligomeric state.
- The non crystalline but densely packed regions of protein are also hexamers, a small

Chapter 5-Assembly of PR : An AFM study

roportion shows presence of pentameric oligomeric state.

- The observed unfolding pattern was similar to the other members of the rhodopsin family.

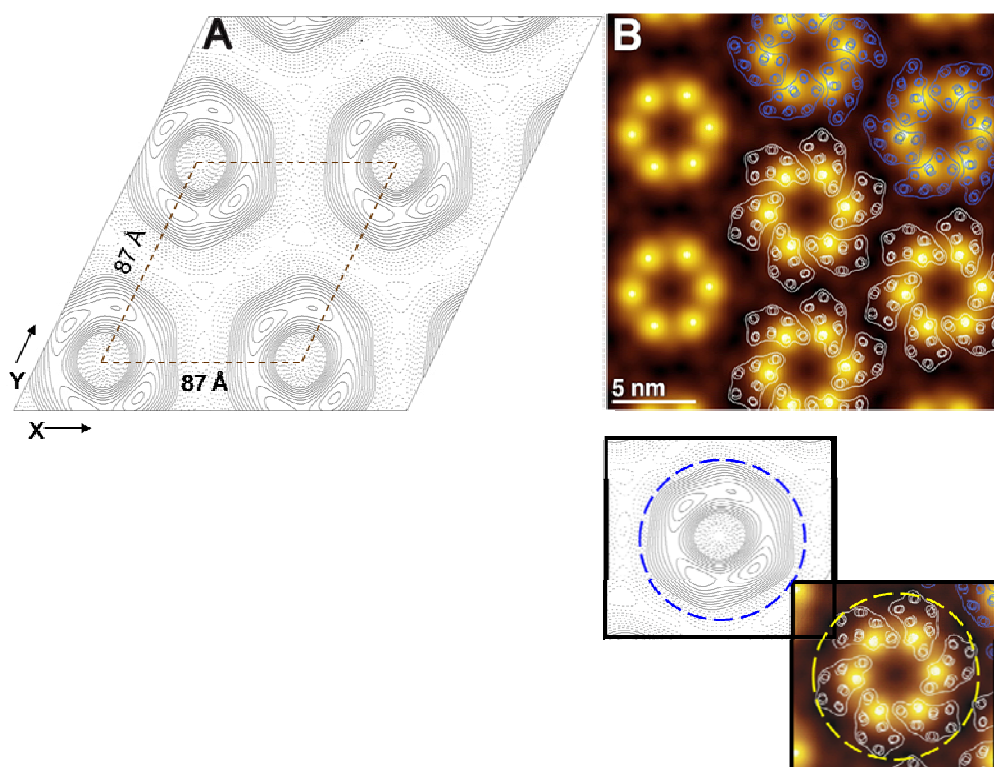


Figure 27 : Comparison of Projection map of PR 2D crystals with AFM micrographs. A: Projection map with one unit cell displayed in red dotted lines. B: AFM topographs showing hexameric oligomeric state in PR 2D crystals. Inset showing a monomers as observed with Electron Microscopy and AFM topographs.

The AFM topographs indicate that the PR exists mainly as hexamers in reconstituted as well as in 2D crystalline state. However, a small proportion of pentamers is also observed. Unlike AFM which can select and observe individual molecules and gives a diffraction pattern, electron microscopy needs larger and more ordered crystalline area for detailed structural information. Presence of different oligomeric states also suggests existence of an inherent inhomogeneity in the reconstituted sample, which might have implications in the analysis of electron microscopy and SSNMR data that involve sample averaging.

Chapter 5-Assembly of PR : An AFM study

The hint for the coexistence of the higher oligomer state was an outcome of the electron microscopy data where the unit cell size was relatively large for a monomer. Other in house biochemical techniques used for characterization such as gel filtration and SDS PAGE were suggestive of only monomeric state. The oligomerization of PR but in the form of trimers is suggested by SDS-PAGE and the broad peaks generated from size exclusion chromatography [144].

5.10 Functional implication

Stable structural segments of BR monomeric suggest appreciable contribution from the intra molecular interactions. However, oligomerization can also contribute significantly to the stabilization. In context to PR which is spectrally tuned to different wavelengths and has potential of generating energy from the solar energy, the relatively high number of PR molecules and slower photocycle suggest a dense packing. Obtaining the 2D crystals under wide range of conditions with varying parameters indicate dominant protein-protein interactions, which indirectly hint towards favorable oligomerization. Similar indication is also provided by presence of huge number of PR molecules present per bacterial cell. This dense packing suggests that the oligomerization process might be favored in nature.

The AFM topographs further show a uniform arrangement of individual PR molecules in the hexamers as well as in pentamers. However, with the available information about PR, it is still unclear whether PR portrays a cooperative phenomenon of photo excitation for the individual molecules in the oligomeric state or it is specific for an individual.

Various spectroscopic studies have been carried out to gain insight into the functional aspect of PR. Most of these studies were performed in the detergent solubilized state where the protein exists as monomer and have shown the active functionality of the protein. If in the detergent solubilized state, the protein is functional it means that the monomeric form of the protein is active. However, the effect of oligomerization on the degree of activity and for what reason the hexamers be useful, is still unknown.

Chapter 6 : Solid State NMR characterization of PR 2D crystals

6.1 Motivation

The SSNMR studies on PR were motivated with the idea of solving the 3D structure by SSNMR. The similarities between BR and PR, and the fact that BR is arranged in 2D arrays within the *Halobacterium salinarium* membrane [93] provided additional support to the motivation. However, information about the PR protobacterial membranes is scarce. After obtaining the suitable 2D crystallization conditions, it was hypothesized that the 2D crystals would provide well-resolved NMR spectra for the structural and detailed mechanistic studies by SSNMR. From earlier work, it is known that the natural 2D crystals of BR did yield very well resolved spectra [95]. Major benefits of applying SSNMR on PR 2D crystals are high sample concentration and homogeneity, which have been used to study various aspects of BR e. g. surface dynamics of BR [145], interactions between the various tryptophans [146], retinal-Schiff base photo isomerization [147], studying the dynamics [148] to cite a few. Furthermore, crystal packing would reduce internal molecular motions, which might interfere with coherent averaging by magic angle sample spinning. Considering the above stated facts the SSNMR was applied on PR 2D crystals for investigation of structural information, preliminary assignments and dynamics of PR in crystalline arrangement. The entire SSNMR data shall be discussed from application perspective for these crystals under the following broad titles:

1. Investigation of lipids in the 2D crystalline samples with ^{31}P measurements from the lipid head groups.
2. Selective ^{15}N isotopic labeling
 - Lysines : Schiff Base chemical shift
 - Methionines : Resolution and dynamics with HETCOR and LG-CP
 - Tryptophans : Assignment with REDOR
3. Selective ^{13}C isotopic labeling
 - Cysteines
 - Histidines
4. Uniform ^{13}C labeling schemes
 - 2- ^{13}C Glycerol labeling

Chapter 6-Solid State NMR characterization of PR 2D crystals

- ^{13}C Selective unlabeled
- U- ^{13}C labeling

6.2 Background

SSNMR has provided atomic-level structural constraints for biomolecules like peptides and proteins which pose challenges for other biophysical techniques based on insolubility, molecular weight, non crystallinity, or other biological characteristics [149]. It has emerged as a powerful tool for resolving structural information of large molecular complexes with the aid of specific methods such as specific labeling schemes. The complexity of the spectra increases with the increasing molecular weight but the technological advancements such as well-designed pulses sequences and multidimensional measurements coupled with higher field strengths aid in either reducing the spectral overlap or increasing the spectral resolution. Recently the structure of nano crystalline protein was determined up to atomic resolution [150]. However, this needs to be combined with optimal sample preparation especially for membrane proteins as was demonstrated for SH3 domain [151, 152].

The NMR spectrum in both solid and solution state result from observed interactions between the nuclear spins in presence of an external magnetic field. The spectral resolution of solution state NMR spectrum is solely based on the averaging of the anisotropic interactions due to the fast tumbling of the molecules. However, this restricts the application of solution state NMR with respect to the molecular weight of the molecules for study. SSNMR on the other hand is not limited with restriction on the molecular weight but widely applicable to such molecules or complexes of biological origin. SSNMR utilizes anisotropic nuclear spin interactions for understanding of structural and functional aspects. Interactions such as chemical shift anisotropy, quadrupolar coupling and dipole dipole coupling are exploited for quantitative information on molecular structure, dynamics and conformation in space. This technique can be applied for structural measurements such as determination of bond length and bond angles without the need of crystal on amorphous and heterogenous biological samples. The additional advantage conferred by SSNMR is the flexibility to study the molecular dynamics of the protein.

6.3 Basic SSNMR Methods

6.3.1 Magic angle spinning (MAS)

Majority of the experiments adopt the MAS in order to remove effects of chemical shift anisotropy and to aid suppression of dipolar coupling effects. It is known that the average of molecular orientation dependence of the nuclear spin interaction is given by a factor of $(3 \cos^2\theta - 1)$, where θ is the angle between the interaction and the magnetic field. Rapid sample rotation projects all interactions on the rotational axis and when the rotation is with respect to the magnetic field then the interaction can be averaged out. To achieve this, the spinning axis of the rotor is oriented at an angle of 54.74° with respect to the static magnetic field B_0 . When the value of θ is set to 54.74° , the average of $(3 \cos^2\theta - 1)$ becomes 0 and the anisotropy interaction averages to zero.

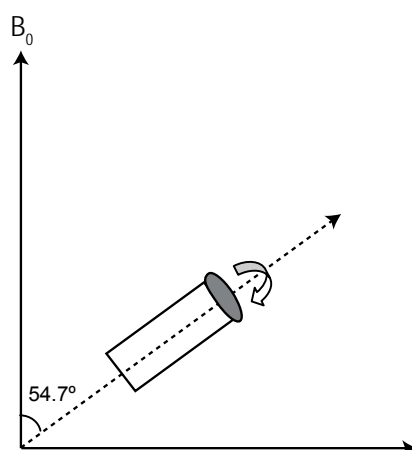


Figure 28 : MAS Picture showing the orientation of the rotor with respect to the external magnetic field of strength B_0 . The rotor is inclined at magic angle, which has a value of 54.7° .

6.3.2 Decoupling

For MAS experiments, the spinning speed widely used is generally below 15 kHz. This spinning frequency is inefficient to eliminate the $^{13}\text{C}-^1\text{H}$, $^{15}\text{N}-^1\text{H}$ and $^1\text{H}-^1\text{H}$ interactions. To eliminate this undesired effect, the carbons or nitrogens are decoupled from protons by means of heteronuclear decoupling. $^1\text{H}-^1\text{H}$ or homonuclear decoupling can be achieved by use of special sequences such

Chapter 6-Solid State NMR characterization of PR 2D crystals

as Lee Goldberg [153]. The common decoupling method is constant wave irradiation (CW), which switches the orientation of protons faster than the NMR time scales. This results in averaged dipolar coupling of zero. Associated with CW are the demerits of sample heating and reduced MAS efficiency. As an improvement over this method, other decoupling methods such as Two Pulse Phase Modulation (TPPM) and Spinal 64 have been introduced. TPPM is the most efficient broadband decoupling method for solids which is based on 2-step phase shifting [154]. The step wise increase in the phase angle of the TPPM sequence in combination with phase cycling proves better for solid samples and is known as small phase incremental alteration with 64 steps or Spinal 64 [155].

6.3.3 Cross polarization (CP)

CP is a technique to aid observation of the rare spin systems for biological samples. Spins of special interest are ^{13}C and ^{15}N which have a low natural abundance of 1.1% and 0.37% respectively and have less gyromagnetic ratio of $\gamma_{^{13}\text{C}} = 67 \cdot 10^6 \text{ rad/sT}$ and $\gamma_{^{15}\text{N}} = -27 \cdot 10^6 \text{ MHz/T}$ respectively, but are the core building blocks of biomolecules. In contrast, the natural abundance of ^1H is 99.99% but the high gyromagnetic ratio of $\gamma_{^1\text{H}} = 267 \cdot 10^6 \text{ rad/sT}$ makes them difficult to detect due to stronger homonuclear dipolar coupling which results in line broadening.

Observation of rare spins such as ^{13}C directly confronts the problems of poor signal with respect to noise and longer relaxation time. These issues are overcome by use of cross polarization where a network of abundant spin transfers the magnetization to the rare spin. Usually ^1H are used for the sensitivity enhancement of rare spins such as ^{13}C and ^{15}N because of their high natural abundance and shorter relaxation time. This polarization transfer is accomplished through the dipolar interaction between the rare and abundant spins and is mediated by Hartmann Hahn match, which permits the magnetization transfer when Larmor frequency of the rare and the abundant spins are exactly matched. This in turn is achieved by adjusting the applied radiofrequency on the two spins as the gyromagnetic ratios are inherent properties.

$$\gamma_{\text{H}} B_{1\text{H}} = \gamma_{\text{C}} B_{1\text{C}}$$

where γ represents the gyromagnetic ratios of the two spins and B_1 , the applied radio frequency.

Chapter 6-Solid State NMR characterization of PR 2D crystals

This 1D experiment offers high sensitivity spectra for rare spins by eliminating broadening from chemical shift anisotropy and dipolar coupling. This technique does not consider the effect of dipolar coupling between the abundant spin system and hence decoupling is applied while the signal from the rare spin is recorded. When coupled with MAS, the spinning should not be too fast with respect the dipolar coupling which mediate the transfer of magnetization. The basic pulse sequence of CP is shown below.

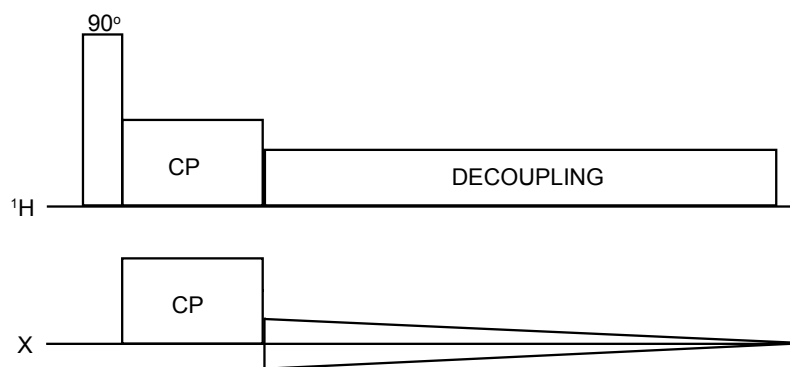


Figure 29 : The pulse sequence of cross polarization. The magnetization is induced with a 90° pulse on ^1H and then the bulk magnetization is transferred to the rare spin via Hartmann Hahn match. The ^1H are decoupled while the free induction decay of the rare spin is acquired.

6.3.4 Recoupling

It is a method to reintroduce the dipolar couplings under MAS condition. The reintroduction is achieved with the help of rational resonance, REDOR or symmetry based pulse sequences. The sequence is used to measure the dipolar couplings between the spins in a spin pair system. The most practical example is the suppression of the natural abundance in a specifically labeled amino acid. In practice, this is accomplished with the help of rotor synchronized C type sequences (CN_n^Y). These sequences have blocks of 360° pulses, which are applied over fixed rotor periods with a definite phase increment [156].

6.4 Investigation of lipids in the 2D crystalline samples with ^{31}P measurements from the lipid head groups

6.4.1 Motivation

Lipid protein interactions are essential for successful 2D crystallization and for protein activity. The lipids are known to provide stability to the crystal of BR and the composition of lipid and density is shown to be variable for the cytoplasmic and extracellular sides [157]. The crystal structure of BR at 1.55 Å resolution indicates a bilayer of 18 tightly bound lipid chains, which forms a ring like structure around the protein in the crystal. It also indicates that the contacts between the trimers in the membrane plane are mediated almost exclusively by lipids [158]. In some other membrane proteins like the aquaporin where the structure is determined by electron crystallography of 2D crystals and by X-Ray crystallography of 3D crystals, reveals presence of nine lipids per aquaporin monomer, which adopt a wide variety of conformations and tightly fill the space between the adjacent aquaporin tetramers [159]. In order to gain an insight into the arrangement of the lipid and to characterize DOPC, the lipid used for crystallization for PR, was investigated.

6.4.2 Importance of lipids

Lipids, which are amphipathic in nature, form the major components of the biological membranes. The amphipathic nature of the lipids is responsible for the structural basis of the biomembranes and hence form an integral part of the membrane protein characterization. The lipids typically consist of a glycerol backbone and attached to this are the 2 organic fatty acid side chains with varying degree of unsaturation and chain length with ester bond and one phosphate group. All lipids have 2 phases, an ordered gel phase (L_{β}) and a disordered liquid crystalline phase (L_{α}). The lipids are characterized by specific phase transition temperature. It is defined as a temperature, which induces change from one phase to the other. The kind of fatty acid side chains play an important role in the membrane protein reconstitution and crystallization. The appropriate selection of lipid and phase appears to be very important for crystallographic and NMR studies. E.g. the structure of the BR-trimer lipid complex suggests complementary ways in which the lipids stabilize oligomeric rings of membrane proteins and achieve an asymmetric distribution in biological membranes [107]. The involvement of lipids is also known to influence certain properties in BR, such as the regulation of the pK for the purple

Chapter 6-Solid State NMR characterization of PR 2D crystals

to blue transition caused by deionization, and the reformation of trimers from monomers after exposure of the purple membrane to detergent. An important role for the neutral lipid known as squalene is found to provide the functional stability of the fast-decaying M-intermediate [102].

Study of Lipids, known as ‘lipidomics’ constitutes a vast area for detailed investigation due to the involvement of lipids in various aspects of structural biology. There are various techniques used for the analysis of lipids like Chromatography (HPLC and TLC) and for separation of lipid mixtures [160], Mass spectrometry (ESI /APCI/ MALDI) for estimation of lipid composition of complex mixtures with negligible amount of fragmentation, FTIR for biochemical processes e.g. hydration and conformational changes [161, 162], studies based on characteristic band position [163], Neutron and X-Ray diffraction to determine the phospholipids structures [164] and fluorescence by chemical modification with a fluorophore. Amongst all these techniques FTIR, diffraction [165], and fluorescence [166] have been shown to aid the study related to the membrane lipid interactions. However, the modern technique, which annuls in terms of obtaining structural information, is the ^{31}P SSNMR.

6.4.3 Advantages of ^{31}P for lipid investigation

The phosphorous head group in the lipid molecule confers several advantages. It is NMR active isotope with a natural abundance of 100% along with ^1H and ^{19}F and possesses high positive gyro magnetic ratio. The sensitivity of ^{31}P detection is next to ^1H . The higher sensitivity means detection under dilute concentration and lower field strengths. Each molecule of lipid has just one ^{31}P molecule hence it provides unique isotropic chemical shift. By virtue of relatively less number of ^{31}P nuclei, the spectra is less complicated and overlapping as compared to ^1H or ^{13}C [167]. The chemical shift anisotropy values for ^{31}P are also indicative of the phase of lipid and dispersion.

6.4.4 Results and Discussion

The lipids are characterized by transition temperatures and exhibit different properties and behavior depending on the temperature of measurement. The lipid used for characterization is DOPC and has a phase transition temperature of -24°C . All the measurements were carried out at 280 K, which is above the DOPC main phase transition temperature. Figure 30 a shows direct

Chapter 6-Solid State NMR characterization of PR 2D crystals

polarized ^{31}P spectra under proton decoupling at low spinning speed (3 kHz) where two major resonances were observed at 3.6 ppm and -0.6 ppm. While the less shielded resonance is rather narrow and disappears under cross polarization (figure 30 b), the peak at -0.6 ppm shows significant line-broadening (2.5 ppm) and is surrounded by spinning sidebands indicating large chemical shift anisotropy.

The CP spectrum of the PR 2D crystals shows increased line broadening. This increased line width in figure 30 b can be attributed to the fast chemical exchange between protein-bound and non-bound lipids or altered lipid dynamics within the 2D crystal. The line broadening may also be caused due to the inhomogeneity in the sample. The narrow lipid signals in figure 30 a, found at around 3.6 ppm do not show any significant anisotropy. These could be co-purified *E.coli* lipids or lipids in residual amounts of small unilamellar vesicles.

For control measurements, a comparison with a spectrum of DOPC bilayers at the same temperature and spinning speed was acquired. The spectra shows comparable isotropic and anisotropic chemical shifts but reduced line-broadening (0.1 ppm) (figure 30 c). The spinning sidebands in figure 30 c correspond to an axially symmetric CSA tensor typical for fluid lipid bilayers. The rotational diffusion of lipids is not restricted despite the very small lipid to protein ratio in the 2D crystalline preparation.

The ^{31}P MAS NMR control experiments at above (280 K) and below (220 K) the main lipid phase transition temperature (-24°C) on pure DOPC bilayers and on 2D crystal samples were also carried out. The direct polarization as well as cross polarization spectra for both the temperatures were comparable as shown in figure 31. In all cases, the ^{31}P CSA was always comparable between 2D crystals and DOPC bilayers. This also supports the hypothesis that the lipids in the 2D crystalline arrangement behave lipid bilayers as seen in figure 31.

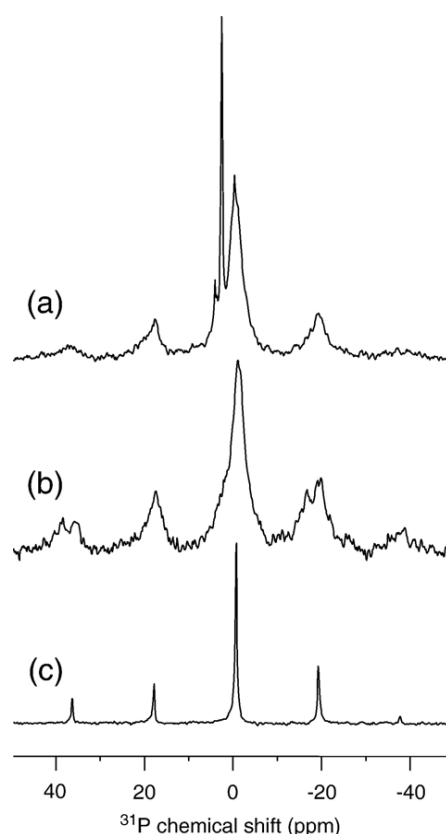


Figure 30 : ^{31}P 1D MAS spectra of PR 2D crystals and DOPC bilayers. ^{31}P direct polarized MAS spectrum (3 kHz spinning) of PR 2D crystals prepared in DOPC (a). The main species at -0.6 ppm shows a large CSA (CSA=33 ppm, $\eta=0.1$), while a minor population at 3.6 ppm is rather narrow and disappears under cross-polarization (b). It could arise from other lipids copurified with PR. For comparison, DOPC lipid bilayers are shown in (c) which show a similar axial symmetric CSA tensor (CSA=33 ppm, $\eta=0$) but reduced line width. Spectra were acquired with 40 k scans at 162 MHz for ^{31}P . The temperature was adjusted to 280 K to ensure a fully fluid lipid bilayer. The chemical shift values are indicated in ppm.

6.4.5 Conclusion

Since the amount of lipid used for the 2D crystallization is infinitesimal and the fact that the type of lipid does not affect the crystallization process, it was important to know their contribution to the overall crystalline arrangement. The likelihood of involvement of lipids in the stabilization of the monomers by forming a tight belt around the individual monomer was high. However, from the ^{31}P data presented for lipids, it is highly suggestive that they behave more like lipid bilayer. Whether DOPC forms a bound belt around PR or whether other bound lipids have been co-

Chapter 6-Solid State NMR characterization of PR 2D crystals

purified together with PR and contribute to the ^{31}P signal cannot be decided at this point but is subject to further studies.

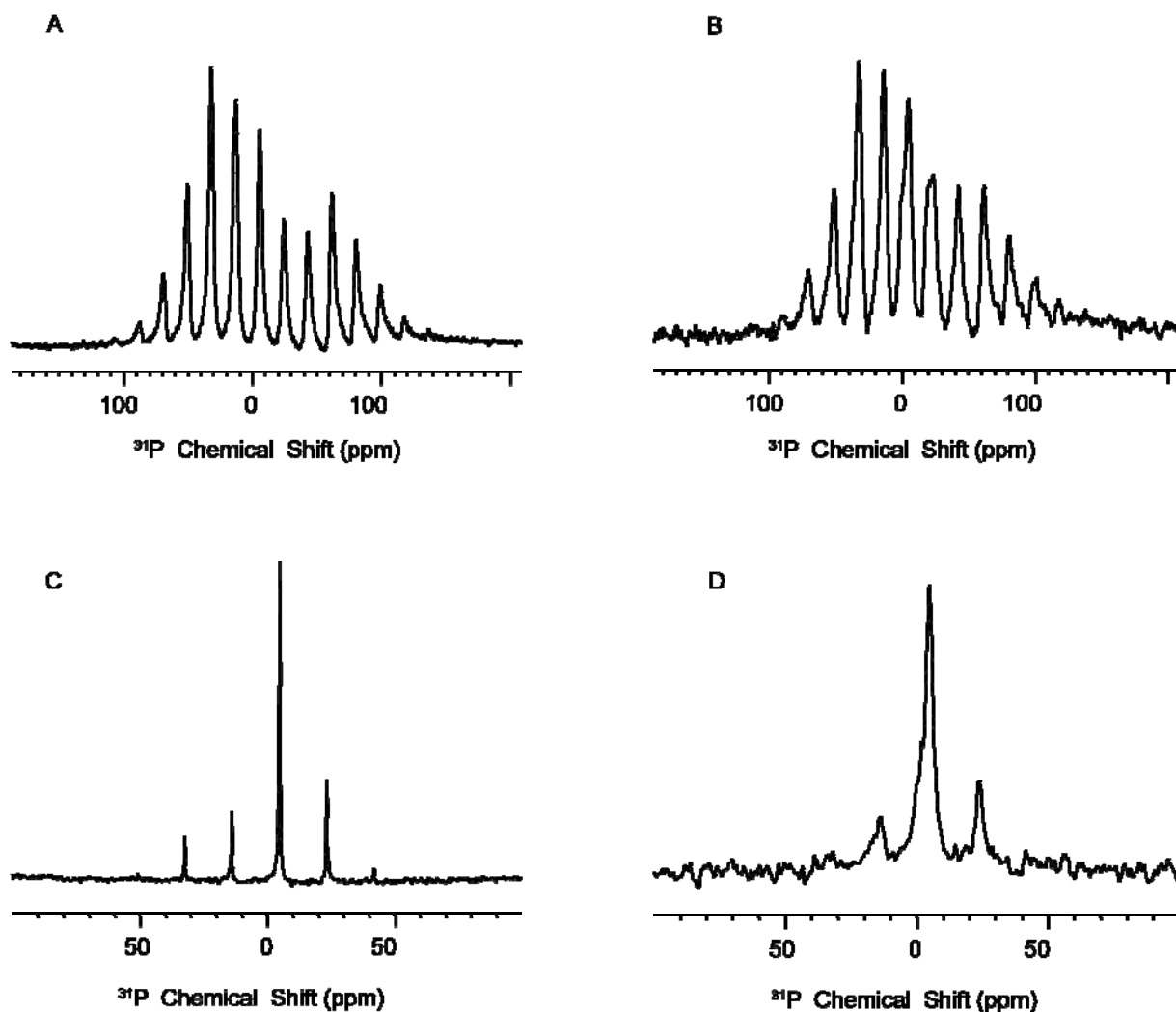


Figure 31 : Comparison spectra of DOPC and PR 2D crystals at different temperatures. A: Cross polarization spectra of DOPC 220 K with line broadening of 50, B: Cross polarization spectra of PR crystals at 220 K with line broadening of 150. C: Direct polarization spectra of DOPC 280 K and line broadening of 50 and D: Direct polarization spectra of PR 2D crystals at 280 K with line broadening of 150. The spectra were collected on 400 MHz spectrometer with spinning speed of 3 kHz. Approx. 9000 scans were collected per spectra. The chemical shift is indicated in ppm.

Further from AFM and EM data, it is evident that there exists an inherent inhomogeneity in the crystalline samples, which is represented by the presence of equally dense reconstituted samples.

Chapter 6-Solid State NMR characterization of PR 2D crystals

It is possible that the ^{31}P spectra are representative of the bulk lipids in the reconstituted samples as the amount of lipids in the reconstituted region is relatively more than the crystalline region and broad line shapes mask the resonances representing the crystalline part.

6.5 Schiff Base characterization with MAS NMR on ^{15}N - ζ -Lys labeled PR

6.5.1 Motivation

A remarkable feature observed in case of retinal proteins especially in BR is a large protein induced shift of the absorption spectra of the chromophore, which gives them characteristic colour. This spectral shift is referred to as opsin shift and is defined as the difference in the energies of maximum visible absorption of the free protonated retinal Schiff base in solution and the light adapted retinal protein complex. The opsin shift is investigated in detail with several approaches [168-170] including SSNMR [171, 172]. This effect refers to the important interactions between chromophore and protein. It is shown that the deionization or acidification affects the opsin shift for BR [173, 174] and is also suggested that the change in the surface pH, affects the chromophore.

In case of PR, the chromophore retinal is bound to the protein via a Schiff base to lysine 231 and in context to these reports; it is highly probable that it might be involved in the similar interactions. In order to investigate such sensitive interactions, it is important to check the proper folding of protein and to ensure the native environment of the Schiff base. To ensure the correct folding and functionality of the protein the ^{15}N - ζ -Lysine CPMAS spectra were measured in 2D crystalline samples.

6.5.2 Results and Discussion

The ^{15}N CPMAS spectra of ^{15}N labeled lysine was measured at 280 K. Lysine is the most conserved residue within the retinal binding pocket of proteins from the rhodopsin family. In PR, the chromophore retinal is covalently linked via a Schiff base to lysine231. The ^{15}N chemical shift of this Schiff base is highly responsive to its protonation state [147] and an accurate reporter of photocycle intermediates [175]. It has been studied extensively for photoisomerization of retinal proteins [176].

Chapter 6-Solid State NMR characterization of PR 2D crystals

The spectrum in figure 32 reveals a chemical shift of 185 ppm for the protonated Schiff base and 36.6 ppm for the other lysine side chains. The Schiff base chemical shift is almost identical to that in non-crystalline, reconstituted samples which are fully functional as reported previously [68]. In dark-adapted BR, the PSB of the all-trans retinal resonates at 171 ppm and shows a λ_{\max} at 568 nm which is different from PR (185 ppm and 520 nm). While the correlation between chemical shift and λ_{\max} [177], it deviates significantly for PR indicating very strong chromophore–opsin interactions [68, 177]. It is important to note, that Schiff base, backbone amides and lysine side chains cross polarize in non-frozen 2D crystalline samples while low temperatures (230 K) had to be used for the non-crystalline, reconstituted samples [68]. The line width has improved as well from 4.5 ppm to 0.5 ppm for the lysine side chains as a result of 2D crystallization.

For ^{15}N assignment purposes, sample with ^{15}N labeled lysine and ^{15}N histidine was prepared initially at pH 7 and the spectrum obtained is displayed in figure 33. The figure 33 A shows the entire spectrum and gives a clear picture of the side chain resonances. The chemical shift value for the resonance from the free lysines comes at 36.6 ppm and backbone region around 120 ppm. However, the side chain region exhibits more than expected resonances. In all, there were five peaks in the side chain region. The observed resonances had chemical shift values of 184.3 ppm, 178.7 ppm, 175.9 ppm, 170.4 ppm and 164.8 ppm respectively. From our earlier measurement of ^{15}N lysine at pH 8.5, it is known that the chemical shift value for the Schiff base is about 186 ppm. In addition, from BMRB database, the standard ^{15}N chemical shift values for histidine are given as follows: backbone 119.59, $\delta_1 = 189.93$ and $\delta_2 = 176.78$. These chemical shift values are based on solution state measurements and are likely to show deviation for the reconstituted samples especially in crystalline environment. The possible explanation to account for additional peaks is the co-existence of more than one conformational state at pH 7 and resonances arising from mobile 6xHis tag. If the pH of the surrounding environment is below the pKa of proton acceptor, which happens to be in the range of 7.1-7.6, there is a possibility of vectorality of the proton pumping for the protein. From the structural point of view, it indicates that the protein has heterogeneous arrangement, which gives rise to the additional peaks in the SSNMR.

Chapter 6-Solid State NMR characterization of PR 2D crystals

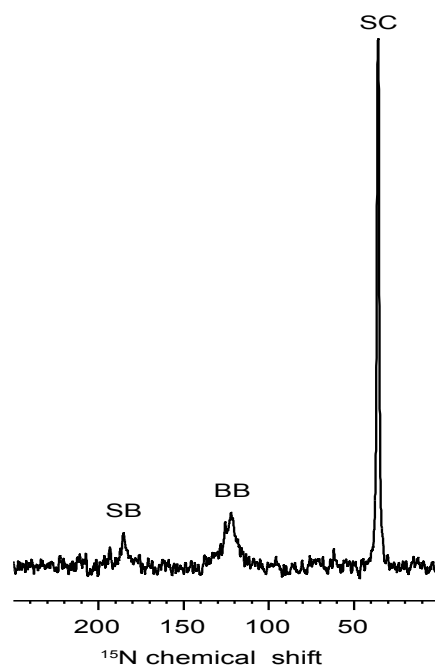


Figure 32 : ^{15}N -CP-MAS spectrum of ^{15}N - ζ -Lysine 2D crystalline PR shows the protonated Schiff base (SB) at 185 ppm. The spectra recorded on 600 MHz at 11 K Hz spinning speed and 30 k scans were accumulated at 280 K. The free lysine or the side chains (SC) appear at 36.6 ppm and the backbone resonance at 120 ppm. The spectra is processed with line broadening of 25.

For improved spectral resolution, the ^{15}N uniformly labeled samples were measured on 850 MHz spectrometer and spectra was collected as shown in figure 33 B. The spectra shows free lysines at 36.6 ppm and backbone resonances show better resolution. Resonances from the aromatic region could also be seen but it was not possible to differentiate due to spectral overlap. The most interesting region in the spectrum is shown in the inset, which compares well with the earlier ^{15}N lysine spectra. This is the region, where the resonances from the side chains of histidine and lysines are expected. The region shows similarity with the multiple peaks as has been shown in figure 33 A. The peaks at 185 and 165 ppm are relatively sharp and well defined. The peak at 185 ppm is from the Schiff base and most likely the other peak at 165 ppm is originating from the structured location of histidine 75. The resonances which lie in between these two peaks are probably because of the 6xHis tag, which displays mobility and hence the reason for the broadening of the peaks. However, this can only be confirmed with ^{15}N spectra of histidine75 mutant.

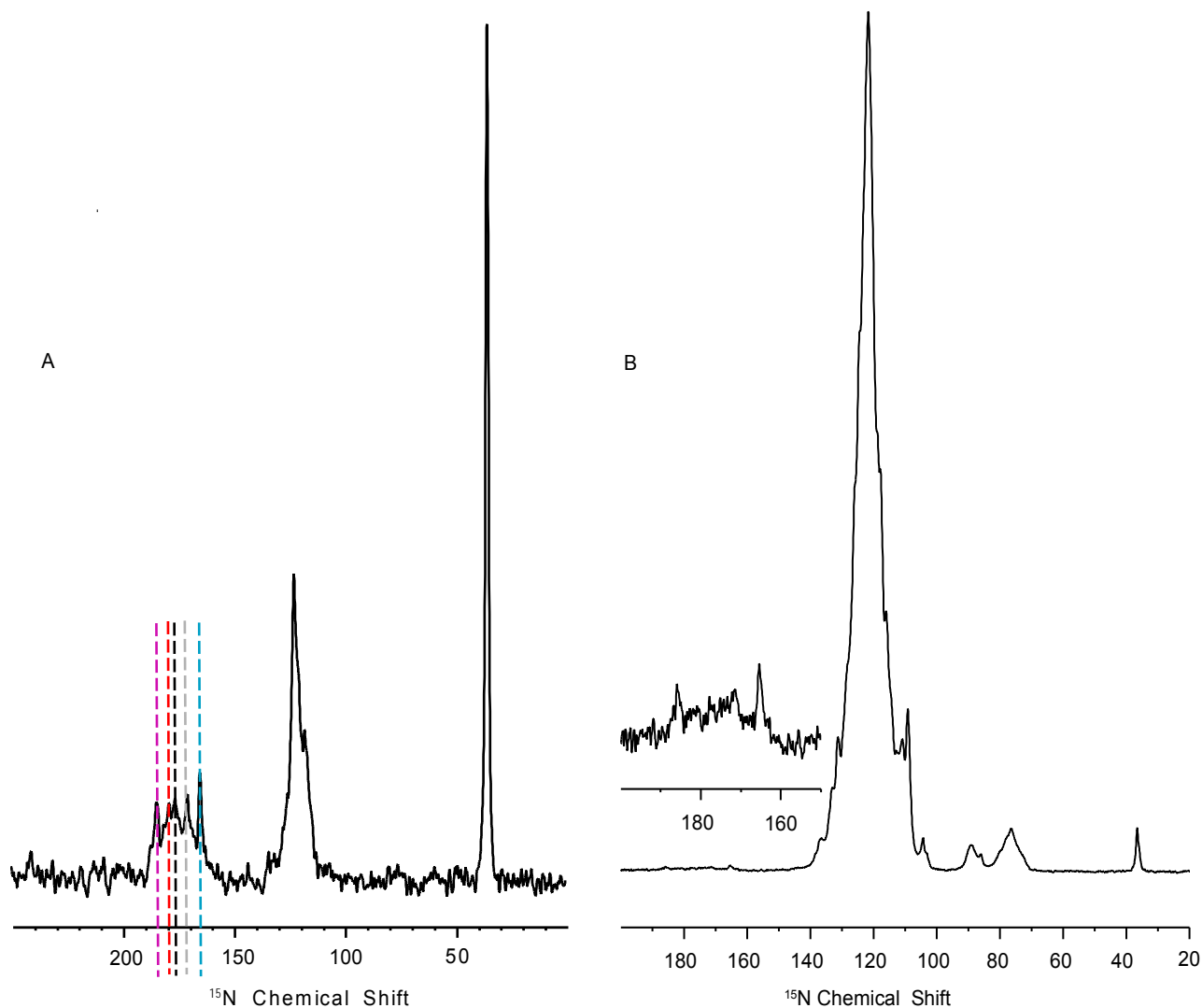


Figure 33 : A: ^{15}N CPMAS of lysine and histidine labeled sample at pH 7. The observed resonances appear at purple: 184.3 ppm, red: 178.7 ppm, black: 176 ppm , grey: 170.4 ppm and blue at 164.8 ppm respectively in the side chain region. The spectra were acquired at 280 K with 10 kHz spinning frequency and ~ 100 K scans were accumulated on 400 MHz spectrometer. Line broadening of 25 is applied. B: ^{15}N CPMAS from uniformly labeled samples of PR 2D crystals at pH 8.5. The spectra was collected at 850 MHz Bruker spectrometer with a spinning speed of 10 kHz and temperature of 280 K. 23 K scans were collected and line broadening of zero is applied.

6.6 ^{15}N characterization of Methionines

6.6.1 Motivation

Chapter 6-Solid State NMR characterization of PR 2D crystals

Magic angle sample spinning for determination of set of oriental constraints for specifically labeled samples was used for BR. The advantage conferred is of improved resolution and sensitivity. This approach was applied for BR for characterization of methionines where 6 out of 9 residues are located in the helical region [29]. The ^{15}N CPMAS allowed the resolution of 7 methionines and further their assignment [95]. In case of PR, there are 10 methionines out of which 9 are located in the helical region as shown in figure 34. This distribution of methionines is quite similar to the arrangement in BR. It also suggests that the information so obtained will be reflective of the behavior of helical region. On the basis of above available literature and the feasibility of isotope labeling the ^{15}N methionine in PR 2D crystals, methionines were investigated.

The initial investigation aimed to observe the extent of resolution by means of CPMAS and later to obtain a greater insight into the resolution, 2D experiments such as 2D Heteronuclear correlation were performed. Attempts to measure helix mobility by ^{15}N - ^1H dipolar couplings using Lee-Goldberg cross-polarization were also made.

Some results of this section are published in *Biochimica et Biophysica Acta* 1768 (2007) 3012–3019.

6.6.2 Approach

The experiments used for characterization of Methionines were ^{15}N CPMAS, ^{15}N - ^1H Heteronuclear experiment and ^{15}N - ^1H Lee-Goldberg Cross Polarization. The basic principle of CPMAS has been discussed before and the principle of HETCOR and LG-CP shall be discussed in the following paragraphs.

6.6.3 ^{15}N - ^1H Heteronuclear experiment

HETCOR experiments display spatial correlation between 2 heteronuclear species. Here in this case it was used for ^1H - ^{15}N correlation. HETCOR is a 2 dimensional experiment where ^1H evolution takes place during ^1H - ^1H decoupling which is achieved with FSLG. This is followed by a CP step to transfer the magnetization to ^{15}N and further by ^{15}N detection.

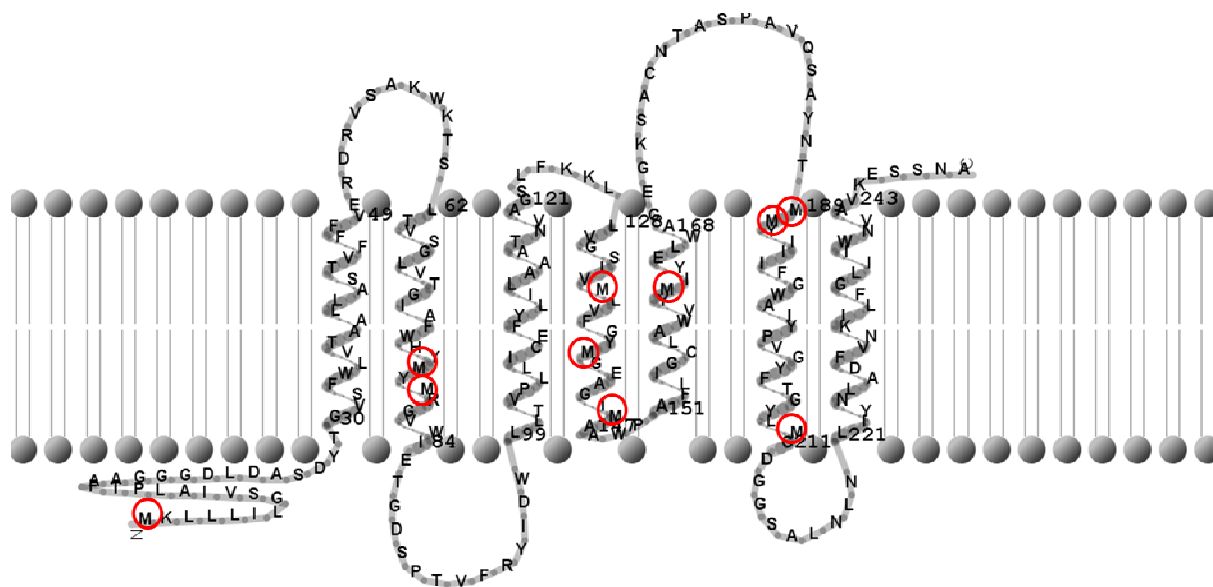


Figure 34 : Topology model of PR showing the location of methionines in the amino acid sequence. Methionines at positions 77, 79, 134, 140, 146, 162, 189, 190, 210 are located in the helical region. The Methionines are circled in red.

6.6.3.1 HETCOR experimental parameters

^{15}N - ^1H 2D Heteronuclear spectroscopy was performed using frequency switched Lee–Goldburg decoupling [178] as described in [179] at an effective proton decoupling field of 85 kHz during the evolution period and two pulse phase modulation proton decoupling at 64 kHz during the acquisition period. 2 k scans in the ω_2 dimension and 64 rows in the ω_1 dimension were acquired using time-proportional phase increments. Here ^1H evolve under homonuclear ^1H - ^1H decoupling using FSLG and ^{15}N detection is done by CP. The scaling factor for the ω_1 dimension was determined to be 0.57. A spinning rate of 14 kHz was used. HETCOR experiments were carried out using a Bruker Avance 400.

6.6.4 ^{15}N - ^1H LG-CP experiment

The LG-CP experiment refers to ^1H - ^{15}N CP measurement while ^1H are decoupled from each other during the Hartmann Hahn transfer step. By variations of the CP contact time, a 2D spectrum can be acquired, which correlates ^1H - ^{15}N dipolar couplings to ^{15}N chemical shifts and the dipolar coupling is scaled to 0.57[178].

Chapter 6-Solid State NMR characterization of PR 2D crystals

Cross polarization Lee Goldberg is an example of chemical shift dipolar correlation experiment for studying molecular dynamics. In 2D LG-CP method, the CP contact time is incremented to produce 2D spectrum, which contains the ^{15}N high-resolution spectrum along one spectral dimension and corresponding ^{15}N - ^1H dipolar powder pattern along the other axis. For this measurement, a normal CP measurement is coupled with homonuclear ^1H - ^1H decoupling method. The effective magnetization transfer during CP is mediated via strong homo nuclear dipolar coupling. Motionally averaged ^1H - ^{15}N dipolar couplings can be used to access the molecular dynamics at the site of ^{15}N label in the protein. The ^1H - ^1H interactions are largely suppressed by applying off resonance radio frequency field that results in an effective field pointing along an axis tilted by magic angle with respect to the direction of external magnetic field at the same time proton carbon dipolar interaction is reintroduced via Hartmann Hahn condition imposed on effective radiofrequency fields experienced by nuclei.

6.6.4.1 ^{15}N - ^1H LG-CP experimental parameters

^{15}N chemical shift - ^{15}N - ^1H dipolar correlation spectra were acquired using LG-CP. The contact time was incremented by 30 μs 128 times resulting in a t_1 evolution time of 3.84 ms. Experiments were carried out at 12 kHz sample spinning. The ^{15}N spin-lock field was adjusted to the first order sideband condition. Only cosine-modulated data were collected and a real Fourier transformation was applied to the indirect dimension. To remove the dominant zero frequency peak caused by the signal increase with increasing contact time, an exponential baseline correction was applied prior to Fourier transformation. LG-CP experiments were carried out using a Bruker Avance 400.

6.6.5 Results and Discussion

Nuclear spin relaxation times provide a direct and unambiguous measure of the presence of molecular dynamics in “solid samples”. The most widely used approach is to study deuterium NMR line shape and measure relaxation rates. Measurements of ^{15}N -nuclear longitudinal relaxation rates in microcrystalline sample of the protein have provided a qualitative description of the site-specific backbone dynamics in the solid state [180]. With recent advances in SSNMR, it became possible to obtain dynamic information on a per-residue basis using uniformly labeled

Chapter 6-Solid State NMR characterization of PR 2D crystals

protein samples [181]. And here we have made similar attempt to measure the protein dynamics with ^{15}N specifically labeled samples of methionines.

In ^{15}N - ^1H HETCOR experiments as shown in figure 35 a, most peaks are found around 120 ppm but cross-peak intensities are also seen at 123 ppm and 117.5 ppm. This data indicates that highly ordered protein samples in 2D crystalline form in a non-frozen state provide well resolved spectra even of side chain resonance. 9 out of 10 methionines (77, 79, 134, 140, 146, 162, 189, 190, 210) are buried inside the transmembranous region and only methionine189 is located at the interface as shown in the topology model in figure 34. Compared to BR, these resonances did show a similar line width of 0.7 ppm but a smaller chemical shift dispersion of (6 ppm vs. 11 ppm) [95]. Cross-polarization at 280 K is possible, which indicates restricted protein dynamics.

The LG-CP experiment has been carried out first on crystalline ^{15}N -acetyl-leucine, where a rigid-limit, scaled dipolar splitting of 4.7 kHz is found (figure 35 b). In PR, at 280 K, all ^{15}N - ^1H methionine dipolar couplings are smaller with variations from residue to residue (in average 3.7 kHz). This corresponds to an order parameter of 0.8. A comparison between 1D slice through the spectra of ^{15}N -acetyl-leucine and ^{15}N -Met labeled PR is shown in the figure 35 d and e. It has been shown earlier that the rigid segments exhibit strong dipolar couplings and thus large splittings in the LG-CP spectra whereas the mobile groups show diminished coupling strengths [182]. To obtain an overall view, the same experiment was carried out on uniformly ^{15}N labeled PR. The spectrum obtained at 280 K figure 35 f deviates clearly from the rigid-limit case shown in figure 35 d but also from the selectively labeled sample in figure 35 e. The spectrum in figure 35 e shows a reduction in splitting but not a significant change in line shape compared to the rigid-limit case, while figure 35 f reveals a line shape expected.

The determination of molecular dynamics of proteins is one of the major challenges in understanding their structure-function relationship of a membrane protein. Relationships SSNMR spectroscopy is a powerful method for studying internal dynamics for motions typically on the 10^{-2} to 10^{-12} s time scale. Correlation times and activation energies for specific models of motion have been determined using this technique. Previous models have shown that internal dynamics are very sensitive and subjective to packing in crystalline amino acids [183].

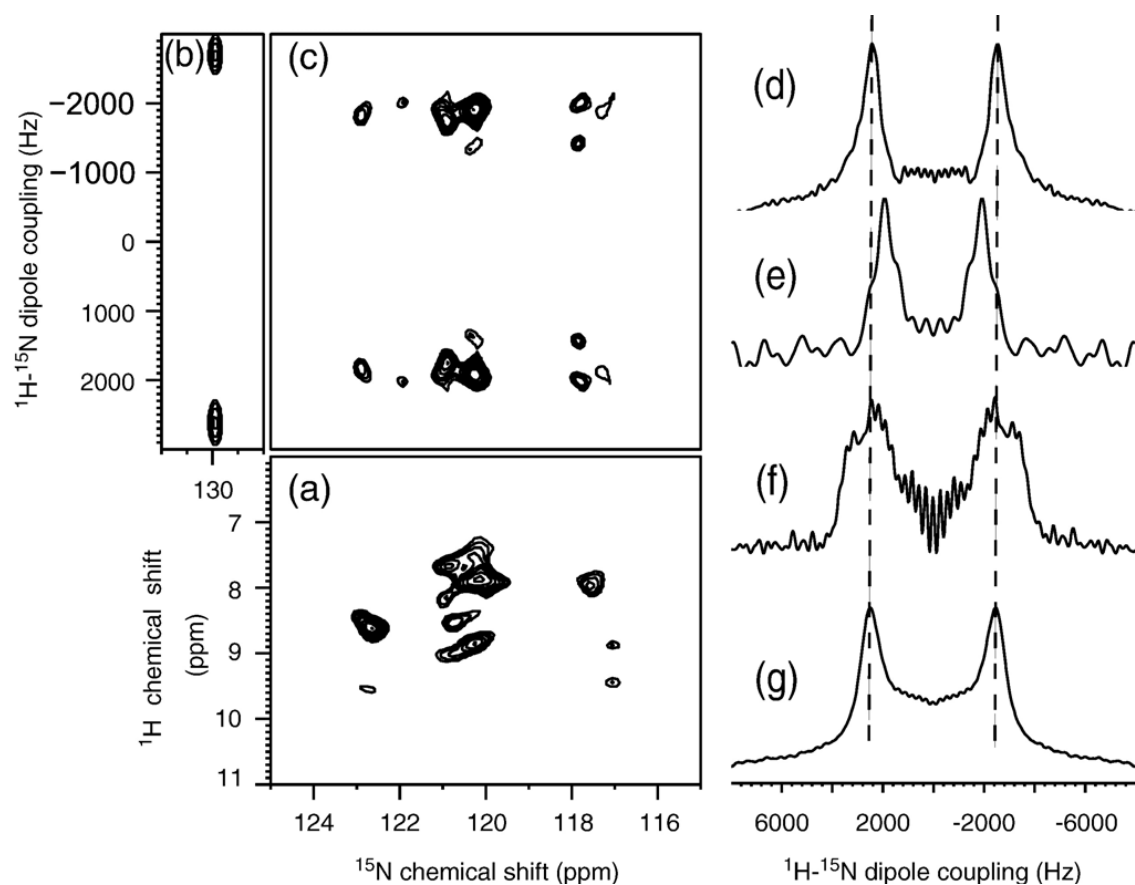


Figure 35 : ^{15}N - ^1H HETCOR experiment of ^{15}N -Met PR reveals major intensities around 120 ppm but also at 123 and 117.5 ppm. The spectra was acquired with 1100 points in the direct dimension and 128 points in the indirect dimension. 1096 transients were accumulated per slice and acquisition time of 49 msec was used (a). The 2D ^{15}N - ^1H LG-CP spectrum of ^{15}N -acetyl-leucine shows a rigid-limit dipolar splitting of 4.7 kHz. The spectrum was acquired with 684 points in the direct dimension and 128 points in the indirect dimension. 2 transients were accumulated per slice and acquisition time of 48 msec was used (b), while the ^{15}N -Met resonances in PR show reduced dipolar splitting with an average value of 3.7 kHz indicating helix mobility despite 2D crystalline arrangement. The spectrum was acquired with 684 points in the direct dimension and 128 points in the indirect dimension. 4096 transients were accumulated per slice and acquisition time of 48 msec was used. (c). A slice through the ^{15}N -acetyl-leucine spectrum at 130 ppm is shown in (d) and compared with ^{15}N -Met PR at 120 ppm in (e). The LG-CP spectrum of U- ^{15}N PR (slice taken at 120 ppm) (f) deviates significantly from (e) indicating motions in PR caused by nonuniaxially motional averaging. Upon lowering the temperature to 220 K, the spectrum approaches a line shape expected for the rigid-limit case (d). All spectra are acquired at a 400 MHz for ^{15}N and 280 K except (e) where the temperature was adjusted to 220 K. All the chemical shifts are indicated in ppm and dipolar coupling in Hz.

Chapter 6-Solid State NMR characterization of PR 2D crystals

The reduced splitting observed for methionines could partially be explained by their involvement in strong hydrogen bonds within the PR α -helices. However, must contain some motional averaging due to small angle wobbling of these individual residues, liberation of the peptide plane, or general fluctuations of the helices around their axis. The dependence of Lee–Goldberg cross-polarization line shapes on molecular motions had been discussed extensively [153]. Uniaxially motional averaging would just reduce the observed dipolar splitting while non uniaxially dipolar averaging causes alterations in the spectral line shape such as broadening and additional wings on both sites of the spectrum.

6.6.6 Conclusions

The ^{15}N - ^1H HETCOR measurements show that it is possible to resolve individual methionines in second dimension, which was not possible with ^{15}N methionine labeled 1D spectra. The major conclusion from the ^{15}N - ^1H LG-CP measurements is the presence of helix mobility despite the crystalline packing of the protein. The helix mobility, which is observed, in effect may be the representation of the bulk mobility of the inherently inhomogeneous samples and is open to further investigation.

6.7 ^{15}N Tryptophan assignments with Rotational Echo double Resonance (REDOR)

6.7.1 Motivation

Biochemically tryptophan is highly hydrophobic residue and has potential of hydrogen bonding. This residue has a large indole (benzopyrrole) side chain, which is comprised of two fused aromatic rings. Due to its aromatic nature character, it can form π - π interactions. The indole ring is considerably separated from the hydrogen bonding part of the molecule. Such a spatial arrangement allows hydrophobic as well as hydrogen bonding interactions [184].

Membrane proteins have significantly higher content of tryptophan as compared to soluble proteins. Within the subunits, they form hydrogen bonds with carboxyl oxygen of the main chain and thereby conferring stability to the protein. On the surface, these are positioned to form

Chapter 6-Solid State NMR characterization of PR 2D crystals

hydrogen bonds with the lipid head groups. This indicates involvement of tryptophan in anchoring of the protein subunits within the bilayer.

PR has 10 tryptophans in the entire sequence and the ^{15}N tryptophan CPMAS spectra showed a significant resolution of resonances as shown in the figure 38. The resonances from the side chain as well as backbone were very well separated. Previous attempts made on ^{15}N methionines labeled preparations on BR [95] and recent reports on ^{15}N tryptophan in rhodopsin [185] have suggested the possibility of the assignment of well separated resonances with Rotational echo double resonance. Considering the comparable resolution of ^{15}N tryptophan spectra in PR with the above reported assignments for BR and Rhodopsin, similar measurements were attempted. Another reason for this attempt was to assign the tryptophan 197, which is highly conserved and if assigned might provide an anchor point for the assignment purposes in the spectra from fully labeled samples in multi dimensional experiments.

6.7.2 Approach

REDOR is a high-resolution SSNMR heteronuclear MAS recoupling method, which employs MAS and CP to measure the distance between two selected labeled heteronuclei, such as ^{13}C - ^{15}N in the molecule or can be used for assignment purpose of a selected spin pair in a specifically labeled sample. This method is particularly used here for recoupling of C'_{i-1} - N_i dipolar coupling for assignment purpose. The pulse sequence of REDOR is given in figure 36.

Using CP, the ^{15}N magnetization is enhanced. A set of 180° pulses on ^{13}C channel, which are separated with the rotor rotation (as shown in figure 36) interfere with the averaging of the ^{13}C - ^{15}N dipolar coupling by MAS. Experimentally, 2 data sets are acquired with (S) and without dephasing (S0) in order to compensate for the spin relaxation during recoupling. The difference between a ^{15}N NMR spectrum obtained with ^{13}C π pulses and one obtained with no ^{13}C π pulses, measures the ^{13}C - ^{15}N coupling. The difference signals for the ^{15}N spectra of the sample are comparable, but weaker than that for the carbon directly bonded to ^{13}C [186]. These C-N distances are generally of the order of 4-6 Å. This is of particular interest in special cases like amide bond, where carbonyl is ^{13}C labeled and amide has ^{15}N label. In general, maximizing a

Chapter 6-Solid State NMR characterization of PR 2D crystals

REDOR difference signal for a given dipolar coupling requires selection of both pulse location and number of rotor cycles. The signal intensity reduces for the dephased spectrum because of incomplete refocusing and this reduction in the signal intensity is given by

$$\Delta S/S = KD^2N^2v^2$$

where $\Delta S = (S - S_0)$, N is the number of rotor cycles during the evolution period, v is the spinning speed, D is the dipolar coupling constant and K is the dimensionless constant whose value is 1.066 [187]. The pulse program of the REDOR is depicted below in figure 36.

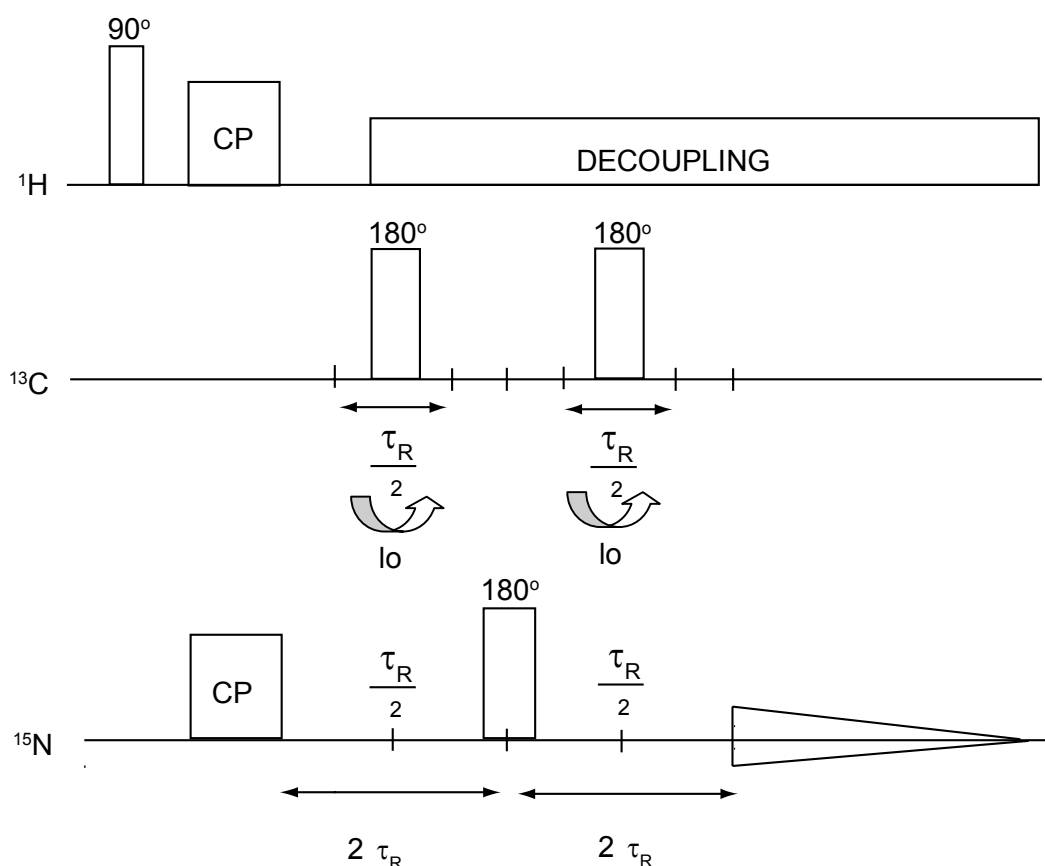


Figure 36 : Pulse sequence for REDOR. ^{15}N magnetization is prepared by a cross-polarization transfer from protons and then evolves under proton decoupling and the influence of two ^{13}C π pulses per rotor period. The first ^{13}C π pulse is placed at one-half the rotor period and the second ^{13}C π pulse occurs at the completion of each rotor period. A single ^{15}N π pulse replaces the ^{13}C π pulse in the middle of the evolution period and refocuses isotropic chemical shifts. The ^{13}C channel is turned on while acquiring spectrum with dephasing. The arrows indicate the no of cycles (lo) which corresponds to 51.

Chapter 6-Solid State NMR characterization of PR 2D crystals

6.7.3 Results and Discussion

Tryptophans in the PR sequence are present at positions 34, 58, 74, 83, 98, 149, 159, 127, 197 and 239. Out of these, tryptophans at residue number 58, 98 and 149 are located in the loop region and rest all are in the helical region as shown in figure 37.

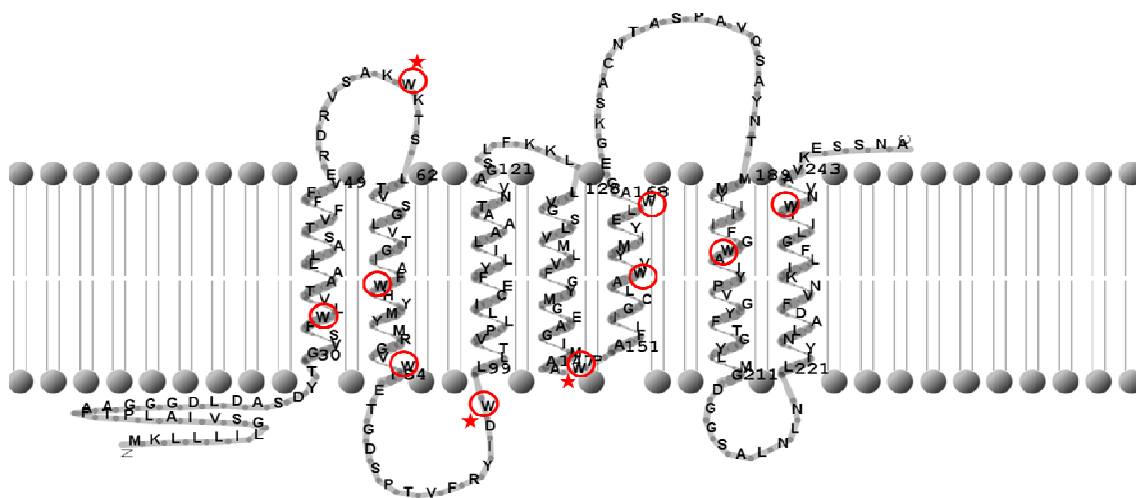


Figure 37 : The topology plot of PR amino acid sequence with 10 tryptophans circled in red. The tryptophans in the loop region are indicated with a star.

The primary requirement for assignment with REDOR, the samples need to be specifically labeled with ^{13}C at the carbonyl carbon of the (i-1) residue and ^{15}N of the N-H in the amide bond of the i^{th} residue, which is tryptophan. With reference to the amino acid sequence, the following unique pairs were identified and specifically labeled.

Table 8: Details of the tryptophan residues in wildtype GPR sequence.

Residue number	location	(i-1) residue $^{13}\text{C}=\text{O}$	i^{th} residue $^{15}\text{N}-\text{H}$	Designation	Sample
34	Helical	Phenylalanine	Trptophan	Phe-Trp	F ₃₃ -W ₃₄
58	Loop	Lysine	Tryptophan	Lys-Trp	K ₅₇ -W ₅₈
74	Helical	Phenylalanine	Tryptophan	Phe-Trp	F ₇₃ -W ₇₄
83	Helical	Valine	Tryptophan	Val-Trp	V ₈₂ -W ₈₃

Chapter 6-Solid State NMR characterization of PR 2D crystals

98	Interface	Aspartic Acid	Tryptophan	Asp-Trp	D ₉₇ -W ₉₈
149	Loop	Alanine	Tryptophan	Ala-Trp	A ₁₄₈ -W ₁₄₉
159	Helical	Alanine	Tryptophan	Ala-Trp	A ₁₅₈ -W ₁₅₉
167	Helical	Leucine	Tryptophan	Leu-Trp	L ₁₆₆ -W ₁₆₇
197	Helical	Glycine	Tryptophan	Gly-Trp	G ₁₉₆ -W ₁₉₇
239	Helical	Isoleucine	Tryptophan	Iso-Trp	I ₂₃₈ -W ₂₃₉

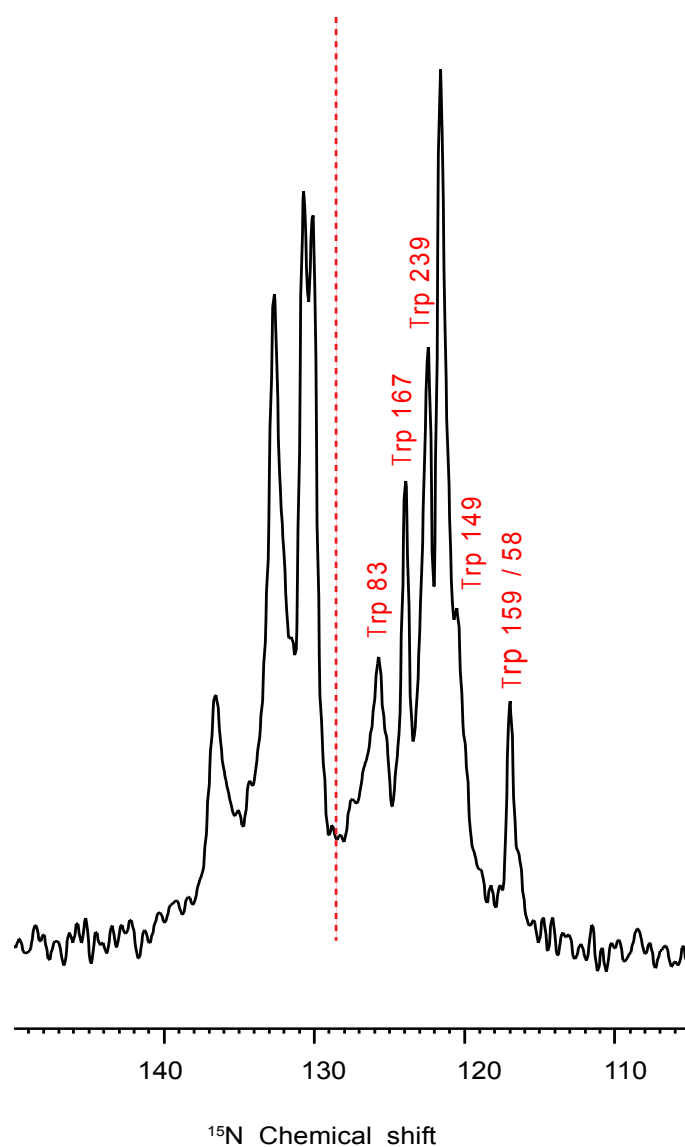


Figure 38 : ¹⁵N CPMAS spectra of α,ϵ -¹⁵N-tryptophan labeled at the backbone as well as in the side chain nitrogen.

Chapter 6-Solid State NMR characterization of PR 2D crystals

The resonances in the region between 115-130 ppm belong to the backbone and between 130-140 ppm arise from the side chain and are separated with a dashed line. The spectrum was collected at 600 MHz spectrometer at 280 K with a spinning frequency of 10 kHz and contact time of 1500 msec. The spectra is processed with zero line broadening. Approx 15 K scans were collected. The chemical shift values are indicated in ppm.

Figure 38 shows the resolution obtained with CPMAS of α,ϵ - ^{15}N tryptophan spectra, which was used as a standard spectra to compare the resolution of different preparations and hence the reproducibility of the sample preparations. The spectra shows clear demarcation of resonances from the backbone and the side chains regions. The resonances in the region between 115-130 ppm belong to the backbone and between 130-140 ppm arise from the side chain.

The REDOR experiments were initially set on a small tripeptide, ^{13}C - ^{15}N MLF for optimization of all the parameters like the 180° pulses, setting of the carrier frequencies and optimization of the number of dephasing cycles. For all these, measurements 51 rotor periods ($l_0=51$), which corresponded to dephasing time of ~ 5.1 μsec , were used after optimization to observe the maximum dephasing of the peaks for the ^{13}C - ^{15}N spin pair. The outcome of 8 such uniquely labeled pairs is discussed below. For the sake of convenience, the results are discussed in two groups.

Group A

The first group includes assignment of those tryptophan residues where the difference of the non dephased spectra and the dephased spectra was absolutely clear as can be seen in the figure 39. As indicated before, the spectra are collected first without dephasing and later with dephasing. These spectra are recorded under identical set of parameters and then compared. The results of the spectra with dephasing showed reduced intensity of the resonance in the ^{15}N CPMAS spectra of tryptophan, which was directly bonded to the ^{13}C labeled carbonyl. However, the overall shape of the ^{15}N CPMAS spectra remained the same. The difference spectra were derived in order to assign the ^{15}N chemical shift value as shown in figure 39. The chemical shift value for respective side chains is also reported wherever applicable.

In case of figure 39 c, the difference spectra shows more than one resonance. From direct visual observation of the overlapping of the 2 spectra i. e one with dephasing and other one without, it appears that the resonance at 125.16 ppm is the actual difference peak. The other resonances at ~ 120 ppm and ~ 130 ppm can arise from the backbone and the side chain natural abundance

Chapter 6-Solid State NMR characterization of PR 2D crystals

respectively. This additionally observed difference peaks could also result from partial scrambling of the valine label into isoleucine and leucine, which share the biosynthetic pathway with valine, or from the close proximity of the labels in space due to folded nature of protein. In context to this, the chemical shift value of 125.16 is most likely but not completely undebateable.

Group B

This group involves those spin pairs which did not yield clear difference spectra from the non dephased and dephased spectra respectively as shown in figure 40. In three of these spectra the resolution and signal was not comparable to the earlier group. The probable explanation is involvement of scrambling to certain extent, which reduces the dephasing effect. E.g Alanine degrading to pyruvate and glutamate, lysine to acetyl Co-A and glycine to serine and pyruvate. There is a remote possibility of the slight change in the biochemical preparation and batch-to-batch variation, which cannot be ruled out completely. However, in effect, this should not produce such a significant difference as the crystals can be obtained under wide range of conditions and slight insignificant handling error will not make a remarkable impact on the spectra.

Other reason could be insufficient number of dephasing cycles to observe the dephasing effect. In principle, 51 dephasing cycles have yielded significant dephasing for other samples but it may exhibit deviations from spin pair to spin pair.

In all there are 10 tryptophans and at given resolution on 600 MHz, there are only 6 isolated resonances in the backbone region. This indicates that the remaining 4 are obscured. In such a case, there is very little chance to observe the dephasing even if it is present.

From figure 40 A and B it can be seen that there is no difference peak for samples G₁₉₆-W₁₉₇ and D₉₇-W₉₈. For figure 40.C there are 2 peaks just above noise which appear at 121.48 and 116.81 ppm respectively. Since this is a sample labeled with Alanine and Alanines appear at position A₁₅₈-W₁₅₉ or A₁₄₈-W₁₄₉ respectively, the assignment is unambiguous. The D part of figure 40 shows a difference peak at 116.19 ppm. Although this peak is well isolated from the rest of the

Chapter 6-Solid State NMR characterization of PR 2D crystals

peaks, the resolution of the spectra is not satisfactory but can be tentatively assigned to K₅₇-W₅₈. The location of difference peaks is indicated by dashed lines in the figure 40.

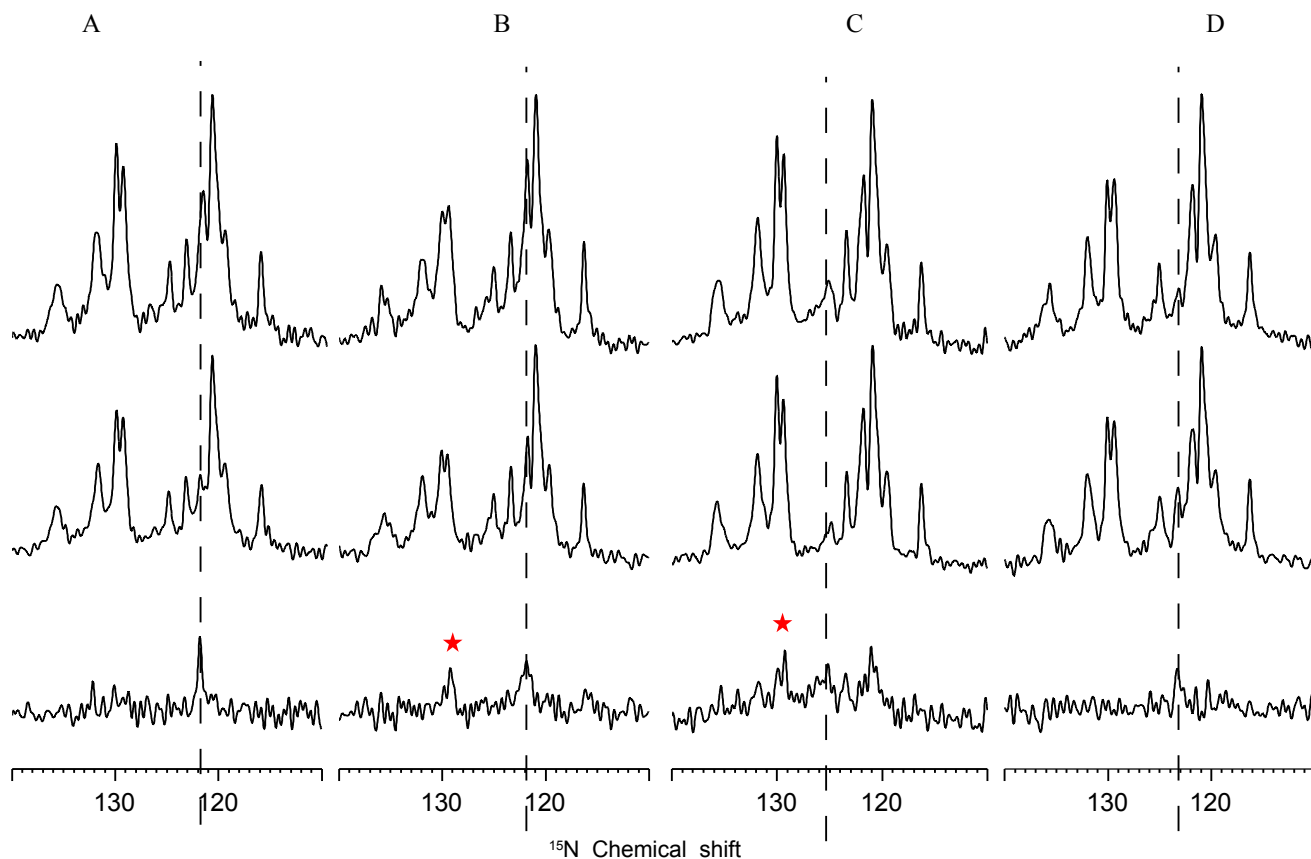


Figure 39 : REDOR spectra for group A. Each data set has 3 spectra. The top one indicates the spectrum without dephasing , middle one represents with dephasing and the spectra at the bottom summarizes the difference of the non dephased and the dephased spectra. The spectra are recorded on 600 MHz at 280 K with 10 kHz spinning speed. Since the amount of sample for each case is different, the number of scans accumulated vary from 25 K to 120 K. A: I₂₃₈-W₂₃₉, B: F₃₃-W₃₄ or F₇₃-W₇₄ C: V₈₂-W₈₃, D: L₁₆₆-W₁₆₇. The resonances at ~130 ppm in B and C part of the figure may arise due to the natural abundance of the side chains (indicated with a red star) and the peak at ~120 in C part may arise either due to the natural abundance of the backbone or close spatial proximity of the labels. The chemical shift values are indicated in ppm.

6.7.4 Conclusion

In conclusion, with the given resolution of ¹⁵N CPMAS spectra it was possible to apply REDOR for assignment of tryptophan with specific labeling scheme. In all five tryptophans could be assigned unambiguously. They include tryptophan at residues 58, 83, 149, 167 and 239. The ¹⁵N

Chapter 6-Solid State NMR characterization of PR 2D crystals

chemical shift values of these four tryptophans along with tentative assignment of tryptophan at 159 position. The assignment of tryptophan 159 is tentative because there is a slight indication from the inconclusive MnCl_2 exchange experiments for the broadening of peak and also the dephasing with REDOR was not conclusive. The dephasing effect for this particular peak was observed in ^{13}C carbonyl labeled phenylalanine as well as ^{13}C carbonyl labeled alanine samples adding to uncertainty. The final assignment is summarized in the following table.

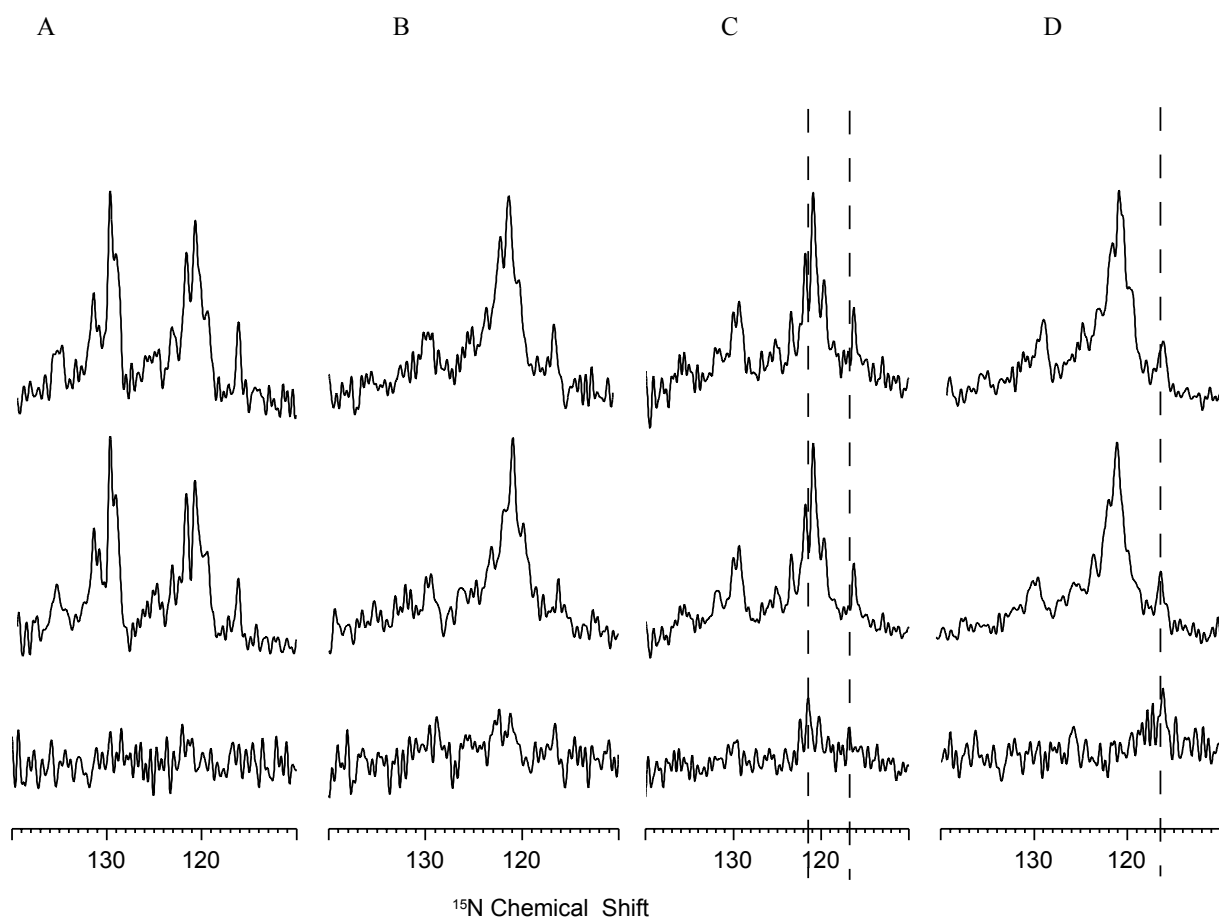


Figure 40: REDOR spectra for group B. Each data set has 3 spectra. The top one indicates the spectrum without dephasing, middle one represents with dephasing and the spectra at the bottom summarize the difference of the non dephased and the dephased spectra. The spectra are recorded on 600 MHz at 280 K with 10 kHz spinning speed. Since the amount of sample for each case is different, the number of scans accumulated vary from 25 K to 120 K. A : $\text{G}_{196}\text{-W}_{197}$, B : $\text{D}_{97}\text{-W}_{98}$, C : $\text{A}_{158}\text{-W}_{159}$ or $\text{A}_{148}\text{-W}_{149}$, D : $\text{K}_{57}\text{-W}_{58}$. The chemical shift values are indicated in ppm.

Chapter 6-Solid State NMR characterization of PR 2D crystals

Table 9 : Summary of tryptophan assignments.

Residue number	Sample	Location	Backbone Chemical shift	Side chain Chemical shift	Comments
Trp 34 / 74	F ₃₃ -W ₃₄ or F ₇₃ -W ₇₄	helical	121.84 ppm	128.64/129.86	Because there are 2 F-W pairs, the assignment cannot be precisely said for a particular F-W pair.
Trp 58 /159	K ₅₇ -W ₅₈	loop	116.19 ppm??	XXX	Because there are 2 A-W pairs, the assignment cannot be precisely said for a particular A-W pair. But there is slight indication from D ₂ O exchange experiment for this assignment.
Trp 83	V ₈₂ -W ₈₃	helical	125.16 ppm	125.16	Although additional difference peak appear but after overlapping the 2 spectra, the reported chemical shift value appears to be most probable but is still ambiguous.
Trp 149	A ₁₄₈ -W ₁₄₉	loop	119.68 ppm	XXX	Unambiguous assignment
Trp 159	A ₁₅₈ -W ₁₅₉	helical	116.98 ppm ??	XXX	Because there are 2 A-W pairs, the assignment cannot be precisely said for a particular F-Apair.
Trp 167	L ₁₆₆ -W ₁₆₇	helical	123.42 ppm	XXX	Unambiguous assignment
Trp 239	I ₂₃₈ -W ₂₃₉	helical	121.81 ppm	XXX	Unambiguous assignment

6.8 Selective ¹³C characterization of PR 2D crystals

6.8.1 U ¹³C Cysteine

6.8.1.1 Motivation

Chapter 6-Solid State NMR characterization of PR 2D crystals

In some of the studies performed on PR, it is reported that the molecular weight of *E.coli* produced PR was determined to be 36,000, approximately 9,000 more than the 27,000 predicted by the DNA sequence as judged by the SDS PAGE analysis. This has been explained on the basis of the post-translational modification of one or more of the cysteine residues [188]. Cysteine residues appear only thrice in the entire sequence of PR. They appear at residue numbers 107, 156 and 175 as shown in figure 41. First two are located in the helical region, where as the last one locates in the loop region. Since the number of cysteine residues is limited to three, it should be possible to observe individual cysteine resonances in a one dimensional experiment. This will help in the evaluation of the extent of resolution with the optimal sample preparation and at the same time provide the starting point for the assignment in the homo and heteronuclear 2D and 3D spectra in the future experiments.

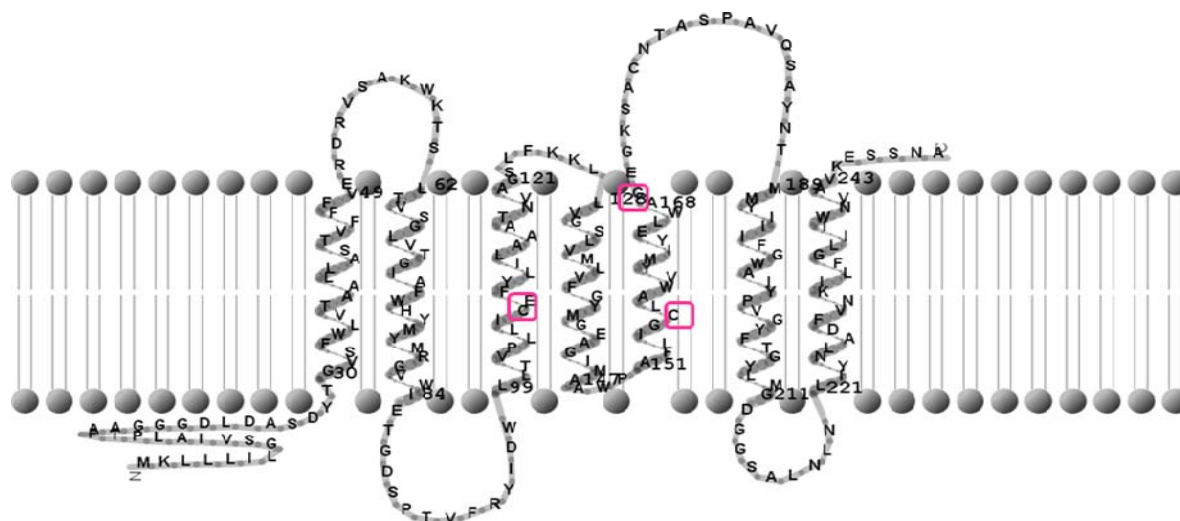


Figure 41 : The topology plot of PR amino acid sequence with 3 cysteines circled in pink.

6.8.1.2 Conclusion

From this perspective, the CPMAS spectra for U-¹³C cysteine in the crystalline preparation were measured. It was observed that the CPMAS spectra had significant contributions from the ¹³C

Chapter 6-Solid State NMR characterization of PR 2D crystals

natural abundance, which obscured the precise chemical shift measurements. In order to eliminate the background signal from the ^{13}C natural abundance double quantum filtered measurements were performed on the same samples. The CPMAS and DQF spectra are shown in the figure 42 A and 42 B. respectively.

Since the PR sequence has just 3 cysteines, it was expected that the individual cysteines would be observed in DQF. However, we could not resolve the individual cysteines except for the $\text{C}\alpha$ region where 2 peaks were observed. Based on this DQF measurement, we arrive at the following chemical shift region for these residues. The carbonyls at 174.75 ppm, $\text{C}\alpha$ at 59.46 and 61.66 ppm and $\text{C}\beta$ at 23.06 and 24.71 ppm respectively.

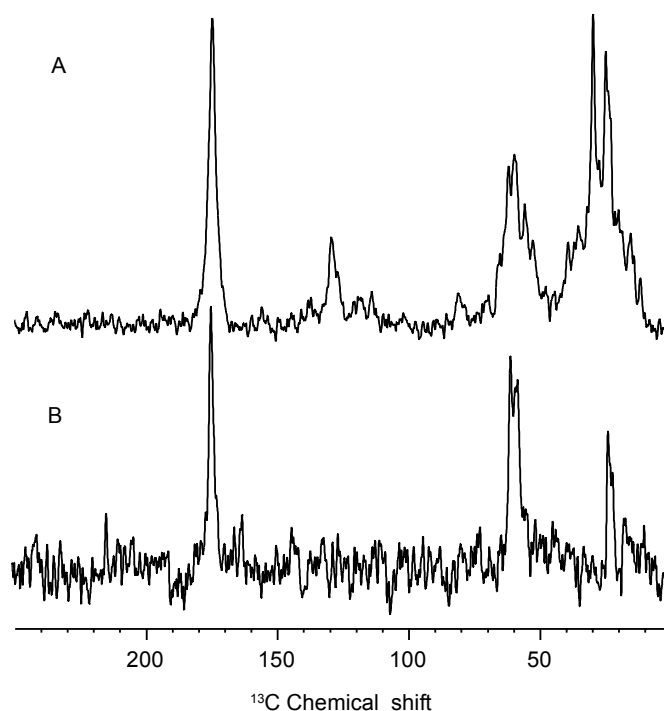


Figure 42 : ^{13}C spectra of specifically labeled cysteine. (A) CPMAS spectra (B) DQF spectra. The spectra were collected at 280 K with spinning speed of 10 kHz on Bruker 400 MHz spectrometer. Based on the DQF measurement carbonyls were assigned to 174.75 ppm, $\text{C}\alpha$ at 59.46 and 61.66 ppm and $\text{C}\beta$ at 23.06 and 24.71 ppm

Chapter 6-Solid State NMR characterization of PR 2D crystals

respectively. Line broadening of 50 is used for processing of spectra. Approx 2 K and 61 K scans were acquired respectively. The chemical shift values are indicated in ppm.

6.8.2 $U^{13}C$ Histidine

6.8.2.1 Motivation

Histidine 75 is the single histidine residue in the entire PR sequence as shown in figure 43 and is highly conserved. It has a pka of 7.2 and the protonated and deprotonated forms are widely separated in the NMR spectra. The deprotonated form resonates at ~ 250 ppm and protonated at ~ 180 ppm. The protonated and deprotonated states of histidine are likely to have an indication towards the functionality of PR and the direction of proton pumping in the natural environment and hence was investigated.

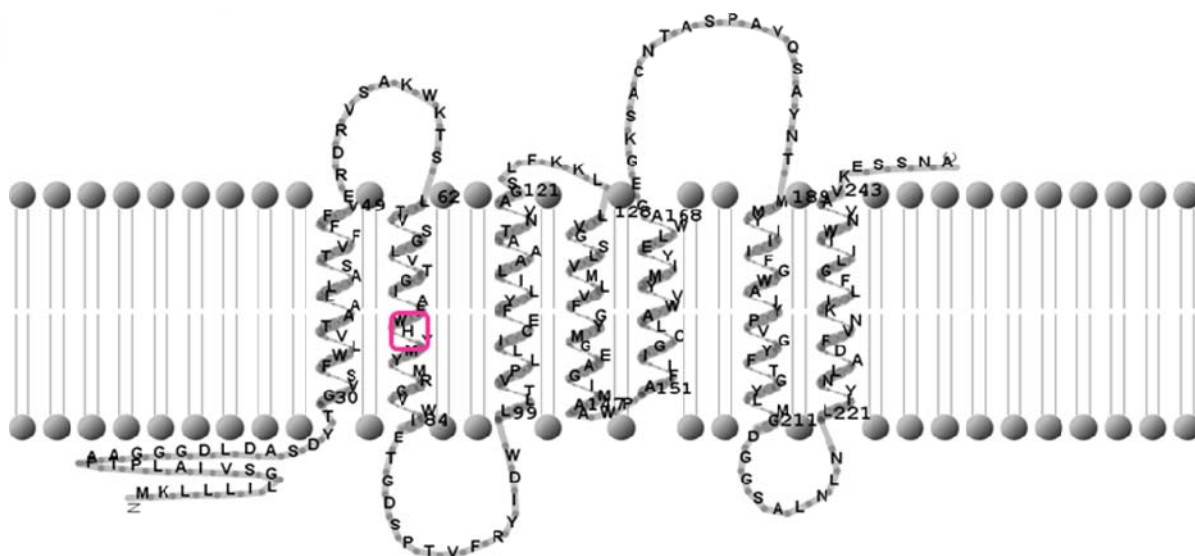


Figure 43 : The topology plot of PR amino acid sequence with histidine 75 circled in pink.

6.8.2.2 Conclusion

Similar to the cysteines where the CPMAS spectra had contributions from the natural abundance,

Chapter 6-Solid State NMR characterization of PR 2D crystals

the histidine too observed similar effect. As a result the DQF measurement was performed. Based on DQF measurements the chemical shift values for histidine were derived and can be tentatively assigned to $C\alpha=56.13$ ppm, $C\beta=26.72$ ppm, $C\gamma=129.6$ ppm, $C\delta_1=136.29$ ppm, $C\delta_2=113.2$ ppm and $CO=176.2$ ppm respectively.

In view of the above stated importance of histidine and its solitary position in the sequence, the CPMAS and the DQF spectra were attempted and are shown in figure 44 A and 44 B respectively. The poorly resolved side chain resonances correlates well with the similar resolution for the ^{15}N histidine and lysine labeled spectra as shown in figure 33. However, it should be noted that that there is 6x His tag, which was not cleaved prior to these measurements.

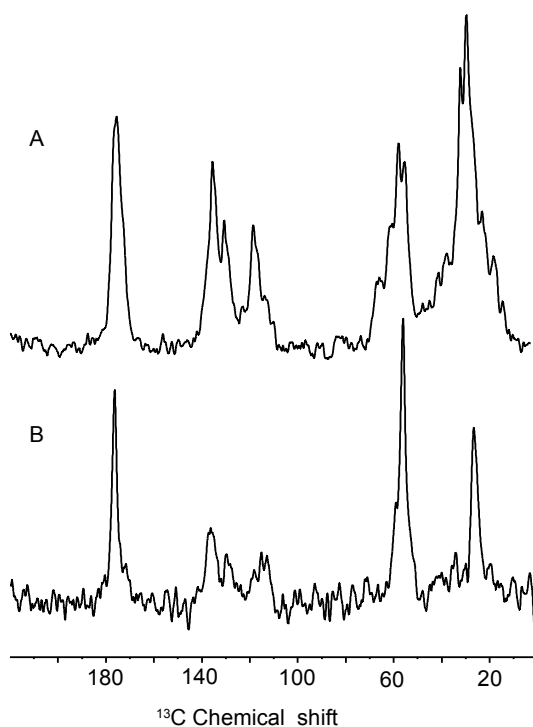


Figure 44 : ^{13}C 1D CPMAS spectra of specifically labeled histidine. (A) CPMAS spectra (B) DQF double quantum filtered spectra. The spectra were collected at 280 K with spinning speed of 10 kHz on Bruker 400 MHz spectrometer. The spectra is processed with line broadening of 100 Approx 2 K and 61 K scans were acquired respectively. The chemical shift values are indicated in ppm.

6.9 Uniform ^{13}C characterization of PR 2D crystals

6.9.1 Uniformly labeled ^{13}C samples

Chapter 6-Solid State NMR characterization of PR 2D crystals

6.9.1.1 Motivation

Based on Electron Microscopy data of PR 2D crystals, it is evident that the protein is in the restricted mobility state. As per our initial hypothesis, this restricted mobility and homogeneity of the protein should yield well-resolved spectra. In order to observe this, the first step to begin was to make U-¹³C sample and obtain the first picture of the line shapes and the resolution obtained with crystalline preparation. This sample preparation and measurement was important for the initial optimization of parameters for further experiments.

6.9.2 Approach

As introduced before, MAS was applied on the samples and Cross polarization and Direct polarization spectra were collected at different temperatures. The temperature scan on the U-¹³C samples was performed in order to optimize the measuring parameters. Once the initial parameters were optimized selectively labeled and unlabeled samples were measured to determine the specific line shapes.

6.9.3 Temperature scan

The set of CPMAS and DPMAS was acquired over a range of temperatures from 210 K upto 285 K as shown in the figure 45. The spectra were collected at 210 K, 225 K, 240 K, 260 K, 280 K and 285 K respectively. By comparison, between the two spectra at the same temperature, it was observed that the pattern of spectra is comparable. This observation indicates that the protein is in restricted mobility arrangement. The intensity of signal with CPMAS was approx 1.5 times more than that of DPMAS signal.

When the intensity of the overall signal at different temperatures was compared, it was observed that the intensity of signal reduces by a factor of 4 as the temperature was raised from 210 K to 285 K. The loss of signal intensity at higher temperatures could be explained based on reduced CP efficiency due to increasing molecular motion. The trend of reduction in the signal intensity, with increasing temperature was similar for CPMAS and DPMAS measurements.

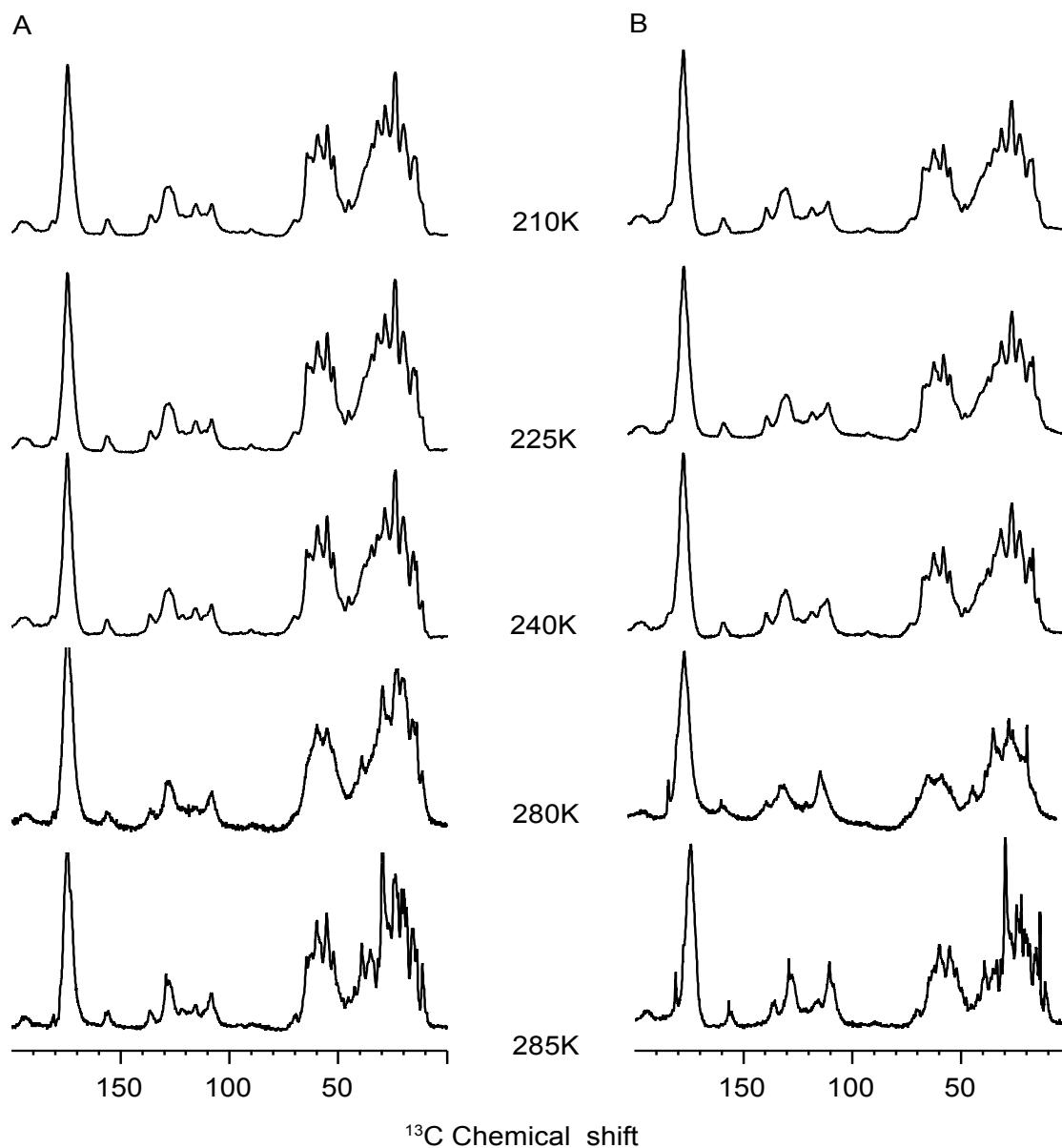


Figure 45 : Temperature scan of U-¹³C PR crystalline samples (A) Cross polarization and (B) Direct polarization spectra of U ¹³C PR 2D crystals over a range of temperature. The spectra were acquired on Bruker 600 MHz spectrometer with 10 kHz spinning frequency. A total of 8 mg sample was used and 512 scans were accumulated. The spectra clearly indicate increased resolution at higher temperature. The chemical shift values are depicted in ppm units and line broadening of 10 is applied for processing. All the spectra are normalized to the carbonyl peak intensity at 180 ppm. The chemical shift values are indicated in ppm.

6.9.1.4 Conclusion

The improved resolution at room temperature is indicative of tight and orderly packing of the protein. However, the measurements at higher temperatures are unpractical for long-term sensitive measurements due to the risk of dehydration, which may cause protein to denature. In order to avoid this unfavorable situation but at the same time not compromising on resolution and signal, a temperature of 280 K was chosen as the optimized temperature for further measurements. 280 K is just about the freezing temperature so the biological loss to the sample for the long term experiments can be delayed if not completely avoided.

6.10 ^{13}C labeled samples with different labeling schemes

6.10.1 Motivation

The main purpose of using the different labeling schemes is to reduce the spectral overlap and the effects from line broadening encountered in uniformly ^{13}C -labeled proteins. The selectivity and extent of labeling can contribute to simplification of the NMR spectra. The labeling sites can be selectively labeled by supplying specifically ^{13}C -labeled glucose or differentially labeled glycerol as the sole carbon source in the expression medium. Certain carbon sites with ^{13}C at high levels can be labeled while the other sites remain completely unlabeled. This facilitates resonance assignment and the measurement of long-range distances. The differential labeling pattern achieved is due to the cyclic nature of the enzymatic reactions, which spread the single label in the starting compound to multiple positions in the carbon skeletons of the cascading amino acids [189].

For this, two different kinds of samples were prepared. One was 2- ^{13}C glycerol labeled and the other one spin diluted or selectively unlabeled sample. Both of these labeling schemes were carried out using *E.coli* expression system.

6.10.1.1 2- ^{13}C Glycerol labeled samples

Chapter 6-Solid State NMR characterization of PR 2D crystals

Isotope labeling is primary requirement for sequence specific resonance assignment and for estimation of distance restraints and torsion angle. Limited by the poor efficiency of the ^{15}N - ^{13}C polarization transfer and the limited resolution of the proton spectra, ^{13}C - ^{13}C homonuclear restraints are of utmost importance for the structural determination. These measurements are obscured in the fully labeled ^{13}C samples by dipolar truncation [190, 191]. There are several ways to overcome this effect but a combination of recoupling method and dilution of ^{13}C spin with differential labeling is attempted [192].

For our measurements, 2- ^{13}C Glycerol was used as a label to reduce the spectral overlap by reduction of dipolar truncation effect and for observation of long-range interaction. For further discussion, this sample shall be referred to as “2- ^{13}C Glycerol labeled PR”. The detailed labeling pattern expected to be observed with 2- ^{13}C glycerol labeling is shown in the following picture 46.

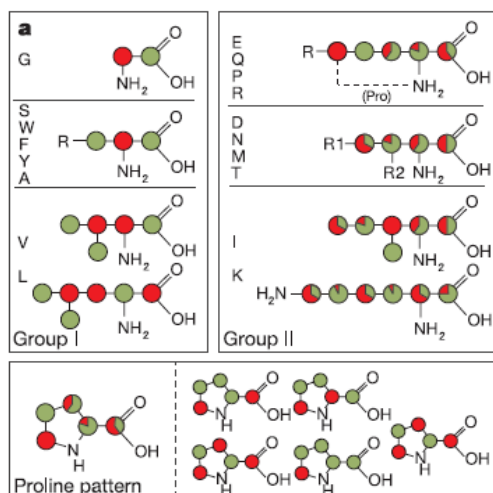


Figure 46 : Differential labeling patterns with 1-3 ^{13}C glycerol and 2 ^{13}C glycerol. The green colour corresponds to the degree of ^{13}C labeling pattern obtained by growth on [1,3- ^{13}C] glycerol; the opposite labeling pattern, obtained by growth on [2- ^{13}C] glycerol, is represented in red. In cases with mixed labeling, the percentage label from [2- ^{13}C] glycerol and [1,3- ^{13}C] glycerol for a particular atom is represented using relative red/green coloring. This picture is taken from [152].

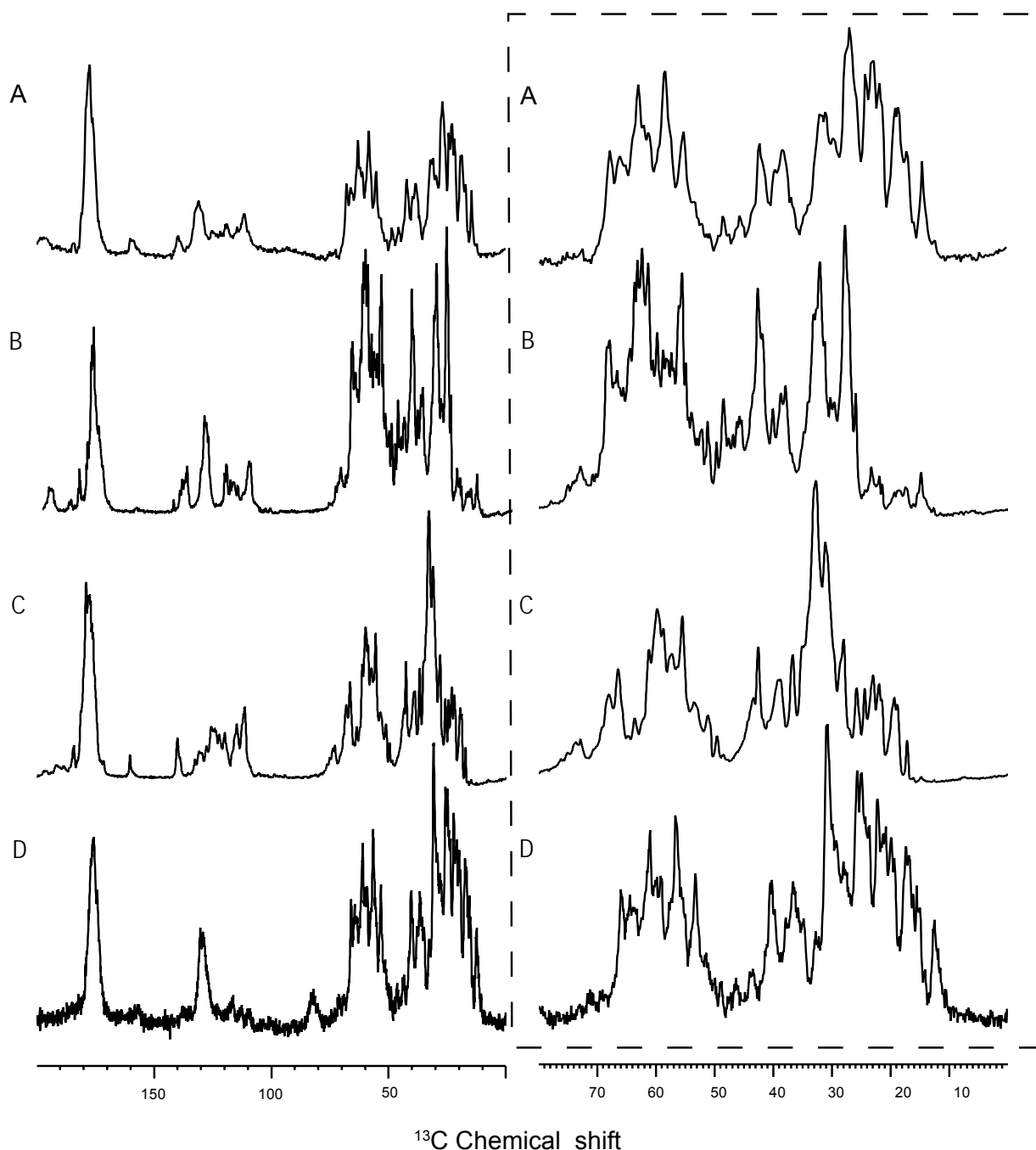


Figure 47 : Comparison of different labeling schemes with U- ^{13}C spectra of PR in 2D crystalline arrangement. (A) U- ^{13}C sample measured on Bruker 600 MHz spectrometer at 280 K and a spinning speed of 10 kHz. For processing zero line broadening is applied and approx 100 K scans were accumulated. (B) $2\text{-}^{13}\text{C}$ -Glycerol labeled measured on Bruker 600 MHz spectrometer at 280 K and a spinning speed of 10 kHz. For processing zero line broadening is applied and approx 100 K scans were accumulated. (C) Selectively unlabeled sample measured on Bruker 600 MHz spectrometer at 280 K and a spinning speed of 10 kHz. For processing zero line broadening is applied and approx

Chapter 6-Solid State NMR characterization of PR 2D crystals

100 K scans were accumulated (D) U-¹³C sample measured on Bruker 850 MHz spectrometer at 280 K and a spinning speed of 10 kHz. For processing zero line broadening is applied and approx 100 scans were accumulated. The region between the 0-70 ppm indicates the aliphatic region. Between 100 -150 ppm indicates the aromatic region and rest is the carbonyl region. The chemical shift values are shown in ppm. The boxed region displays detailed picture of the aliphatic region of the corresponding spectra.

6.10.1.2 Selectively unlabeled U-¹³C Glucose labeled sample

Selectively unlabeled or reverse labeling scheme was first reported for studying the phenylalanine residues of the protein [193]. The positive side effects of the reduced labeling are simplification of the assignment of the long-range correlations and an overall improved resolution as a result of suppressing homonuclear one-bond *J*-couplings. The dipolar truncation effect also plays an important role for simplification of the spectra. For preparation of such spin-diluted samples unlabeled of 9 amino acids was carried out. These include Alanine, Glycine, Isoleucine, Leucine, Phenylalanine, Serine, Threonine, Valine and Tyrosine. For further discussions this sample shall be referred to as “U-¹³C spin diluted sample”

Figure 47 indicates the comparative spectral resolution with different labeling schemes. The boxed region highlights the aliphatic regions in the corresponding 1D CPMAS spectra on the left.

6.10.1.3 ¹³C - ¹³C 2D Homonuclear correlation measurements on U-¹³C labeled samples

6.10.1.3.1 Motivation

¹³C-¹³C 2D homonuclear experiments measure the through space correlations and have the ability for assignment of all carbon resonances of one amino acid residue as well as long distance restraints with a single measurement. Such experiments rely on dipolar coupling for the magnetization transfer in a distance dependent manner between nuclei. These homonuclear measurements are widely popular as it is comparatively easier to set up the experiment and sidetracks the problems associated with the measurement of ¹H signals and low efficient magnetization transfers between ¹³C and ¹⁵N nuclei.

6.10.1.3.2 Approach

Rotational resonance NMR provides a unique approach for obtaining high-resolution structural data in membrane systems and has been used to establish intermolecular contacts [194]. It is an established method for long range distance measurements in reconstituted membrane proteins [195]. It is a homonuclear recoupling technique under MAS where through space dipole dipole coupling is reintroduced and hence measured without application of any specific radio frequency pulse [196]. The primary goal of the rotational resonance experiment is to determine the dipolar / coupling constant from which the internuclear distance may be calculated. Carbon-carbon separations as large as 6.8Å have been successfully determined. Under rotational resonance condition the chemical shift difference between the two homonuclear spin ω_1 and ω_2 is equal to $n\omega_R$ and the rotational resonance condition is represented as

$$n\omega_R = (\omega_1 - \omega_2)$$

where $n = \pm 1, \pm 2$, ω_R is the sample spinning speed and ω_1 and ω_2 are the isotropic resonant frequencies of spins 1 and 2 respectively.

Under this specified condition, the dipolar coupling interaction is reintroduced but just between spins 1 and 2. The need of reintroduction of dipolar couplings say for ^{13}C - ^{13}C arises because of the low gyro magnetic ratio of ^{13}C and because of the fact that ^{13}C - ^{13}C dipolar couplings are of the order 2 kHz which cannot be detected at higher spinning speed [196]. At rotational resonance the ^{13}C - ^1H dipolar couplings aid the ^{13}C spectral overlap which is needed for magnetization transfer [197]. The rotational resonance condition is applied for time “ t ” which is equal to the integral number of rotor periods to allow exchange of magnetization between the two spins. The constant wave irradiation has to match the multiples of the spinning speed. The line shapes obtained can be simulated and the values of homonuclear dipolar constants can be calculated. The basic pulse sequence of DARR is shown in figure 48.

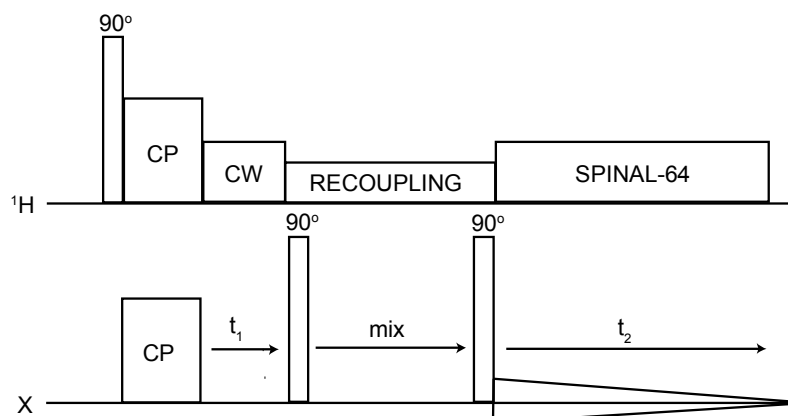


Figure 48 : DARR pulse sequence indicating the first 90° pulse on proton channel, followed by cross polarization where the magnetization is transferred to the X nuclei. Weak proton decoupling occurs during the heteronuclear evolution time. The 90° pulse on X nuclei transfers the magnetization to the z-axis. After second mixing time, the 90° pulse flips the magnetization back to the X-Y plane. Finally, the signal is detected with proton decoupling.

6.10.2 Results and Discussion

6.10.2.1 U- ^{13}C uniformly labeled samples

Initial optimization of the parameters was carried out on ^{13}C labeled glycine. Thereafter the fine optimization of the parameters was done on the sample itself. For arriving at the best appropriate mixing time for the ^{13}C - ^{13}C homonuclear measurements, a set of DARRs with different mixing time were recorded and analyzed prior to the actual measurements. The different mixing times used for the buildup curves were 25 ms, 50 ms, 75 ms, 100 ms, 125 ms, 150 ms, 175 ms, 200 ms, 250 ms, 300 ms, 800 ms and 1.2 sec. From these experiments, using the python scripts (developed by Dr. Jacob Lopez, personal communication) the buildup curves for a set of 3- 5 cross peaks were calculated for the spin diluted as well as the 2- ^{13}C glycerol labeled samples as shown in figure 49 A and 49 B. The buildups are clearly seen in the analysis and a range of optimal mixing times was calculate as shown in figure 50. Based on these buildup curve analysis, the optimum mixing time for U- ^{13}C was calculated to be ~ 125 msec. For calculation of the buildups representative cross peaks from different parts of the spectra were selected and are explained in the following figure and legend.

Chapter 6-Solid State NMR characterization of PR 2D crystals

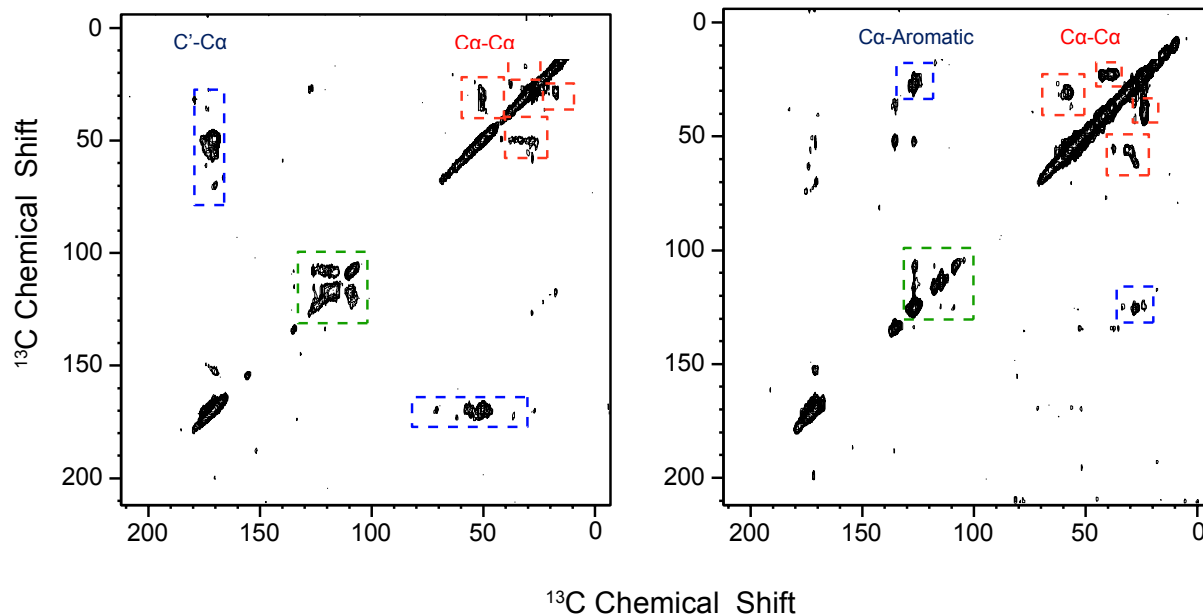


Figure 49 : Overview of the 2D DARRs used for calculation of the buildups. A) spin diluted uniformly ^{13}C labeled PR 2D crystals B) 2 ^{13}C -Glycerol labeled PR 2D crystals. The DARRs displayed were used for buildup curves and were acquired with 300 ms mixing time and measured at 280 K at a 10 kHz MAS spin rate. The spectrum was acquired with 1956 points in the direct dimension and 128 points in the indirect dimension. Both spectra were measured at 600 MHz spectrometer using TPPI and 128 transients per slice. For processing exponential line broadening of 20 Hz in the direct dimension and a squared sine modulation in the indirect dimension was applied. The cross peaks used for calculation of buildup curves were selected from different regions of the spectra. E.g. red blocks indicate the cross peaks between the aliphatic regions and green represent the cross peaks between the aromatics and blue cross peaks between either a) carbonyls and aliphatic region or b) aromatics and aliphatics. The chemical shift values are indicated in ppm.

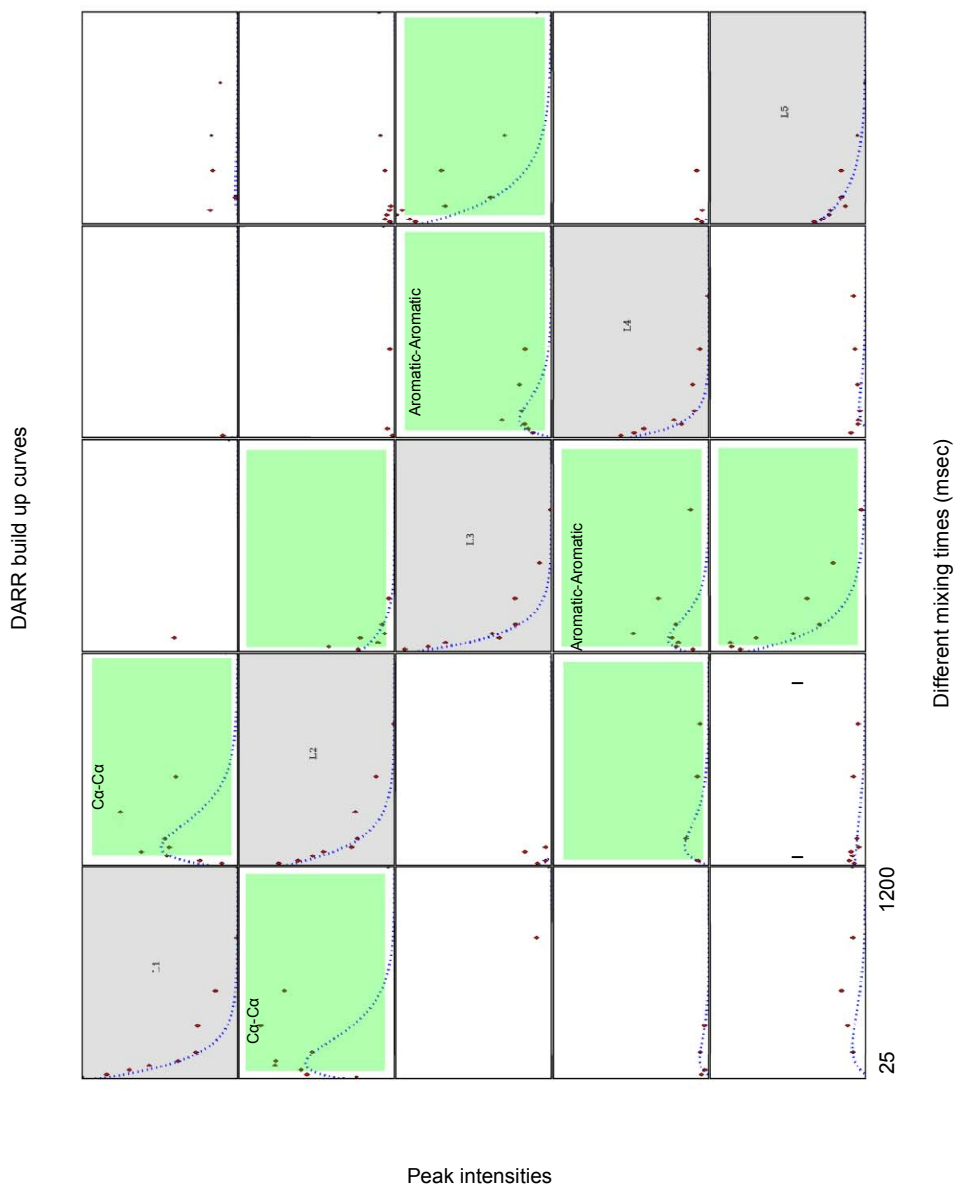


Figure 50 : Overview of diagonal and cross-peak buildup at different mixing times fitted using the full matrix approach for the “ ^{2-13}C glycerol PR labeled” sample. Horizontal axes represents in individual graphs represent the mixing time from 25 msec to 1.2 sec. The vertical axes represent the diagonal and cross-peak volumes scaled individually from 0 to 1 for each graph. The filled red circles show measured peak volumes while the dotted blue line represents the best fit to the data points using the full matrix analysis. The diagonal peaks are represented by the grey boxes and the green boxes indicate the buildup pattern for the selected cross peak.

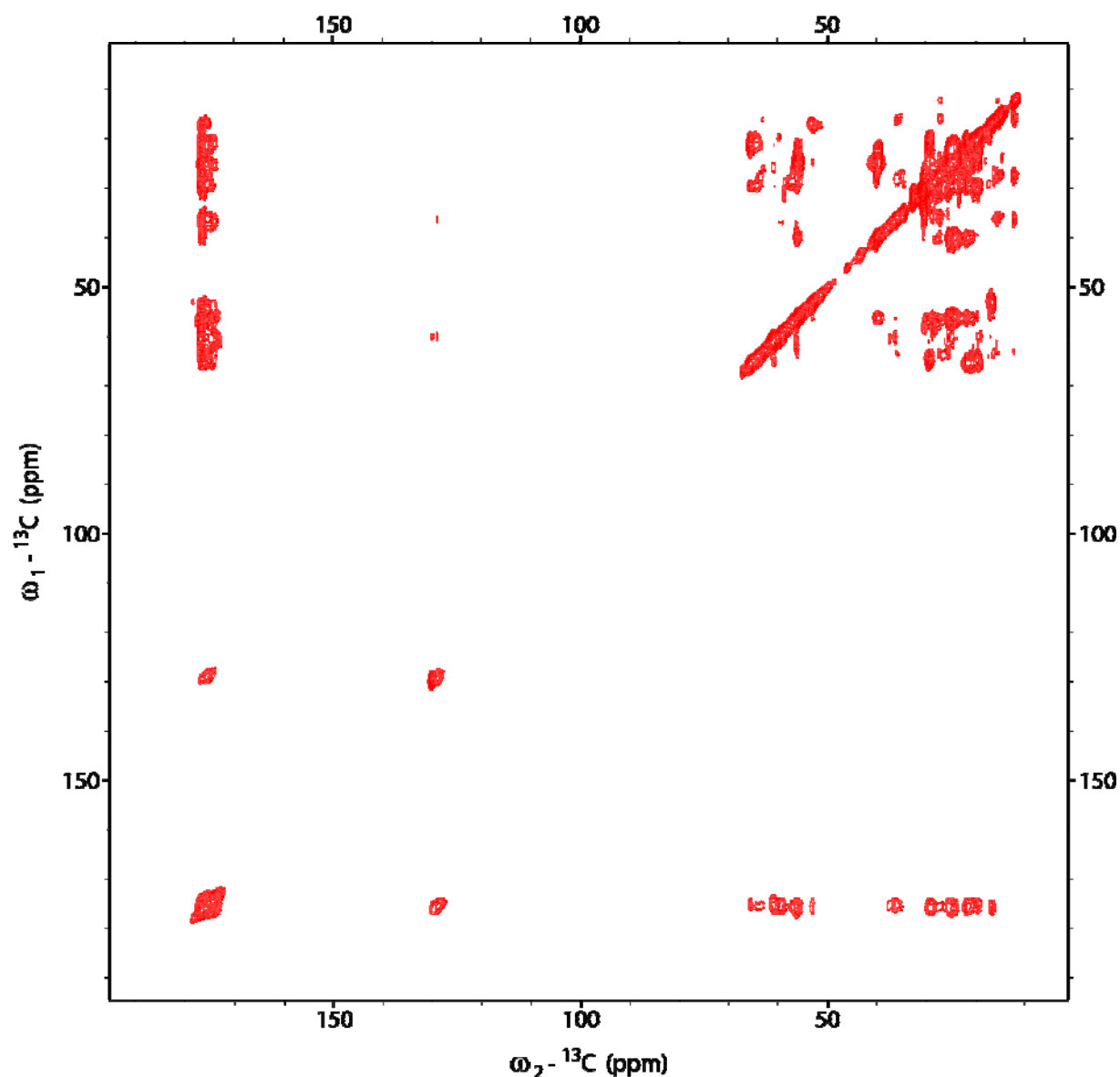


Figure 51 : 2D ^{13}C - ^{13}C DARR experiment on uniformly labeled ^{13}C labeled 2D crystalline PR with 125 msec mixing time. The DARR was measured at 280 K and 10 kHz spinning speed. The spectra were acquired in phase sensitive mode on Bruker 850 MHz spectrometer. The spectrum was acquired with 1796 points in the direct dimension and 256 points in the indirect dimension. 512 transients were collected per slice. The spectrum was processed with exponential line broadening of 20 Hz in the direct dimension and a squared sine modulation in the indirect dimension. Only positive contour levels are shown. The chemical shift values are indicated in ppm.

The 2D DARR spectra with 125 msec mixing time acquired on 850 MHz spectrometer with U^{13}C labeled PR 2D crystalline preparation is shown in figure 51. The spectra shows improved resolution as compared to the earlier spectra, which were measured on 600 MHz. However direct

Chapter 6-Solid State NMR characterization of PR 2D crystals

comparison is not possible because the earlier mixing time was in the range of 25 msec. This short mixing time is known to yield interresidue crosspeaks. Further comparison with the earlier 2D spectra shows some improvement in the resolution especially in the aliphatic region. The 1D spectra recorded at 850 MHz spectrometer have already shown to have improved resolution in the aliphatic region as shown in figure 47. Similarly, it was expected that the spectral overlap would be reduced to certain extent in the 2D DARRs. In some regions especially for alanines, isoleucine, serines, threonines and the glutamic acid, which are normally well separated, showed slight improvement as shown in the figure 52, 53, 54 and 55. Figure 52, 53, 54 and 55 are regions extracted from the figure 51 and have different contour levels.

The alanines, isoleucines and particularly glutamic acid had earlier shown no spectral resolution. The best observed resolution was in the region of glutamic acid. where almost all the 7 glutamic acid could be resolved as shown in figure 55. The serine and threonines showed no traces of existence in the previous spectra with shorter mixing time. However, they could be well observed with the 2D DARRs recorded on 850 MHz spectrometer with 125 msec mixing time.

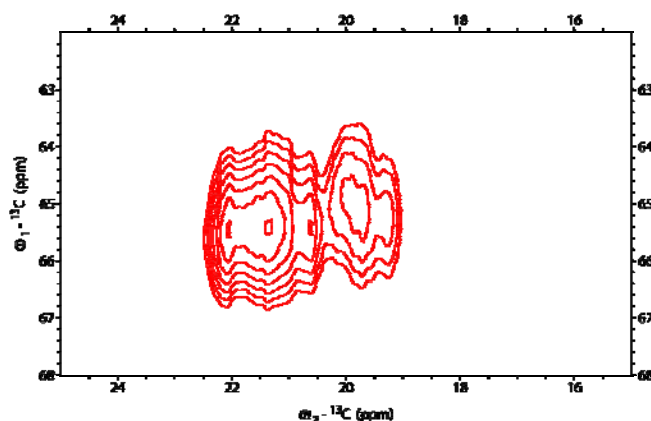


Figure 52: Section of 2D DARRs acquired on 850 MHz spectrometer at 280 K and 10 kHz spinning speed with 125 msec mixing time. The section displays the alanine region. The spectra were acquired in phase sensitive mode on Bruker 850 MHz spectrometer. The spectrum was acquired with 1796 points in the direct dimension and 256 points in the indirect dimension. 512 transients were collected per slice. The spectrum was processed with exponential line broadening of 20 Hz in the direct dimension and a squared sine modulation in the indirect dimension. Only positive contour levels are shown. The chemical shift values are indicated in ppm.

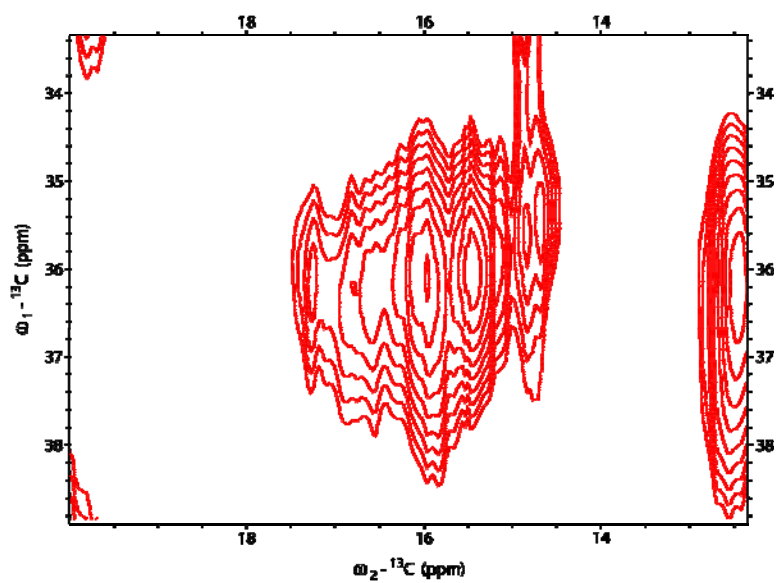


Figure 53 : Section of 2D DARRs acquired on 850 MHz spectrometer with 125 msec mixing time at 280 K and 10 kHz spinning speed. The section displays the isoleucine region. The experimental details are same as figure 52.

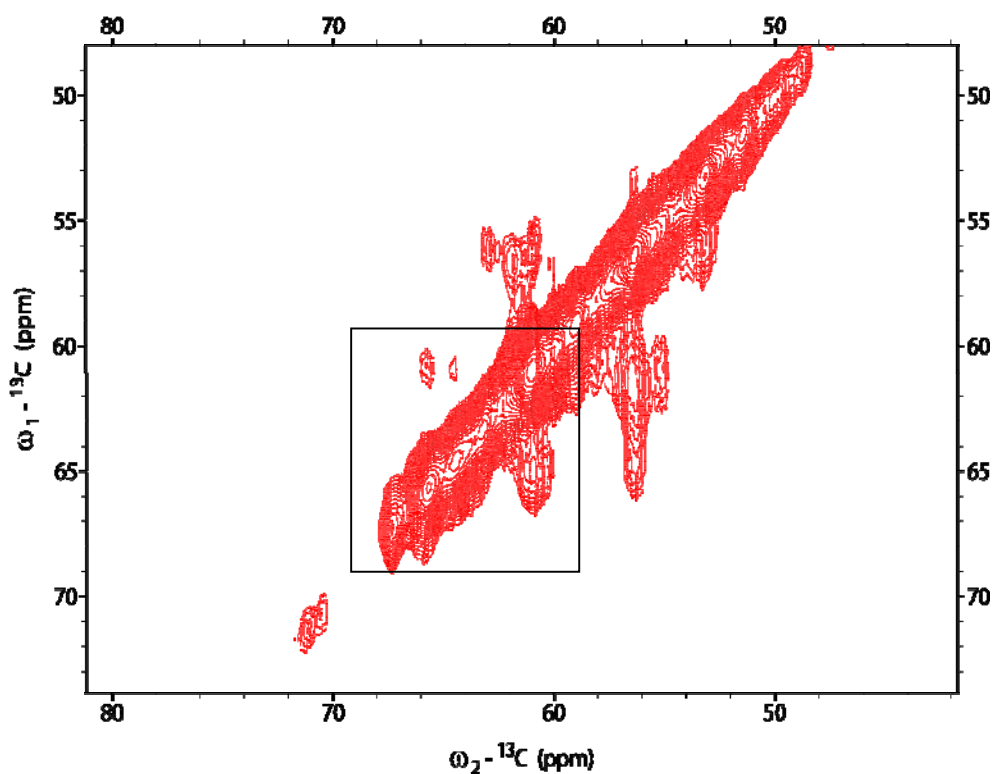


Figure 54 : Section of 2D DARR acquired on 850 MHz spectrometer with 125 msec mixing time at 280 K and 10 kHz spinning speed. The section displays the serine and the threonine, and region for threonines is boxed. The experimental details are same as figure 52.

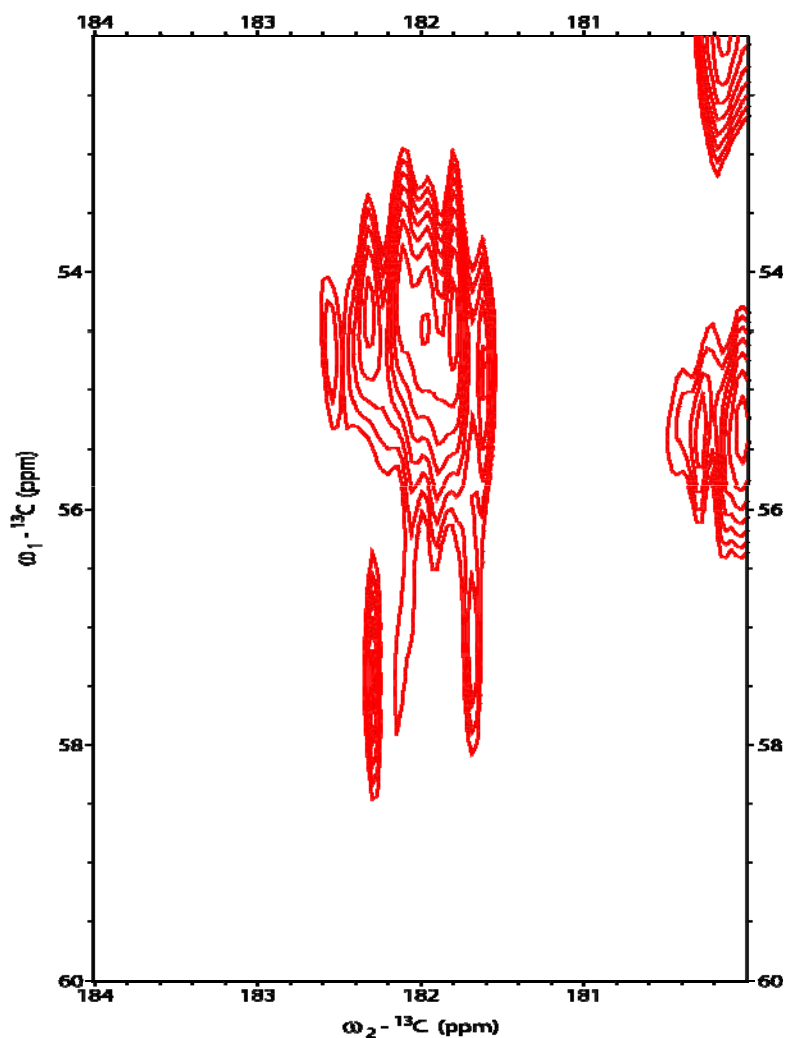


Figure 55 : Section of 2D DARRs acquired on 850 MHz spectrometer with 125 msec mixing time at 280 K and 10 kHz spinning speed. The section displays the glutamic acid region. The experimental details are same as figure 52.

6.10.2.2 ¹³C spin diluted sample

The preparation of spin diluted sample has been already discussed in materials and method section 2.2.1.18. In short, 9 amino acids were selectively unlabeled. The purpose behind selective unlabeled was to reduce the spectral overlap by eliminating the cross peaks due to amino acids that are more abundant and hence obscure the cross peaks between comparatively less abundant residues. For this purpose all the amino acids which occur more than 10 times in the amino acid sequence were unlabeled. The 2D DARR was acquired based on the optimum

Chapter 6-Solid State NMR characterization of PR 2D crystals

mixing time as a result of build up curve analysis. The spectra was collected with 125 msec mixing time and is shown in figure 56.

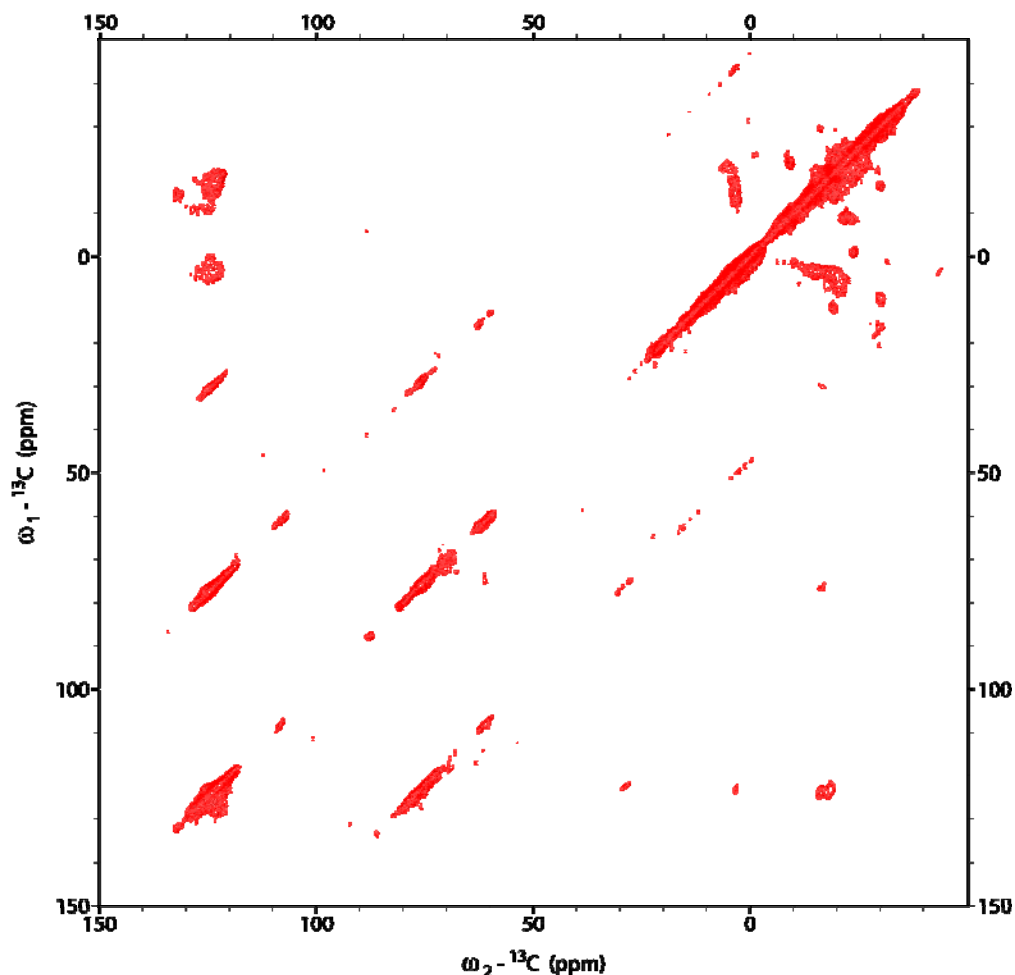


Figure 56 : 2D ${}^{13}\text{C}$ - ${}^{13}\text{C}$ DARR experiment on selectively unlabelled 2D crystalline PR. The DARR was measured at 280 K and 10 kHz spinning speed with 125 msec mixing time. The spectra were acquired in phase sensitive mode on Bruker 850 MHz spectrometer. The spectrum was acquired with 1796 points in the direct dimension and 256 points in the indirect dimension. 64 transients were collected per slice. The spectrum was processed with exponential line broadening of 20 Hz in the direct dimension and a squared sine modulation in the indirect dimension. Only positive contour levels are shown. The chemical shift values are indicted in ppm.

For comparison of the reduced spectral overlap the detailed picture of the aliphatic region is displayed in figure 57 A for the U- ${}^{13}\text{C}$ labeled sample and 57 B for the selectively unlabeled sample for the same mixing time of 125 msec. It is clear that there is a reduction in the spectral

Chapter 6-Solid State NMR characterization of PR 2D crystals

overlap. However all the aminoacids, which were finally labeled, had similar range of chemical shift values and hence individual identification of group types was not possible.

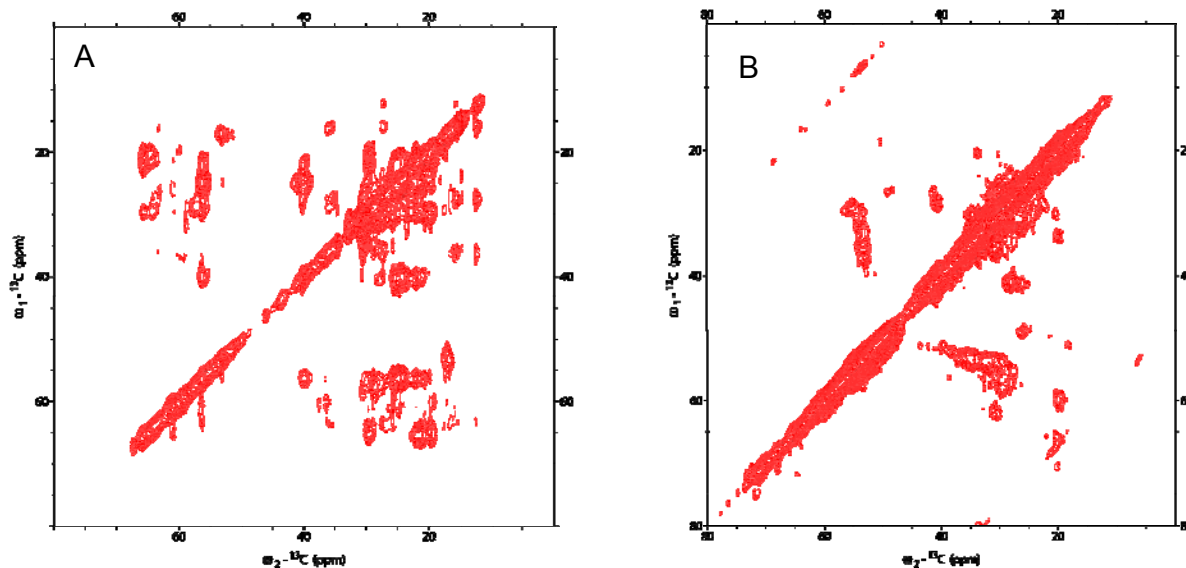


Figure 57 : ^{13}C - ^{13}C homonuclear correlation DARR spectra for uniformly labeled ^{13}C PR 2D crystals and ^{13}C spin diluted PR 2D crystals. The data was acquired with 125 msec mixing time. The spectrum is same as described as figure 51 and figure 56 and here only aliphatic region is shown.

6.10.3 Conclusions

In principle it is possible to achieve a good signal to noise with feasible number of scans and increments in the indirect dimension. This is achievable because of the dense packing the protein in the 2D crystalline state. The improved resolution as judged by the resolution of 7 glutamic acids in the 2D DARR spectra are encouraging as it can be inferred that the individual amino acids can be resolved despite seven transmembranous overlapping helices. The selective unlabeled for reduction in the spectral overlap can be successfully applied, however for such unlabeled, aminoacids with well-separated chemical shift region should be chosen.

In the light of these measurements, it appears that the high resolution spectra for PR 2D crystals is achievable. However, more efficient labeling schemes are required for further characterization. Improvements can be made biochemically by removing the slight impurities, which might have hindered better crystal formation. Since the 2D crystallization can be achieved under wide range of conditions, further modification of these conditions e.g. crystallization without the histag, crystallization with different variants of PR or crystallization using special lipids as described by

Chapter 6-Solid State NMR characterization of PR 2D crystals

Liang et al [109] can be a good starting point. In the light of data presented in this thesis, there is an explicit evidence for inhomogeneity in the protein. Further attempts involving trials to achieve a completely homogenous sample prior to the crystallization would be worth the efforts.

Appendix

Appendix

Abbreviations

ATP	Adenosine Tri Phosphate
CaCl ₂	Calcium Chloride
DAG	Diacyl glycerol
DGK	Diacyl Glycerol kinase
DTT	Dithiothreitol
EDTA	Ethylenediaminetetraacetic acid
EGTA	Ethylene glycol tetraacetic acid
MgCl ₂	Magnesium Chloride
Na(CH ₃ COO)	Sodium Acetate
NADH	Nicotinamide Adenine Dinucleotide Phosphate
NiCl ₂	Nickel Chloride
NMR	Nuclear Magnetic Resoance
PA	Phosphatidic Acid
PEG	Poly Ethylene Glycol
PIPES	1,4-piperazinediethanesulfonic acid
Zn(CH ₃ COO) ₂	Zinc Acetate

Motivation

The major focus of this project was to attempt for 2D crystallization of Diacyl Glycerol kinase, a small membrane protein from *Salmomella typhimurium*, to obtain an optimal sample preparation and set up 3D crystallization trials, which could later be used for structural and functional studies with solid state NMR.

This protein was a one of the targets of ProAMP project, which aimed at structural and functional characterization of small membrane protein targets. The inherent idea was to focus on small membrane protein for complete proteomic, bioinformatics and functional analysis for prediction of relevant targets in pathogens. It also included implementation of 2D and 3D crystallization screens with the selected target and development of novel NMR techniques to

Appendix

obtain structural and functional information in either solid state or liquid state NMR methods.

Diacyl glycerol kinase

DGK is a typical membrane protein and it has 3 alpha helical transmembranous regions [198]. It has a conserved catalytic domain and an array of other conserved motifs that are thought to play a role in lipid-protein and protein-protein interactions in various signaling pathways. Functionally it phosphorylates the second-messenger DAG to phosphatidic acid. Since DAG is regenerated at the (plasma) membrane, DGK is therefore believed to be activated there [199]. The functionally active unit of DGK is thought to be a trimer [200]. This protein has virtually no detectable sequence homology to other kinases and lacks sequence motifs typically present in enzymes catalyzing phosphoryl transfer [201, 202]. The molecular weight of this smallest known kinase is 13 kDa and number of amino acid residues are 122. The protein is over-expressed in *E.coli* to yield ~30 mg of protein per liter of culture [203]. The topology plot of the protein is shown in figure 58.

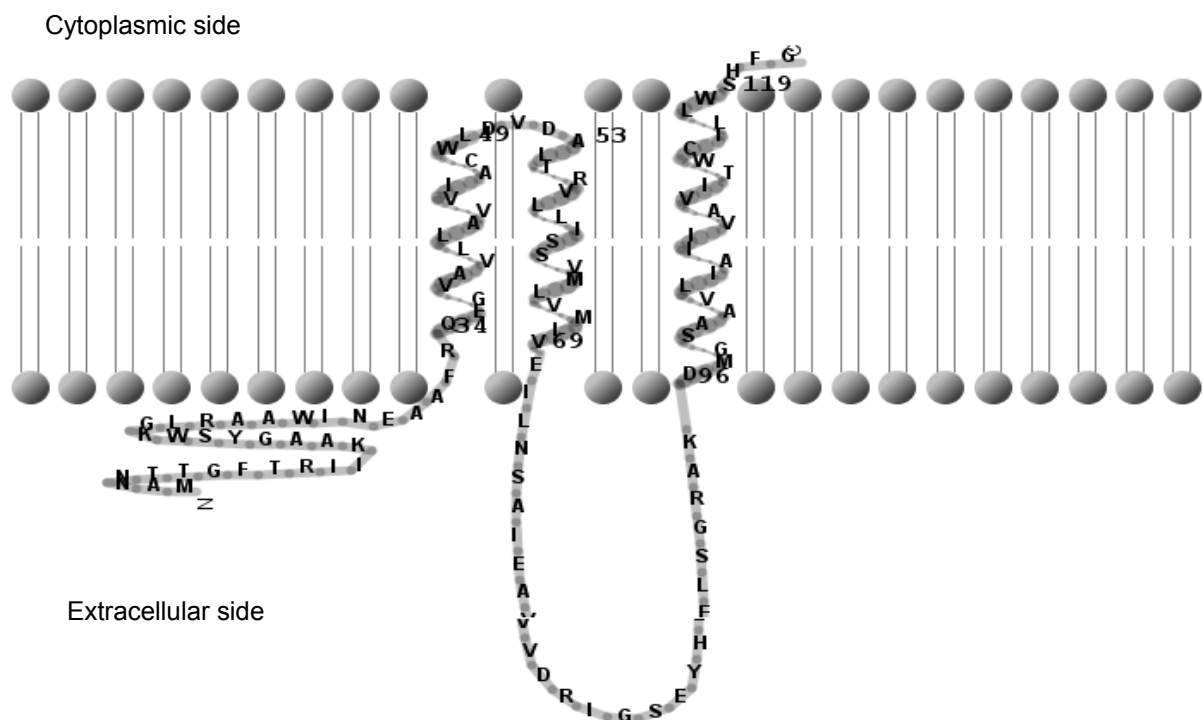


Figure 58 : Topology plot of Diacylglycerol kinase. The SwissProt sequence accession number is P0ABN1.

Appendix

3D crystallization

Previous attempts with DGK from *E.coli* were successful in obtaining 3D crystals but they did not diffract. However, these 3D crystals yielded well resolved NMR spectra [204]. In context to this, initial trials for 3D crystallizations for DGK from *Salmonella typhimurium* were attempted with the intention of obtaining 3D crystals, which could be used for structural and functional studies with solid state NMR and if further improvements in sample preparation would be possible. For setting up the 3D crystallization trials, the sitting drop method was employed.

Principle of sitting drop crystallization

The sitting drop vapor diffusion technique is generally used for the crystallization of macromolecules. A drop composed of a mixture of sample and reagent is placed in vapor equilibration with a liquid reservoir of reagent. Typically, the drop contains a lower reagent concentration than the reservoir. To achieve equilibrium, water vapors leave the drop and eventually lands up in the reservoir. When water leaves the drop, the sample experiences super saturation. Both the sample and reagent increase in concentration as water leaves the drop for the reservoir. Equilibration is reached when the reagent concentration in the drop is approximately the same as that in the reservoir.

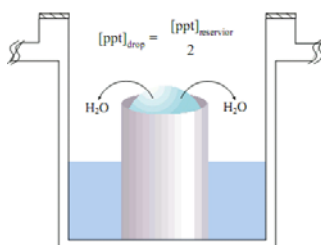


Figure 59: Picture depicting the principle of sitting drop crystallization. Courtesy: <http://www.hamptonresearch.com>

In a 24 well microtitre plate at a given time several crystallization conditions were set. Typically in one well 4.5 μ l of 5 mg/ml of protein, 3 μ l of buffer and 1 μ l of dATP from a stock solution of 100 mM in water was added. This mixture was placed on the central cavity/well and the outer well contained 500 μ l of the same buffer. The plates were sealed and incubated at room temperature. After 2 days, some crystals were observed as shown in the figure 60.

Appendix

The composition of different buffers used for crystallization trials is given below.

1. 50 mM Sodium formate (pH 3,5) or Sodium acetate (pH 4,5) buffer
2. 22.5% PEG 400 (v/v)
3. 15 mM CaCl₂ or MgCl₂
4. 10 mM Zn(CH₃COO)₂ or NiCl₂

Results

The 3D crystallization of DGK from *S.typhimurium* was taken up as a side project and hence only few trials were carried out. As an outcome of the 3D crystallization trials, we obtained 3D crystals in 6 of the following conditions. Although the crystals were observed with low power light microscope in the microtitre plates, they were small for the 3D crystallographic analysis. One of these crystals obtained in condition “A” was checked for diffraction pattern at Max Planck Institute of Biophysics, Frankfurt. However, the crystal failed to give any diffraction pattern.

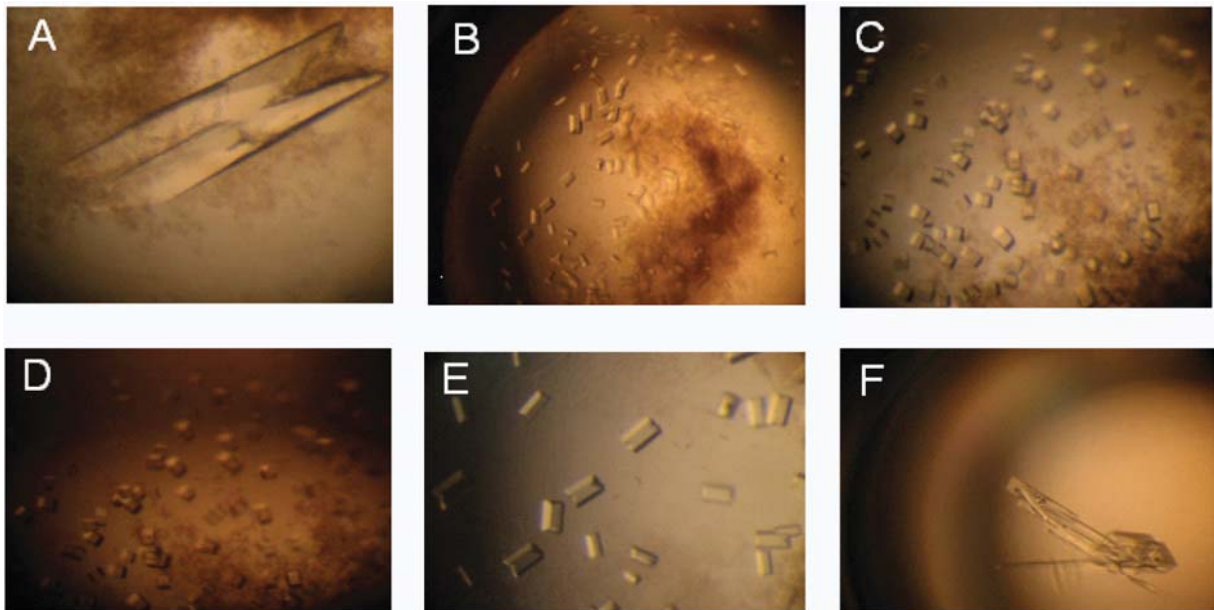


Figure 60: 3D Crystallization Trials of DGK from *Salmonella typhimurium*.

Appendix

The different conditions used for the screen are summarized in the following table.

Table 10: Summary of 3D crystallization screens for DGK.

Legend	Crystallization Condition
A	50 mM Sodium Formate + 15 mM MgCl ₂ + 10 mM NiCl ₂ +22.5% PEG 400
B	50 mM Sodium Formate + 15 mM CaCl ₂ + 10 mM NiCl ₂ +22.5% PEG 400
C	50 mM Sodium Formate + 15 mM MgCl ₂ + 10 mM Zn(CH ₃ COO) ₂ + 22.5% PEG 400
D	50mM Sodium Acetate + 15 mM CaCl ₂ +10 mM NiCl ₂ + 22.5% PEG 400
E	50 mM Sodium Formate +15 mM CaCl ₂ + 10 mM Zn(CH ₃ COO) ₂ +22.5% PEG 400
F	50 mM Sodium Acetate +15 mM MgCl ₂ + 10 mM Zn(CH ₃ COO) ₂ +22.5% PEG 400

2D crystallization

The major aim of screening for 2D crystallization was to obtain an optimal reconstitution protocol where the membrane protein is orderly arranged in the lipid bilayer and is functionally active. Earlier it has been shown that well diffracting 2D crystals can provide a structural model for membrane proteins based on cryo-electron microscopy [96]. The motivation for 2D crystallization was 2 fold. First to obtain well diffracting 2D crystals for structural analysis by cryo-electron microscopy and second to achieve optimum concentration of protein for solid state NMR spectroscopic analysis for structure determination [152]. The orderly arrangement of protein is also likely to aid in the resolution of the solid state NMR spectra by achieving narrow line widths [205].

For this purpose, a detailed 2D crystallization screen was planned and subsequent screening with electron microscopy was carried out. There were different screens based on known physical and

Appendix

chemical parameters, which are known to influence the process of 2D crystallization such as temperature, pH, salts, concentration and additives [108]. An over view of these screens is provided in the following table.

Table 11: Summary of 2D crystallization screens for DGK.

Parameter	Analyzed range of parameter
Temperature	4°C, 20°C, 30°C, 37°C
pH of dialysis buffer	3, 4, 5, 6, 7, 8, 9, 10, 11
Concentration of protein	1-3 mg/ml
Detergents for solubilization of lipid	DPC, DDM, OG
Lipids	<i>E.coli</i> Lipids, DOPC
Divalent Salts (concentration range (mM))	MgCl ₂ (5, 10, 25, 50, 100)
Monovalant salts (concentration range (mM))	NaCl (50, 100, 250)
Dialysis duration(days)	3, 5, 7, 10, 15
Detergent : lipid (mol ratio)	1:1, 1:2
Buffers (20 mM, 50 mM, and 100mM)	Acetate, Formate, Hepes, Phosphate
Additives	Glycerol (10%, 20%)
Mode of detergent removal	Biobeads, Dialysis
Protein : Lipid (mol ratio)	1:15, 1:25, 1:50, 1:100

The different screens based on the above listed parameters and the given range of concentrations was tested and was individually examined with electron microscopy. However, a combination of multiple parameters was also used.

Results

As an outcome of the different 2D crystallization screens, we obtained a reconstitution protocol for dense packing of the protein in the lipid bilayer. The electron micrographs showed multiple stacking of the lipid layers, which can be attributed to either excess of lipid or the salt concentration of the buffer used for reconstitution. The protein was not crystallized, however the extent of dense packing of the protein can be observed in the corresponding freeze fracture picture in figure 63 D. No large, isolated sheets or vesicles which were suitable for cryo electron microscopy were obtained.

Appendix

Based on all the 2D crystallization attempts the optimum dialysis condition has following parameters. Buffer containing 40 mM Na(CH₃COO), 10 mM MgCl₂, 0.2 mM DTT, 3 mM NaN₃, 20 % Glycerol with pH of 4.5 and at temperature ~ 20°C and protein concentration of 1 mg/ml. When screened for activity, with the activity assay described in materials and methods section, the samples which were reconstituted with 20% glycerol gave maximum activity as compared to the samples reconstituted without glycerol. From the additive screen it was conclusive that 20% glycerol was required for optimal reconstitution. The specific activity was measured at different points of dialysis and different salts in the dialysis buffer. The bar plot displaying the effect of different salt concentrations for day 5 dialysis is shown in figure 61 and figure 62.

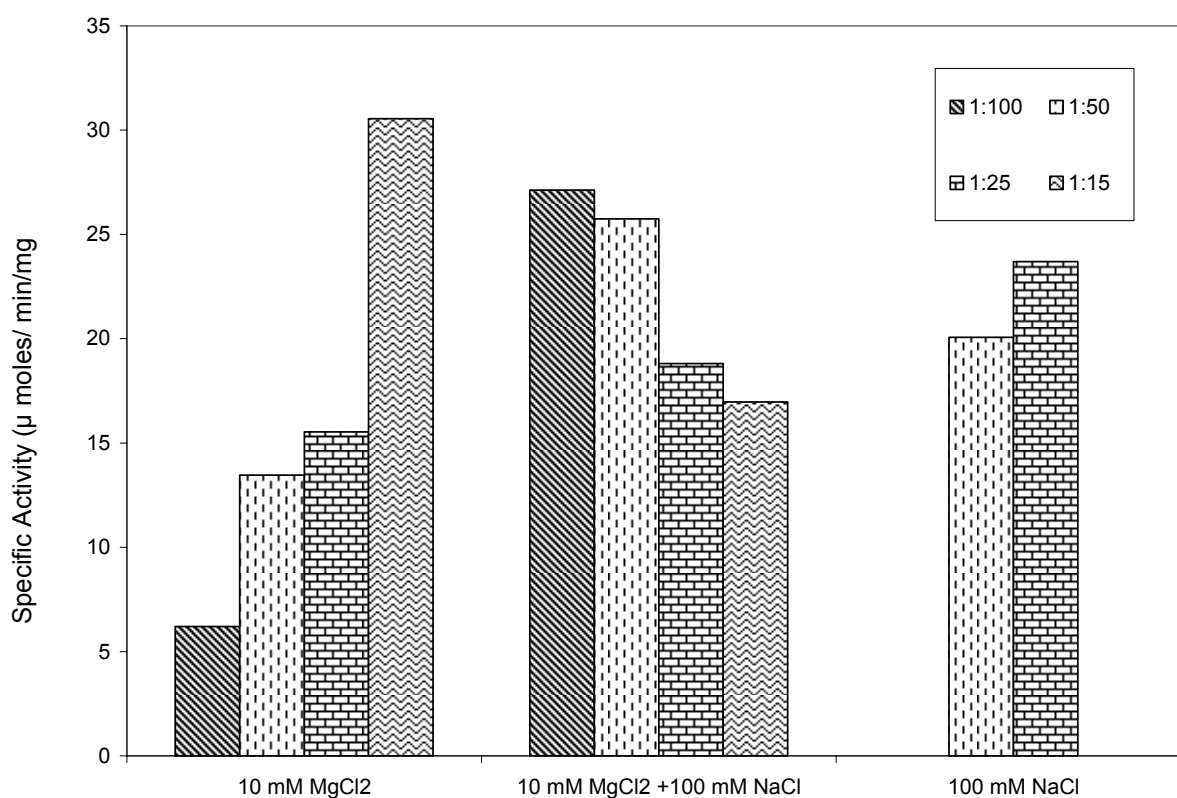


Figure 61 : Specific activity of DGK under different reconstitution and salt conditions with 20% glycerol in the dialysis buffer. The legends in the picture indicate the different Protein : Lipid ratio used for analyzing the specific activity at day 5 under different salt conditions. The maximum specific activity is observed at protein to lipid ratio of 1:15 and with only 10 mM MgCl₂ concentration in the buffer containing 20% glycerol in the sodium acetate buffer at pH 4.5.

Appendix

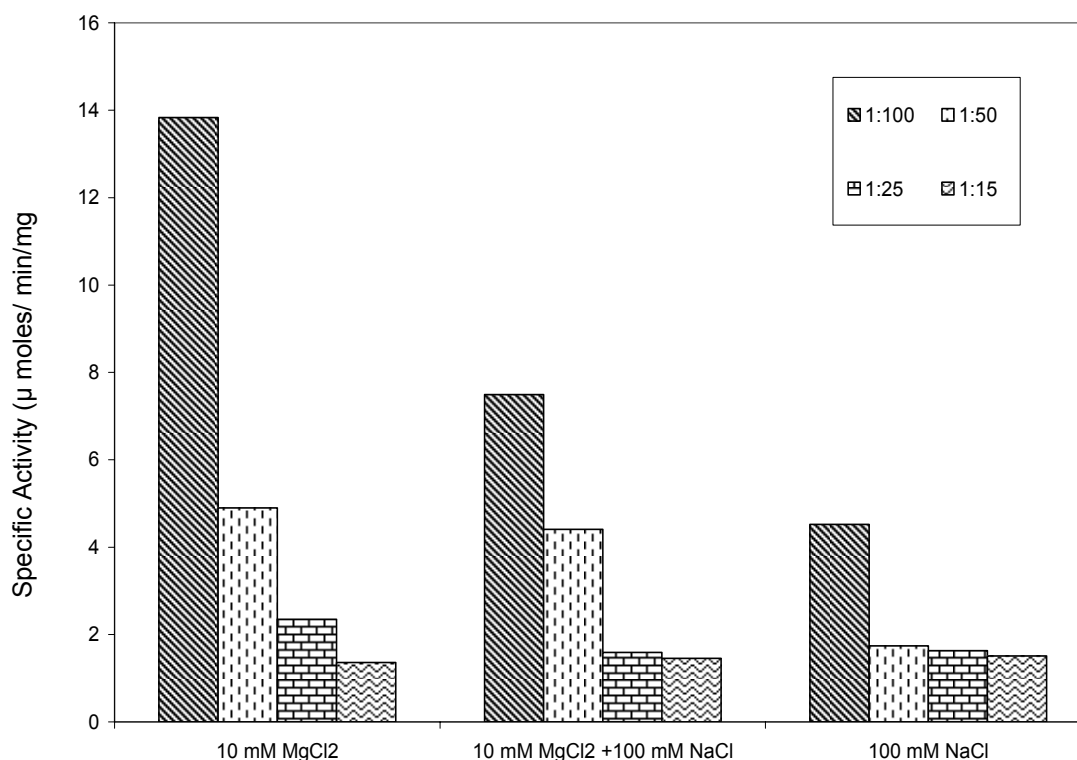


Figure 62 : Specific activity of DGK under different reconstitution and salt conditions without glycerol in the dialysis buffer. The legends in the picture indicate the different Protein: Lipid ratio used for analyzing the specific activity at day 5 under different salt conditions. The maximum specific activity is observed at protein to lipid ratio of 1:100 and with 10 mM MgCl₂ concentration in the buffer without glycerol in the sodium acetate buffer at pH 4.5.

When screened for activity, with the routine activity assay, the samples, which were reconstituted with 20% glycerol, gave maximum activity as compared to the samples reconstituted without glycerol. From the additive screen it was conclusive that 20% glycerol was required for optimal reconstitution. The corresponding incorporation of protein was analyzed with freeze fracture and has been explained in the following figure 63.

Appendix

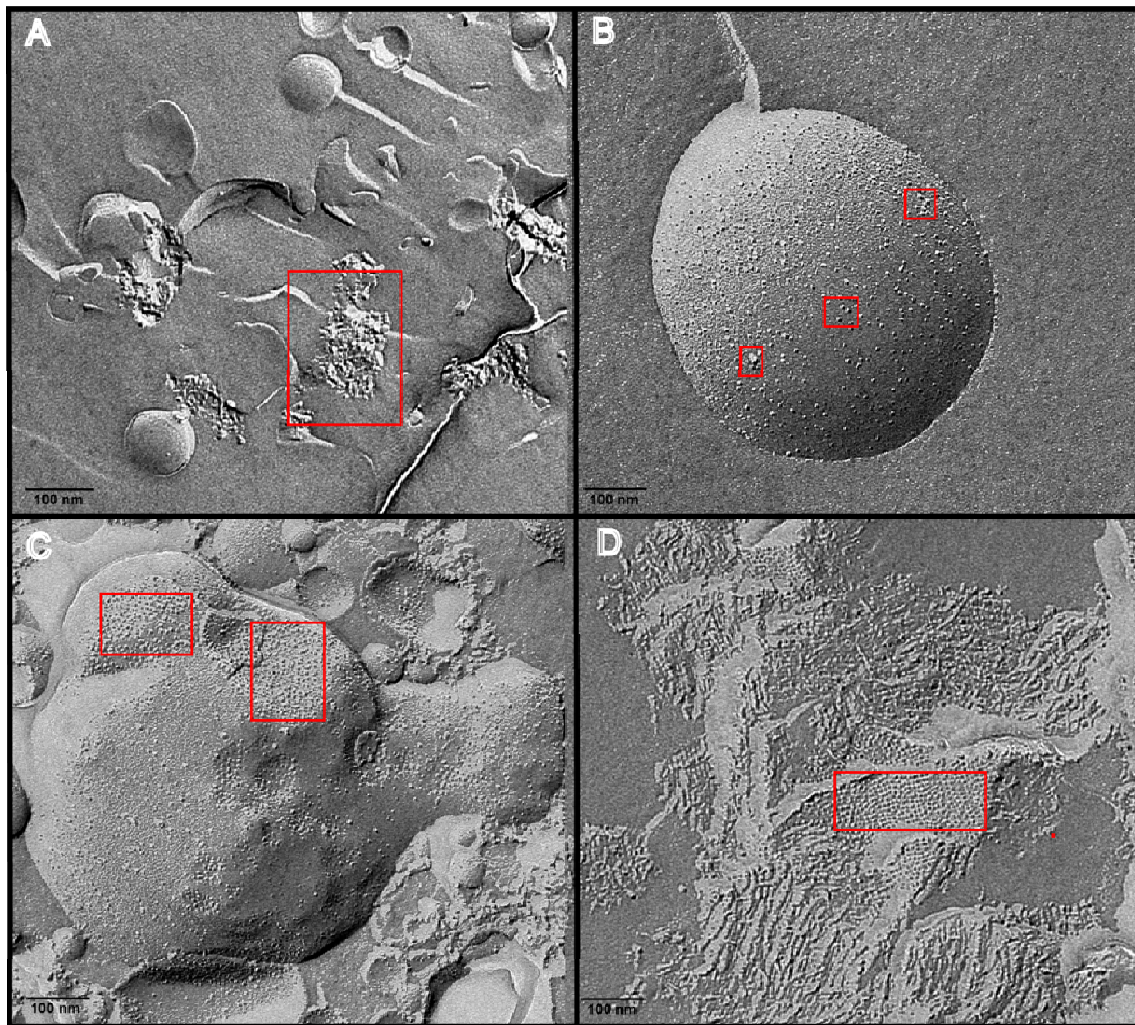


Figure 63 : Freeze fracture pictures of DGK. A: Protein aggregates with no glycerol in the dialysis buffer. B: incorporation of protein with 5% glycerol in the dialysis buffer. C: incorporation of more amount of protein with 10% glycerol in the dialysis buffer and finally D: presence of multiple stacks of incorporated protein with 20% glycerol in the dialysis buffer. The protein precipitate or incorporation is highlighted in black squares.

Conclusions

For the available data, it can be concluded that the DGK from *Salmonella typhimurium* can be densely reconstituted in the lipid bilayers but it does not form 2D crystals. However, this dense packing of the protein in the lipidic environment can be used for solid state NMR measurements.

Appendix

The 3D crystallization of protein takes place under different set of conditions but the crystals do not diffract. These nano crystals could also serve as solid state NMR samples for improved spectral resolution.

Material and Methods

DGK expression

Expression of wild type DGK was essentially done as described below. His-tagged DGK (Swiss-Prot sequence accession number P00556) was over-expressed in BL (21). Cells from a fresh plate were inoculated in the LB medium with Ampicillin to a final concentration of 100 µg/lit. The cells were grown at 37°C at 220 rpm in LB medium to an Optical Density (at 600) of 0.8. The cells were then induced with 200 µg/ml of IPTG and were grown further for 3-4 hours. The harvesting of cells was carried out by centrifugation at 6500 rpm at 4°C for 15 mins.

Solubilization and purification

For solubilization, the cells are resuspended in 50 ml of Buffer A (50 mM Na₂HPO₄, 300 mM NaCl, pH 7.5) with 1 tablet of protease inhibitor and 3% (w/v) OG. The system is kept stirring at 4°C for 2 hours for isolation of protein from inclusion bodies. After which, it is centrifuged for 30 mins at 10,000 rpm while at 4°C. In the mean time, the Ni NTA is equilibrated with buffer A. After equilibration of the resin, the supernatant containing the detergent solubilized protein is incubated with the resin for 2 hours on ice for purification with the help of 6x His tag. Thereafter the column is loaded and washed with wash buffer with (1.5% of OG with 0.03 M Imidazole in buffer A) and then with (0.5% of DPC in buffer A). Finally, the protein is eluted with the elution buffer (0.5% of DPC with 2M Imidazole in buffer A).

$$\text{Absorbance} = \epsilon * c * l$$

Where “ ϵ ” is the extinction coefficient of the protein (2.3), “ c ” the concentration of protein in mg/ml and “ l ” the path length of the cuvette (0.3).

The normal yield of protein in LB medium was ~4-5 mg/ml and ~10 mg/lit in defined medium. The purity of protein was verified with the SDS PAGE gel and the protein was approximately over 95% pure.

Appendix

Reconstitution

The detergent solubilized protein was subjected to reconstitution using various screens. Several conditions for optimal reconstitution were tested with electron microscopy and the best condition can be summarized as dialysis in buffer containing 40 mM Na(CH₃COO), 10 mM MgCl₂, 0.2 mM DTT, 3 mM NaN₃, 20% Glycerol with pH of 4.5 and at temperature ~ 20°C. The protein concentration is adjusted to 1mg/ml; protein to lipid mole ratio is 1:25 and DPC: DOPC molar ratio used is 2:1.

Activity assay

DGK activity was determined by a linked-enzyme assay [206, 207]. In which, the DGK reaction is linked to the conversion of NADH to NAD⁺ by pyruvate kinase and lactate dehydrogenase. DGK activity is monitored by oxidation of NADH to NAD⁺ with the corresponding decrease in NADH absorption at 340 nm. Pyruvate kinase and lactate dehydrogenase were added to the assay buffer and incubated at 30°C for 5 min before the addition of DGK. The change in NADH absorption at 340 nm was monitored by using a Jasco UV/Vis spectrophotometer. The assays were initiated by adding DGK to assay mixtures containing pH 6.8 buffer (60 mM PIPES, 50 mM LiCl, 0.1 mM EDTA, 0.1 mM EGTA), 1 mM phosphoenolpyruvate, 3 mM ATP, 2.6 mM sn-1,2-dihex-anoylglycerol, 20 mM Mg²⁺ (acetate salt used), 0.25 mM NADH, and 20 units each of lactic dehydrogenase and pyruvate kinase (from a glycerol-containing stock). The concentration of the reaction mixture was so adjusted that the DGK catalyzed step in the cascade was rate limiting. The maximum activity obtained with the reconstituted samples was ~35 μmol/mg/min.

Once the protein was successfully reconstituted, the amount of active protein was estimated by calculating the specific activity using the activity assay. The activity of the protein is calculated by means of activity assay. Where 100 μl of assay buffer is added to 5 μl of linking enzymes which is a mixture of pyruvate kinase and lactate dehydrogenase. This mixture is incubated at 30°C for 5 mins and then 1 μl of the reconstituted protein is added. The calculations are done as follows.

$$\Delta\text{Abs}/\text{min} = \text{slope of the graph}$$

Appendix

Extinction coefficient value for NADH is $6.22 \times 10^3 \text{ m}^{-1} \text{ cm}^{-1}$.

The value of slope in units of $\Delta\text{Abs}/\text{min}$ can be obtained from the spectra for the given cuvette thickness, which in this case is 3 mm and needs to be converted for 10 mm to obtain the activity in molar units. The value is then converted to unit of moles by multiplying the molar units with the entire volume of the reaction mixture i.e. 106 μl . usually this value is expressed in $\mu\text{moles}/\text{min}$. Finally, to obtain the values for the specific activity, the activity in $\mu\text{ moles}/\text{min}$ is divided by the protein concentration.

References

- [1] H.R. Bigelow, D.S. Petrey, J. Liu, D. Przybylski, B. Rost, Predicting transmembrane beta-barrels in proteomes, *Nucleic Acids Res* 32 (2004) 2566-2577.
- [2] J.L. Popot, D.M. Engelman, Membrane protein folding and oligomerization: the two-stage model, *Biochemistry* 29 (1990) 4031-4037.
- [3] S.H. White, G. von Heijne, The machinery of membrane protein assembly, *Curr Opin Struct Biol* 14 (2004) 397-404.
- [4] N. Grigorieff, T.A. Ceska, K.H. Downing, J.M. Baldwin, R. Henderson, Electron-crystallographic refinement of the structure of bacteriorhodopsin, *JMB* 259 (1996) 393-421.
- [5] Y. Kimura, D.G. Vassylyev, A. Miyazawa, A. Kidera, M. Matsushima, K. Mitsuoka, K. Murata, T. Hirai, Y. Fujiyoshi, Surface of bacteriorhodopsin revealed by high-resolution electron crystallography, *Nature* 389 (1997) 206-211.
- [6] R. Henderson, The purple membrane from *Halobacterium halobium*, *Annu Rev Biophys Bioeng* 6 (1977) 87-109.
- [7] W. Kuhlbrandt, D.N. Wang, Y. Fujiyoshi, Atomic model of plant light-harvesting complex by electron crystallography, *Nature* 367 (1994) 614-621.
- [8] E. Nogales, S.G. Wolf, K.H. Downing, Structure of the alpha beta tubulin dimer by electron crystallography, *Nature* 391 (1998) 199-203.
- [9] K. Murata, K. Mitsuoka, T. Hirai, T. Walz, P. Agre, J.B. Heymann, A. Engel, Y. Fujiyoshi, Structural determinants of water permeation through aquaporin-1, *Nature* 407 (2000) 599-605.
- [10] A. Krebs, P.C. Edwards, C. Villa, J. Li, G.F. Schertler, The three-dimensional structure of bovine rhodopsin determined by electron cryomicroscopy, *JBC* 278 (2003) 50217-50225.
- [11] A. Davies, B.E. Gowen, A.M. Krebs, G.F. Schertler, H.R. Saibil, Three-dimensional structure of an invertebrate rhodopsin and basis for ordered alignment in the photoreceptor membrane, *JMB* 314 (2001) 455-463.
- [12] G.F. Schertler, P.A. Hargrave, Projection structure of frog rhodopsin in two crystal forms, *PNAS* 92 (1995) 11578-11582.
- [13] W. Kuhlbrandt, Bacteriorhodopsin--the movie, *Nature* 406 (2000) 569-570.
- [14] H. Luecke, B. Schobert, H.T. Richter, J.P. Cartailler, J.K. Lanyi, Structural changes in bacteriorhodopsin during ion transport at 2 angstrom resolution, *Science (New York, N.Y)* 286 (1999) 255-261.
- [15] S. Subramaniam, R. Henderson, Molecular mechanism of vectorial proton translocation by bacteriorhodopsin, *Nature* 406 (2000) 653-657.
- [16] S. Subramaniam, M. Gerstein, D. Oesterhelt, R. Henderson, Electron diffraction analysis of structural changes in the photocycle of bacteriorhodopsin, *EMBO J* 12 (1993) 1-8.
- [17] B.G. Han, J. Vonck, R.M. Glaeser, The bacteriorhodopsin photocycle: direct structural study of two substrates of the M-intermediate, *Biophys J* 67 (1994) 1179-1186.
- [18] N. Unwin, Acetylcholine receptor channel imaged in the open state, *Nature* 373 (1995) 37-43.
- [19] J. Vonck, A three-dimensional difference map of the N intermediate in the bacteriorhodopsin photocycle: part of the F helix tilts in the M to N transition, *Biochemistry* 35 (1996) 5870-5878.

Chapter 7—References

- [20] K.R. Vinothkumar, S.H. Smits, W. Kuhlbrandt, pH-induced structural change in a sodium/proton antiporter from *Methanococcus jannaschii*, *EMBO J* 24 (2005) 2720-2729.
- [21] J.L. Rigaud, G. Mosser, J.J. Lacapere, A. Olofsson, D. Levy, J.L. Ranck, Bio-Beads: an efficient strategy for two-dimensional crystallization of membrane proteins, *J. Struct. Biol* 118 (1997) 226-235.
- [22] J. Rigaud, M. Chami, O. Lambert, D. Levy, J. Ranck, Use of detergents in two-dimensional crystallization of membrane proteins, *Biochim Biophys Acta* 1508 (2000) 112-128.
- [23] G. Mosser, Two-dimensional crystallography of transmembrane proteins, *Micron* 32 (2001) 517-540.
- [24] B.K. Jap, M. Zulauf, T. Scheybani, A. Hefti, W. Baumeister, U. Aebi, A. Engel, 2D crystallization: from art to science, *Ultramicroscopy* 46 (1992) 45-84.
- [25] T. Walz, N. Grigorieff, Electron Crystallography of Two-Dimensional Crystals of Membrane Proteins, *J. Struct. Biol* 121 (1998) 142-161.
- [26] L.A. Amos, R. Henderson, P.N. Unwin, Three-dimensional structure determination by electron microscopy of two-dimensional crystals, *Prog Biophys Mol Biol* 39 (1982) 183-231.
- [27] Y. Kim, K. Valentine, S.J. Opella, S.L. Schendel, W.A. Cramer, Solid-state NMR studies of the membrane-bound closed state of the colicin E1 channel domain in lipid bilayers, *Protein Sci* 7 (1998) 342-348.
- [28] K.J. Shon, Y. Kim, L.A. Colnago, S.J. Opella, NMR studies of the structure and dynamics of membrane-bound bacteriophage Pfl coat protein, *Science (New York, N.Y)* 252 (1991) 1303-1305.
- [29] A.J. Mason, S.L. Grage, S.K. Straus, C. Glaubitz, A. Watts, Identifying anisotropic constraints in multiply labeled bacteriorhodopsin by ¹⁵N MAOSS NMR: a general approach to structural studies of membrane proteins, *Biophys J* 86 (2004) 1610-1617.
- [30] Y. Zhou, J.H. Morais-Cabral, A. Kaufman, R. MacKinnon, Chemistry of ion coordination and hydration revealed by a K⁺ channel-Fab complex at 2.0 Å resolution, *Nature* 414 (2001) 43-48.
- [31] D.C. Gadsby, Ion transport: spot the difference, *Nature* 427 (2004) 795-797.
- [32] J.L. Spudich, C.S. Yang, K.H. Jung, E.N. Spudich, Retinylidene proteins: structures and functions from archaea to humans, *Annu Rev Cell Dev Biol* 16 (2000) 365-392.
- [33] D. Oesterhelt, W. Stoeckenius, Rhodopsin-like protein from the purple membrane of *Halobacterium halobium*, *Nat New Biol* 233 (1971) 149-152.
- [34] W.D. Hoff, K.H. Jung, J.L. Spudich, Molecular mechanism of photosignaling by archaeal sensory rhodopsins, *Annu Rev Biophys Biomol Struct* 26 (1997) 223-258.
- [35] J.K. Lanyi, Understanding structure and function in the light-driven proton pump bacteriorhodopsin, *J Struct Biol* 124 (1998) 164-178.
- [36] M.X. Ruiz-Gonzalez, I. Marin, New insights into the evolutionary history of type 1 rhodopsins, *J Mol Evol* 58 (2004) 348-358.
- [37] O. Beja, L. Aravind, E.V. Koonin, M.T. Suzuki, A. Hadd, L.P. Nguyen, S.B. Jovanovich, C.M. Gates, R.A. Feldman, J.L. Spudich, E.N. Spudich, E.F. DeLong, Bacterial rhodopsin: evidence for a new type of phototrophy in the sea, *Science (New York, N.Y)* 289 (2000) 1902-1906.
- [38] J.M. Baldwin, G.F. Schertler, V.M. Unger, An alpha-carbon template for the

Chapter 7—References

- transmembrane helices in the rhodopsin family of G-protein-coupled receptors, *JMB* 272 (1997) 144-164.
- [39] K. Palczewski, T. Kumasaka, T. Hori, C.A. Behnke, H. Motoshima, B.A. Fox, I. Le Trong, D.C. Teller, T. Okada, R.E. Stenkamp, M. Yamamoto, M. Miyano, Crystal structure of rhodopsin: A G protein-coupled receptor, *Science* (New York, N.Y. 289 (2000) 739-745.
- [40] S.G. Rasmussen, H.J. Choi, D.M. Rosenbaum, T.S. Kobilka, F.S. Thian, P.C. Edwards, M. Burghammer, V.R. Ratnala, R. Sanishvili, R.F. Fischetti, G.F. Schertler, W.I. Weis, B.K. Kobilka, Crystal structure of the human beta2 adrenergic G-protein-coupled receptor, *Nature* 450 (2007) 383-387.
- [41] V. Cherezov, D.M. Rosenbaum, M.A. Hanson, S.G. Rasmussen, F.S. Thian, T.S. Kobilka, H.J. Choi, P. Kuhn, W.I. Weis, B.K. Kobilka, R.C. Stevens, High-resolution crystal structure of an engineered human beta2-adrenergic G protein-coupled receptor, *Science* (New York, N.Y. 318 (2007) 1258-1265.
- [42] D.M. Rosenbaum, V. Cherezov, M.A. Hanson, S.G. Rasmussen, F.S. Thian, T.S. Kobilka, H.J. Choi, X.J. Yao, W.I. Weis, R.C. Stevens, B.K. Kobilka, GPCR engineering yields high-resolution structural insights into beta2-adrenergic receptor function, *Science* (New York, N.Y. 318 (2007) 1266-1273.
- [43] G. Sabehi, O. Beja, M.T. Suzuki, C.M. Preston, E.F. DeLong, Different SAR86 subgroups harbour divergent proteorhodopsins, *Environ Microbiol* 6 (2004) 903-910.
- [44] D. Man-Aharonovich, G. Sabehi, O.A. Sineshchekov, E.N. Spudich, J.L. Spudich, O. Beja, Characterization of RS29, a blue-green proteorhodopsin variant from the Red Sea, *Photochem Photobiol Sci* 3 (2004) 459-462.
- [45] J.R. de la Torre, L.M. Christianson, O. Beja, M.T. Suzuki, D.M. Karl, J. Heidelberg, E.F. DeLong, Proteorhodopsin genes are distributed among divergent marine bacterial taxa, *PNAS* 100 (2003) 12830-12835.
- [46] G. Sabehi, R. Massana, J.P. Bielawski, M. Rosenberg, E.F. DeLong, O. Beja, Novel Proteorhodopsin variants from the Mediterranean and Red Seas, *Environ Microbiol* 5 (2003) 842-849.
- [47] J.C. Venter, K. Remington, J.F. Heidelberg, A.L. Halpern, D. Rusch, J.A. Eisen, D. Wu, I. Paulsen, K.E. Nelson, W. Nelson, D.E. Fouts, S. Levy, A.H. Knap, M.W. Lomas, K. Nealson, O. White, J. Peterson, J. Hoffman, R. Parsons, H. Baden-Tillson, C. Pfannkoch, Y.H. Rogers, H.O. Smith, Environmental genome shotgun sequencing of the Sargasso Sea, *Science* (New York, N.Y. 304 (2004) 66-74.
- [48] G. Sabehi, A. Loy, K.H. Jung, R. Partha, J.L. Spudich, T. Isaacson, J. Hirschberg, M. Wagner, O. Beja, New insights into metabolic properties of marine bacteria encoding proteorhodopsins, *PLoS Biol* 3 (2005) e273.
- [49] N.U. Frigaard, A. Martinez, T.J. Mincer, E.F. DeLong, Proteorhodopsin lateral gene transfer between marine planktonic Bacteria and Archaea, *Nature* 439 (2006) 847-850.
- [50] S.J. Giovannoni, L. Bibbs, J.C. Cho, M.D. Staples, R. Desiderio, K.L. Vergin, M.S. Rappe, S. Laney, L.J. Wilhelm, H.J. Tripp, E.J. Mathur, D.F. Barofsky, Proteorhodopsin in the ubiquitous marine bacterium SAR11, *Nature* 438 (2005) 82-85.
- [51] D. Man, W. Wang, G. Sabehi, L. Aravind, A.F. Post, R. Massana, E.N. Spudich, J.L. Spudich, O. Beja, Diversification and spectral tuning in marine proteorhodopsins, *EMBO J* 22 (2003) 1725-1731.
- [52] L. Gomez-Consarnau, J.M. Gonzalez, M. Coll-Llado, P. Gourdon, T. Pascher, R. Neutze,

Chapter 7—References

- C. Pedros-Alio, J. Pinhassi, Light stimulates growth of proteorhodopsin-containing marine Flavobacteria, *Nature* 445 (2007) 210-213.
- [53] U. Stingl, R.A. Desiderio, J.C. Cho, K.L. Vergin, S.J. Giovannoni, The SAR92 clade: an abundant coastal clade of culturable marine bacteria possessing proteorhodopsin, *Appl. Envir. Micro* 73 (2007) 2290-2296.
- [54] A.K. Dioumaev, L.S. Brown, J. Shih, E.N. Spudich, J.L. Spudich, J.K. Lanyi, Proton transfers in the photochemical reaction cycle of proteorhodopsin, *Biochemistry* 41 (2002) 5348-5358.
- [55] E.S. Imasheva, K. Shimono, S.P. Balashov, J.M. Wang, U. Zadok, M. Sheves, N. Kamo, J.K. Lanyi, Formation of a long-lived photoproduct with a deprotonated Schiff base in proteorhodopsin, and its enhancement by mutation of Asp227, *Biochemistry* 44 (2005) 10828-10838.
- [56] I.C. Spyropoulos, T.D. Liakopoulos, P.G. Bagos, S.J. Hamodrakas, TMRPres2D: high quality visual representation of transmembrane protein models, *Bioinformatics* 20 (2004) 3258-3260.
- [57] S. Shastri, J. Vonck, N. Pflieger, W. Haase, W. Kuehlbrandt, C. Glaubitz, Proteorhodopsin: Characterisation of 2D crystals by electron microscopy and solid state NMR, *Biochim Biophys Acta Biomem* 1768 (2007) 3012-3019.
- [58] J. McCarren, E.F. DeLong, Proteorhodopsin photosystem gene clusters exhibit co-evolutionary trends and shared ancestry among diverse marine microbial phyla, *Environ Microbiol* 9 (2007) 846-858.
- [59] O. Beja, E.N. Spudich, J.L. Spudich, M. Leclerc, E.F. DeLong, Proteorhodopsin phototrophy in the ocean, *Nature* 411 (2001) 786-789.
- [60] G. Sabehi, B.C. Kirkup, M. Rozenberg, N. Stambler, M.F. Polz, O. Beja, Adaptation and spectral tuning in divergent marine proteorhodopsins from the eastern Mediterranean and the Sargasso Seas, *The ISME journal* 1 (2007) 48-55.
- [61] B.J. Campbell, L.A. Waidner, M.T. Cottrell, D.L. Kirchman, Abundant proteorhodopsin genes in the North Atlantic Ocean, *Environ Microbiol* 10 (2008) 99-109.
- [62] G.G. Kochendoerfer, S.W. Lin, T.P. Sakmar, R.A. Mathies, How color visual pigments are tuned, *Trends Biochem Sci* 24 (1999) 300-305.
- [63] S. Subramaniam, D.A. Greenhalgh, P. Rath, K.J. Rothschild, H.G. Khorana, Replacement of leucine-93 by alanine or threonine slows down the decay of the N and O intermediates in the photocycle of bacteriorhodopsin: implications for proton uptake and 13-cis-retinal---all-trans-retinal reisomerization, *PNAS* 88 (1991) 6873-6877.
- [64] B.R. Kelemen, M. Du, R.B. Jensen, Proteorhodopsin in living color: diversity of spectral properties within living bacterial cells, *Biochim Biophys Acta* 1618 (2003) 25-32.
- [65] J.R. Hillebrecht, J. Galan, R. Rangarajan, L. Ramos, K. McCleary, D.E. Ward, J.A. Stuart, R.R. Birge, Structure, function, and wavelength selection in blue-absorbing proteorhodopsin, *Biochemistry* 45 (2006) 1579-1590.
- [66] B. Scharf, B. Pevec, B. Hess, M. Engelhard, Biochemical and photochemical properties of the photophobic receptors from *Halobacterium halobium* and *Natronobacterium pharaonis*, *European journal of biochemistry / FEBS* 206 (1992) 359-366.
- [67] T. Friedrich, S. Geibel, R. Kalmbach, I. Chizhov, K. Ataka, J. Heberle, M. Engelhard, E. Bamberg, Proteorhodopsin is a light-driven proton pump with variable vectoriality, *JMB* 321 (2002) 821-838.
- [68] N. Pflieger, M. Lorch, A.C. Woerner, S. Shastri, C. Glaubitz, Characterisation of Schiff

Chapter 7—References

- base and chromophore in green proteorhodopsin by solid-state NMR, *J Biomol NMR* 40 (2008) 15-21.
- [69] W.W. Wang, O.A. Sineshchekov, E.N. Spudich, J.L. Spudich, Spectroscopic and photochemical characterization of a deep ocean proteorhodopsin, *JBC* 278 (2003) 33985-33991.
- [70] V. Bergo, J.J. Amsden, E.N. Spudich, J.L. Spudich, K.J. Rothschild, Structural changes in the photoactive site of proteorhodopsin during the primary photoreaction, *Biochemistry* 43 (2004) 9075-9083.
- [71] M. Lakatos, G. Varo, The influence of water on the photochemical reaction cycle of proteorhodopsin at low and high pH, *J Photochem Photobiol B* 73 (2004) 177-182.
- [72] M. Lakatos, J.K. Lanyi, J. Szakacs, G. Varo, The photochemical reaction cycle of proteorhodopsin at low pH, *Biophys J* 84 (2003) 3252-3256.
- [73] G. Varo, L.S. Brown, M. Lakatos, J.K. Lanyi, Characterization of the photochemical reaction cycle of proteorhodopsin, *Biophys J* 84 (2003) 1202-1207.
- [74] R. Huber, T. Kohler, M.O. Lenz, E. Bamberg, R. Kalmbach, M. Engelhard, J. Wachtveitl, pH-dependent photoisomerization of retinal in proteorhodopsin, *Biochemistry* 44 (2005) 1800-1806.
- [75] R.H.B. Clayton, Spectrophotometric seawater pH measurements :total hydrogen ion concentration scale calibration of m-cresol purple and at sea results., *Deep-Sea Res.* 40 (1993) 2115-2129
- [76] P.C. Mowery, R.H. Lozier, Q. Chae, Y.W. Tseng, M. Taylor, W. Stoeckenius, Effect of acid pH on the absorption spectra and photoreactions of bacteriorhodopsin, *Biochemistry* 18 (1979) 4100-4107.
- [77] S.P. Balashov, E.S. Imasheva, R. Govindjee, T.G. Ebrey, Titration of aspartate-85 in bacteriorhodopsin: what it says about chromophore isomerization and proton release, *Biophys J* 70 (1996) 473-481.
- [78] A.K. Dioumaev, J.M. Wang, Z. Balint, G. Varo, J.K. Lanyi, Proton transport by proteorhodopsin requires that the retinal Schiff base counterion Asp-97 be anionic, *Biochemistry* 42 (2003) 6582-6587.
- [79] R.M. Morris, M.S. Rappe, S.A. Connon, K.L. Vergin, W.A. Siebold, C.A. Carlson, S.J. Giovannoni, SAR11 clade dominates ocean surface bacterioplankton communities, *Nature* 420 (2002) 806-810.
- [80] S.C. Schuster, S. Khan, The bacterial flagellar motor, *Annu Rev Biophys Biomol Struct* 23 (1994) 509-539.
- [81] R.M. Manab, *E.coli and salmonella: cellular and molecular biology*, Am Soc Microbiol (2005).
- [82] E. Racker, W. Stoeckenius, Reconstitution of purple membrane vesicles catalyzing light-driven proton uptake and adenosine triphosphate formation, *JBC* 249 (1974) 662-663.
- [83] J.M. Walter, D. Greenfield, C. Bustamante, J. Liphardt, Light-powering *Escherichia coli* with proteorhodopsin, *PNAS* 104 (2007) 2408-2412.
- [84] D. Oesterhelt, W. Stoeckenius, Functions of a new photoreceptor membrane, *PNAS* 70 (1973) 2853-2857.
- [85] A. Danon, W. Stoeckenius, Photophosphorylation in *Halobacterium halobium*, *PNAS* 71 (1974) 1234-1238.
- [86] A. Martinez, A.S. Bradley, J.R. Waldbauer, R.E. Summons, E.F. DeLong, Proteorhodopsin photosystem gene expression enables photophosphorylation in a

Chapter 7—References

- heterologous host, PNAS 104 (2007) 5590-5595.
- [87] A. Royant, P. Nollert, K. Edman, R. Neutze, E.M. Landau, E. Pebay-Peyroula, J. Navarro, X-ray structure of sensory rhodopsin II at 2.1-Å resolution, PNAS 98 (2001) 10131-10136.
- [88] R. Rangarajan, J.F. Galan, G. Whited, R.R. Birge, Mechanism of spectral tuning in green-absorbing proteorhodopsin, Biochemistry 46 (2007) 12679-12686.
- [89] Y. Mukohata, K. Ihara, T. Tamura, Y. Sugiyama, Halobacterial rhodopsins, J Biochem 125 (1999) 649-657.
- [90] R.J. Dunn, N.R. Hackett, J.M. McCoy, B.H. Chao, K. Kimura, H.G. Khorana, Structure-function studies on bacteriorhodopsin. I. Expression of the bacterio-opsin gene in Escherichia coli, JBC 262 (1987) 9246-9254.
- [91] I.P. Hohenfeld, A.A. Wegener, M. Engelhard, Purification of histidine tagged bacteriorhodopsin, pharaonis halorhodopsin and pharaonis sensory rhodopsin II functionally expressed in Escherichia coli, FEBS Lett 442 (1999) 198-202.
- [92] E.F. DeLong, C.M. Preston, T. Mincer, V. Rich, S.J. Hallam, N.U. Frigaard, A. Martinez, M.B. Sullivan, R. Edwards, B.R. Brito, S.W. Chisholm, D.M. Karl, Community genomics among stratified microbial assemblages in the ocean's interior, Science (New York, N.Y.) 311 (2006) 496-503.
- [93] P.N. Unwin, R. Henderson, Molecular structure determination by electron microscopy of unstained crystalline specimens, JMB 94 (1975) 425-440.
- [94] R.A. Crowther, R. Henderson, J.M. Smith, MRc image processing programs, J Struct Biol 116 (1996) 9-16.
- [95] A.J. Mason, G.J. Turner, C. Glaubitz, Conformational heterogeneity of transmembrane residues after the Schiff base reprotonation of bacteriorhodopsin: ¹⁵N CPMAS NMR of D85N/T170C membranes, FEBS 272 (2005) 2152-2164.
- [96] R. Henderson, J.M. Baldwin, T.A. Ceska, F. Zemlin, E. Beckmann, K.H. Downing, Model for the structure of bacteriorhodopsin based on high-resolution electron cryo-microscopy, JMB 213 (1990) 899-929.
- [97] G.G. Prive, Detergents for the stabilization and crystallization of membrane proteins, Methods 41 (2007) 388-397.
- [98] H. Michel, crystallization of membrane proteins, Trends Biochem. Sci. 8 (1983) 3.
- [99] R.M. Garavito, J.P. Rosenbusch, Isolation and crystallization of bacterial porin, Methods Enzymol 125 (1986) 309-328.
- [100] C. Sauter, additives for crystallization of proteins and nucleic acids J Crys Grow 196 (1999) 365-376.
- [101] W. Kuehlbrandt, Three dimensional crystallization of membrane protein, Quat Rev Biophys 21 (1988) 48.
- [102] R.W. Hendler, S. Dracheva, Importance of lipids for bacteriorhodopsin structure, photocycle, and function, Biochemistry (Mosc) 66 (2001) 1311-1314.
- [103] S. Nussberger, K. Dorr, D.N. Wang, W. Kuehlbrandt, Lipid-protein interactions in crystals of plant light-harvesting complex, JMB 234 (1993) 347-356.
- [104] A.K. Mukhopadhyay, S. Dracheva, S. Bose, R.W. Hendler, Control of the integral membrane proton pump, bacteriorhodopsin, by purple membrane lipids of Halobacterium halobium, Biochemistry 35 (1996) 9245-9252.
- [105] C.D. Heyes, M.A. El-Sayed, The role of the native lipids and lattice structure in bacteriorhodopsin protein conformation and stability as studied by temperature-

Chapter 7—References

- dependent Fourier transform-infrared spectroscopy, *JBC* 277 (2002) 29437-29443.
- [106] M. Weik, H. Patzelt, G. Zaccai, D. Oesterhelt, Localization of glycolipids in membranes by in vivo labeling and neutron diffraction, *Mol Cell* 1 (1998) 411-419.
- [107] L. Essen, R. Siegert, W.D. Lehmann, D. Oesterhelt, Lipid patches in membrane protein oligomers: crystal structure of the bacteriorhodopsin-lipid complex, *PNAS* 95 (1998) 11673-11678.
- [108] I. Schmidt-Krey, Electron crystallography of membrane proteins: two-dimensional crystallization and screening by electron microscopy, *Methods* (San Diego, Calif 41 (2007) 417-426.
- [109] H. Liang, G. Whited, C. Nguyen, G.D. Stucky, The directed cooperative assembly of proteorhodopsin into 2D and 3D polarized arrays, *PNAS* 104 (2007) 8212-8217.
- [110] J. Baldiwin, R. Henderson, Measurement and evaluation of electron diffraction pattern from 2 dimensional crystals., *Ultramicroscopy* 14 (1984) 16.
- [111] O.A. Sineschekov, K.H. Jung, J.L. Spudich, Two rhodopsins mediate phototaxis to low- and high-intensity light in *Chlamydomonas reinhardtii*, *PNAS* 99 (2002) 8689-8694.
- [112] G. Metz, F. Siebert, M. Engelhard, Asp85 is the only internal aspartic acid that gets protonated in the M intermediate and the purple-to-blue transition of bacteriorhodopsin. A solid-state ¹³C CP-MAS NMR investigation, *FEBS lett* 303 (1992) 237-241.
- [113] B. Aton, A.G. Doukas, R.H. Callender, B. Becher, T.G. Ebrey, Resonance Raman studies of the purple membrane, *Biochemistry* 16 (1977) 2995-2999.
- [114] P.D. Roepe, P.L. Ahl, J. Herzfeld, J. Lugtenburg, K.J. Rothschild, Tyrosine protonation changes in bacteriorhodopsin. A Fourier transform infrared study of BR548 and its primary photoproduct, *JBC* 263 (1988) 5110-5117.
- [115] Y. Xiao, R. Partha, R. Krebs, M. Braiman, Time-resolved FTIR spectroscopy of the photointermediates involved in fast transient H⁺ release by proteorhodopsin, *J Phys Chem* 109 (2005) 634-641.
- [116] J.H. Hoh, R. Lal, S.A. John, J.P. Revel, M.F. Arnsdorf, Atomic force microscopy and dissection of gap junctions, *Science* (New York, N.Y 253 (1991) 1405-1408.
- [117] B. Drake, C.B. Prater, A.L. Weisenhorn, S.A. Gould, T.R. Albrecht, C.F. Quate, D.S. Cannell, H.G. Hansma, P.K. Hansma, Imaging crystals, polymers, and processes in water with the atomic force microscope, *Science* (New York, N.Y 243 (1989) 1586-1589.
- [118] H. Janovjak, A. Kedrov, D.A. Cisneros, K.T. Sapra, J. Struckmeier, D.J. Muller, Imaging and detecting molecular interactions of single transmembrane proteins, *Neurobiol Aging* 27 (2006) 546-561.
- [119] A. Kedrov, C. Ziegler, H. Janovjak, W. Kuhlbrandt, D.J. Muller, Controlled unfolding and refolding of a single sodium-proton antiporter using atomic force microscopy, *JMB* 340 (2004) 1143-1152.
- [120] A. Kedrov, D.J. Muller, Characterizing folding, structure, molecular interactions and ligand gated activation of single sodium/proton antiporters, *Naunyn Schmiedebergs Arch Pharmacol* 372 (2006) 400-412.
- [121] J.P. Rossell, S. Allen, M.C. Davies, C.J. Roberts, S.J. Tendler, P.M. Williams, Electrostatic interactions observed when imaging proteins with the atomic force microscope, *Ultramicroscopy* 96 (2003) 37-46.
- [122] D. Fotiadis, A. Engel, High-resolution imaging of bacteriorhodopsin by atomic force microscopy, *Meth Mol Biol* (Clifton, N.J 242 (2004) 291-303.
- [123] D.J. Muller, K.T. Sapra, S. Scheuring, A. Kedrov, P.L. Frederix, D. Fotiadis, A. Engel,

Chapter 7—References

- Single-molecule studies of membrane proteins, *Curr Opin Struct Biol* 16 (2006) 489-495.
- [124] M. Kolbe, H. Besir, L.O. Essen, D. Oesterhelt, Structure of the light-driven chloride pump halorhodopsin at 1.8 Å resolution, *Science (New York, N.Y)* 288 (2000) 1390-1396.
- [125] H. Luecke, B. Schobert, J.K. Lanyi, E.N. Spudich, J.L. Spudich, Crystal structure of sensory rhodopsin II at 2.4 angstroms: insights into color tuning and transducer interaction, *Science (New York, N.Y)* 293 (2001) 1499-1503.
- [126] T. Haltia, E. Freire, Forces and factors that contribute to the structural stability of membrane proteins, *Biochim Biophys Acta* 1228 (1995) 1-27.
- [127] K.T. Sapra, H. Besir, D. Oesterhelt, D.J. Muller, Characterizing molecular interactions in different bacteriorhodopsin assemblies by single-molecule force spectroscopy, *JMB* 355 (2006) 640-650.
- [128] D.J. Muller, M. Kessler, F. Oesterhelt, C. Moller, D. Oesterhelt, H. Gaub, Stability of bacteriorhodopsin alpha-helices and loops analyzed by single-molecule force spectroscopy, *Biophys J* 83 (2002) 3578-3588.
- [129] D. Fotiadis, Y. Liang, S. Filipek, D.A. Saperstein, A. Engel, K. Palczewski, The G protein-coupled receptor rhodopsin in the native membrane, *FEBS Lett* 564 (2004) 281-288.
- [130] D.J. Muller, D. Fotiadis, S. Scheuring, S.A. Muller, A. Engel, Electrostatically balanced subnanometer imaging of biological specimens by atomic force microscope, *Biophys J* 76 (1999) 1101-1111.
- [131] D.J. Muller, H.J. Sass, S.A. Muller, G. Buldt, A. Engel, Surface structures of native bacteriorhodopsin depend on the molecular packing arrangement in the membrane, *JMB* 285 (1999) 1903-1909.
- [132] F. Oesterhelt, D. Oesterhelt, M. Pfeiffer, A. Engel, H.E. Gaub, D.J. Muller, Unfolding pathways of individual bacteriorhodopsins, *Science (New York, N.Y)* 288 (2000) 143-146.
- [133] H. Janovjak, D.J. Muller, A.D. Humphris, Molecular force modulation spectroscopy revealing the dynamic response of single bacteriorhodopsins, *Biophys J* 88 (2005) 1423-1431.
- [134] D.A. Cisneros, D. Oesterhelt, D.J. Muller, Probing origins of molecular interactions stabilizing the membrane proteins halorhodopsin and bacteriorhodopsin, *Structure* 13 (2005) 235-242.
- [135] A. Kedrov, H. Janovjak, K.T. Sapra, D.J. Muller, Deciphering molecular interactions of native membrane proteins by single-molecule force spectroscopy, *Annu Rev Biophys Biomol Struct* 36 (2007) 233-260.
- [136] A.L. Klyszejko, S. Shastri, S.A. Mari, H. Grubmuller, D.J. Muller, C. Glaubitz, Folding and assembly of proteorhodopsin, *JMB* 376 (2008) 35-41.
- [137] D.M. Engelman, T.A. Steitz, The spontaneous insertion of proteins into and across membranes: the helical hairpin hypothesis, *Cell* 23 (1981) 411-422.
- [138] M. Rief, M. Gautel, F. Oesterhelt, J.M. Fernandez, H.E. Gaub, Reversible unfolding of individual titin immunoglobulin domains by AFM, *Science (New York, N.Y)* 276 (1997) 1109-1112.
- [139] M. Carrion-Vazquez, A.F. Oberhauser, S.B. Fowler, P.E. Marszalek, S.E. Broedel, J. Clarke, J.M. Fernandez, Mechanical and chemical unfolding of a single protein: a comparison, *PNAS* 96 (1999) 3694-3699.

Chapter 7—References

- [140] H. Janovjak, M. Kessler, D. Oesterhelt, H. Gaub, D.J. Muller, Unfolding pathways of native bacteriorhodopsin depend on temperature, *EMBO J* 22 (2003) 5220-5229.
- [141] A.E. Blaurock, W. Stoeckenius, Structure of the purple membrane, *Nat New Biol* 233 (1971) 152-155.
- [142] H. Michel, D. Oesterhelt, R. Henderson, Orthorhombic two-dimensional crystal form of purple membrane, *PNAS* 77 (1980) 338-342.
- [143] J.B. Heymann, D.J. Muller, E.M. Landau, J.P. Rosenbusch, E. Pebay-Peyroula, G. Buldt, A. Engel, Charting the surfaces of the purple membrane, *J Struct Biol* 128 (1999) 243-249.
- [144] P. Gourdon, A. Alfredsson, A. Pedersen, E. Malmerberg, M. Nyblom, M. Widell, R. Berntsson, J. Pinhassi, M. Braiman, O. Hansson, N. Bonander, G. Karlsson, R. Neutze, Optimized in vitro and in vivo expression of proteorhodopsin: a seven-transmembrane proton pump, *Prot Exp Puri* 58 (2008) 103-113.
- [145] H. Saito, Y. Kawase, A. Kira, K. Yamamoto, M. Tanio, S. Yamaguchi, S. Tuzi, A. Naito, Surface and dynamic structures of bacteriorhodopsin in a 2D crystal, a distorted or disrupted lattice, as revealed by site-directed solid-state ¹³C NMR, *Photochem Photobiol* 83 (2007) 253-262.
- [146] A.T. Petkova, M. Hatanaka, C.P. Jaroniec, J.G. Hu, M. Belenky, M. Verhoeven, J. Lugtenburg, R.G. Griffin, J. Herzfeld, Tryptophan interactions in bacteriorhodopsin: a heteronuclear solid-state NMR study, *Biochemistry* 41 (2002) 2429-2437.
- [147] M.R. Farrar, K.V. Lakshmi, S.O. Smith, R.S. Brown, J. Raap, J. Lugtenburg, R.G. Griffin, J. Herzfeld, Solid state NMR study of [epsilon-¹³C]Lys-bacteriorhodopsin: Schiff base photoisomerization, *Biophys J* 65 (1993) 310-315.
- [148] H. Saito, S. Yamaguchi, H. Okuda, A. Shiraishi, S. Tuzi, Dynamic aspect of bacteriorhodopsin as a typical membrane protein as revealed by site-directed solid-state ¹³C NMR, *Solid state nuclear magnetic resonance* 25 (2004) 5-14.
- [149] R. Tycko, Biomolecular solid state NMR: advances in structural methodology and applications to peptide and protein fibrils, *Ann. Rev. Phys.Chem.* 52 (2001) 575-606.
- [150] W.T. Franks, B.J. Wylie, H.L. Schmidt, A.J. Nieuwkoop, R.M. Mayrhofer, G.J. Shah, D.T. Graesser, C.M. Rienstra, Dipole tensor-based atomic-resolution structure determination of a nanocrystalline protein by solid-state NMR, *PNAS* 105 (2008) 4621-4626.
- [151] A. Watts, S.K. Straus, S.L. Grage, M. Kamihira, Y.H. Lam, X. Zhao, Membrane protein structure determination using solid-state NMR, *Meth Mol Biol (Clifton, N.J)* 278 (2004) 403-473.
- [152] F. Castellani, B. van Rossum, A. Diehl, M. Schubert, K. Rehbein, H. Oschkinat, Structure of a protein determined by solid-state magic-angle-spinning NMR spectroscopy, *Nature* 420 (2002) 98-102.
- [153] M. Hong, K. Jakes, D. Huster, Investigation of molecular motions by Lee–Goldburg cross-polarization NMR spectroscopy, *J Phys Chem ,B* 106 (2002) 7355–7364.
- [154] A. Bennett, C.M. Reinstra, R.G. Griffin, heteronuclear decoupling in rotating solids, *J Chem Phys* 103 (1995) 6951.
- [155] B.M. Fung, A.K. Khitrin, K. Ermolaev, An improved broadband decoupling sequence for liquid crystals and solids, *JMR* 142 (2000) 97-101.
- [156] A. Brinkmann, M. Edén, M. Levitt, Synchronous helical pulse sequences in magic-angle spinning nuclear magnetic resonance: Double quantum recoupling of multiple-spin

Chapter 7—References

- systems, *J Chem Phys* 112 (2000) 8539-8554.
- [157] K. Voitchovsky, S. Antoranz Contera, M. Kamihira, A. Watts, J.F. Ryan, Differential stiffness and lipid mobility in the leaflets of purple membranes, *Biophys J* 90 (2006) 2075-2085.
- [158] H. Luecke, B. Schobert, H. Richter, J. Cartailler, J. Lanyi, Structure of bacteriorhodopsin at 1.55 Å resolution, *JMB* 291 (1999) 899-911.
- [159] R.K. Hite, T. Gonen, S.C. Harrison, T. Walz, Interactions of lipids with aquaporin-0 and other membrane proteins, *Pflugers Arch* (2007).
- [160] B.L. Peterson, B.S. Cummings, A review of chromatographic methods for the assessment of phospholipids in biological samples, *Biomed Chromatogr* 20 (2006) 227-243.
- [161] D. Amia, A. Natalelloa, G. Taylorc, G. Tononc, S.M. Doglia, Structural analysis of protein inclusion bodies by Fourier transform infrared microspectroscopy, *Biochimica et Biophysica Acta (BBA) - Proteins & Proteomics* 1764 (2006) 793.
- [162] S.A. Tatulian, Attenuated total reflection Fourier transform infrared spectroscopy: a method of choice for studying membrane proteins and lipids, *Biochemistry* 42 (2003) 11898-11907.
- [163] S.A. Tatulian, Toward understanding interfacial activation of secretory phospholipase A2 (PLA2): membrane surface properties and membrane-induced structural changes in the enzyme contribute synergistically to PLA2 activation, *Biophys J* 80 (2001) 789-800.
- [164] J.F. Nagle, S. Tristram-Nagle, Structure of lipid bilayers, *Biochim Biophys Acta* 1469 (2000) 159-195.
- [165] T. Salditt, Lipid-peptide interaction in oriented bilayers probed by interface-sensitive scattering methods, *Curr Opin Struct Biol* 13 (2003) 467-478.
- [166] D. Marguet, P.F. Lenne, H. Rigneault, H.T. He, Dynamics in the plasma membrane: how to combine fluidity and order, *EMBO J* 25 (2006) 3446-3457.
- [167] I.D. Campbell, C.M. Dobson, The application of high resolution nuclear magnetic resonance to biological systems, *Meth Biochem Anal* 25 (1979) 1-133.
- [168] B. Honig, A.D. Greenberg, U. Dinur, T.G. Ebrey, Visual-pigment spectra: implications of the protonation of the retinal Schiff base, *Biochemistry* 15 (1976) 4593-4599.
- [169] J.L. Spudich, D.A. McCain, K. Nakanishi, M. Okabe, N. Shimizu, H. Rodman, B. Honig, R.A. Bogomolni, Chromophore/protein interaction in bacterial sensory rhodopsin and bacteriorhodopsin, *Biophys J* 49 (1986) 479-483.
- [170] S.O. Smith, I. Hornung, R. van der Steen, J.A. Pardoen, M.S. Braiman, J. Lugtenburg, R.A. Mathies, Are C14-C15 single bond isomerizations of the retinal chromophore involved in the proton-pumping mechanism of bacteriorhodopsin?, *PNAS* 83 (1986) 967-971.
- [171] G.S. Harbison, J. Herzfeld, R.G. Griffin, Solid-state nitrogen-15 nuclear magnetic resonance study of the Schiff base in bacteriorhodopsin, *Biochemistry* 22 (1983) 1-4.
- [172] S.O. Smith, I. Palings, V. Copie, D.P. Raleigh, J. Courtin, J.A. Pardoen, J. Lugtenburg, R.A. Mathies, R.G. Griffin, Low-temperature solid-state ¹³C NMR studies of the retinal chromophore in rhodopsin, *Biochemistry* 26 (1987) 1606-1611.
- [173] Y. Kimura, A. Ikegami, W. Stoeckenius, Salt and pH-dependent changes of the purple membrane absorption spectrum, *Photochem Photobiol* 40 (1984) 641-646.
- [174] C.H. Chang, J.G. Chen, R. Govindjee, T. Ebrey, Cation binding by bacteriorhodopsin, *PNAS* 82 (1985) 396-400.
- [175] J. Herzfeld, J.C. Lansing, Magnetic resonance studies of the bacteriorhodopsin pump

Chapter 7—References

- cycle, *Annu Rev Biophys Biomol Struct* 31 (2002) 73-95.
- [176] H.J. de Groot, S.O. Smith, J. Courtin, E. van den Berg, C. Winkel, J. Lugtenburg, R.G. Griffin, J. Herzfeld, Solid-state ^{13}C and ^{15}N NMR study of the low pH forms of bacteriorhodopsin, *Biochemistry* 29 (1990) 6873-6883.
- [177] J.G. Hu, B.Q. Sun, A.T. Petkova, R.G. Griffin, J. Herzfeld, The predischARGE chromophore in bacteriorhodopsin: a ^{15}N solid-state NMR study of the L photointermediate, *Biochemistry* 36 (1997) 9316-9322.
- [178] M. Lee, W.I. Goldberg, Nuclear magnetic resonance line narrowing by a rotating Rf field, *Phys Rev* 140 (1965) 1261.
- [179] B.J. Rossum, H. Förster, H.J.M. de Groot, High-field and high-speed CP-MAS ^{13}C NMR heteronuclear dipolar-correlation spectroscopy of solids with frequency-switched Lee-Goldberg homonuclear decoupling, *JMR* 124 (1997) 516-519.
- [180] N. Giraud, A. Lesage, F. Penin, M. Blackledge, L. Emsley, Site-Specific Backbone Dynamics from a Crystalline Protein by Solid-State NMR Spectroscopy, *J Am Chem Soc* 126 (2004) 11423-11424.
- [181] B. Reif, Y. Xue, V. Agarwal, M.S. Pavlova, M. Hologne, A. Diehl, Y.E. Ryabov, N.R. Skrynnikov, Protein side-chain dynamics observed by solution- and solid-state NMR: comparative analysis of methyl ^2H relaxation data, *J Am Chem Soc* 128 (2006) 12354-12355.
- [182] X.L. Yao, V.P. Conticello, M. Hong, Investigation of the dynamics of an elastin-mimetic polypeptide using solid-state NMR, *Magn Reson Chem* 42 (2004) 267-275.
- [183] D.A. Torchia, Solid state NMR studies of protein internal dynamics, *Ann. Rev. Biophys. Bioeng* 13 (1984) 125-144.
- [184] M. Schiffer, C.H. Chang, F.J. Stevens, The functions of tryptophan residues in membrane proteins, *Protein engineering* 5 (1992) 213-214.
- [185] K. Werner, I. Lehner, H.K. Dhiman, C. Richter, C. Glaubitz, H. Schwalbe, J. Klein-Seetharaman, H.G. Khorana, Combined solid state and solution NMR studies of alpha,epsilon- ^{15}N labeled bovine rhodopsin, *J Biomol NMR* 37 (2007) 303-312.
- [186] T. Gullion, J. Schaefer, Rotational-Echo Double-Resonance NMR, *JMR* 81 (1989) 196-200.
- [187] S.O. Smith, O.B. Peersen, Solid-state NMR approaches for studying membrane protein structure, *Annu Rev Biophys Biomol Struct* 21 (1992) 25-47.
- [188] R.A. Krebs, U. Alexiev, R. Partha, A.M. DeVita, M.S. Braiman, Detection of fast light-activated H^+ release and M intermediate formation from proteorhodopsin, *BMC physiology* 2 (2002) 5.
- [189] M. Hong, K. Jakes, Selective and extensive ^{13}C labeling of a membrane protein for solid-state NMR investigations, *J Biomol NMR* 14 (1999) 71-74.
- [190] P. Hodgkinson, L. Emsley, The accuracy of distance measurements in solid-state NMR, *JMR* 139 (1999) 46-59.
- [191] S. Kiihne, M.A. Mehta, J.A. Stringer, D.M. Gregory, J.C. Shiels, G.P. Drobny, Distance Measurements by Dipolar Recoupling Two-Dimensional Solid-State NMR *J Phys Chem A* 102 (1998).
- [192] M. Hong, Determination of multiple ϕ -torsion angles in proteins by selective and extensive (^{13}C) labeling and two-dimensional solid-state NMR, *JMR* 139 (1999) 389-401.
- [193] Geerten W. Vuister, Soon-Jong Kim, C. Wu, A. Bax'li, 2D and 3D Nmr-Study of

Chapter 7—References

- Phenylalanine Residues in Proteins by Reverse Isotopic Labeling, *JACS* 116 (1994) 9206-9210.
- [194] S.O. Smith, B.J. Bormann, Determination of helix-helix interactions in membranes by rotational resonance NMR, *PNAS* 92 (1995) 488-491.
- [195] E. Crocker, A.B. Patel, M. Eilers, S. Jayaraman, E. Getmanova, P.J. Reeves, M. Ziliox, H.G. Khorana, M. Sheves, S.O. Smith, Dipolar assisted rotational resonance NMR of tryptophan and tyrosine in rhodopsin, *J Biomol NMR* 29 (2004) 11-20.
- [196] K. Takegoshi, S. Nakamura, T. Terao, ¹³C-¹H dipolar assisted rotational resonance in magic angle spinning NMR, *Chem Phys Letters* 344 (2001) 631-637.
- [197] T.G. Oas, R.G. Griffin, M.H. Levitt, Rotatory resonance recoupling of dipolar interactions in solid state nuclear magnetic resonance, *J Chem Phys* 89 (1988) 692-695.
- [198] C.R. Loomis, J.P. Walsh, R.M. Bell, sn-1,2-Diacylglycerol kinase of *Escherichia coli*. Purification, reconstitution, and partial amino- and carboxyl-terminal analysis, *JBC* 260 (1985) 4091-4097.
- [199] W.J. van Blitterswijk, B. Houssa, Properties and functions of diacylglycerol kinases, *Cellular signalling* 12 (2000) 595-605.
- [200] O. Vinogradova, P. Badola, L. Czerski, F.D. Sonnichsen, C.R. Sanders, 2nd, *Escherichia coli* diacylglycerol kinase: a case study in the application of solution NMR methods to an integral membrane protein, *Biophys J* 72 (1997) 2688-2701.
- [201] C.A. Smith, I. Rayment, Active site comparisons highlight structural similarities between myosin and other P-loop proteins, *Biophys J* 70 (1996) 1590-1602.
- [202] D. Schaap, J. van der Wal, W.J. van Blitterswijk, Consensus sequences for ATP-binding sites in protein kinases do not apply to diacylglycerol kinases, *Biochem J* 304 (Pt 2) (1994) 661-662.
- [203] F.W. Lau, J.U. Bowie, A method for assessing the stability of a membrane protein, *Biochemistry* 36 (1997) 5884-5892.
- [204] M. Lorch, S. Fahem, C. Kaiser, I. Weber, A.J. Mason, J.U. Bowie, C. Glaubitz, How to prepare membrane proteins for solid-state NMR: A case study on the alpha-helical integral membrane protein diacylglycerol kinase from *E. coli*, *Chembiochem* 6 (2005) 1693-1700.
- [205] M. Hiller, L. Krabben, K.R. Vinothkumar, F. Castellani, B.J. van Rossum, W. Kuhlbrandt, H. Oschkinat, Solid-state magic-angle spinning NMR of outer-membrane protein G from *Escherichia coli*, *Chembiochem* 6 (2005) 1679-1684.
- [206] D.S. Waugh, Genetic tools for selective labeling of proteins with alpha-¹⁵N-amino acids, *J Biomol NMR* 8 (1996) 184-192.
- [207] P. Badola, C.R. Sanders, 2nd, *Escherichia coli* diacylglycerol kinase is an evolutionarily optimized membrane enzyme and catalyzes direct phosphoryl transfer, *JBC* 272 (1997) 24176-24182.

Curriculum Vitae

Personal Details

Name	Ms. Sarika Shastri
Birth Date	17/06/1976
Birth Place	Ujjain, India
Nationality	Indian



Academic Details

PhD (Since April 2004)	Under guidance of Prof. Dr. Clemens Glaubitz at Institute of Biophysical Chemistry, J.W.Goethe University, Frankfurt am Main, Germany.
PhD Topic	Characterization of 2D crystals of Proteorhodopsin with Electron Microscopy and Solid State Nuclear Magnetic Resonance.
M.Sc (1998-2000)	Industrial Microbiology from School of Life Sciences, Devi Ahilya University, Indore, India.
M.Sc Thesis	Response of N ₂ fixing Cyanobacteria to ionizing radiations and other environmental stresses. Work carried out at Bhabha Atomic Research Centre, Mumbai, India under supervision of Prof. S.K.Apte.
B.Sc (1995-1998)	Microbiology from Government. Model Autonomous Holkar Science College, Indore, India.

Publications

- [1] **S. Shastri**, J. Vonck, N. Pflieger, W. Haase, W. Kuehlbrandt, C. Glaubitz, Proteorhodopsin: characterisation of 2D crystals by electron microscopy and solid state NMR, *Biochim Biophys Acta* 1768 (2007) 3012-3019.
- [2] A.L. Klyszejko*, **S. Shastri***, S.A. Mari, H. Grubmuller, D.J. Muller, C. Glaubitz, Folding and assembly of proteorhodopsin, *J Mol Biol* 376 (2008) 35-41.
(* contributed equally)
- [3] J.J. Lopez, C. Kaiser, **S. Shastri**, C. Glaubitz, Double quantum filtering homonuclear MAS NMR correlation spectra: a tool for membrane protein studies, *J Biomol NMR* 41 (2008) 97-104.
- [4] N. Pflieger, M. Lorch, A.C. Woerner, **S. Shastri**, C. Glaubitz, Characterisation of Schiff base and chromophore in green proteorhodopsin by solid-state NMR, *J Biomol NMR* 40 (2008) 15-21.
- [5] Shastri YM, D. Bergis, N. Povse, V. Schäfer, **S. Shastri**, M. Weindel, H. Ackermann, O. Schröder, J. Stein Comparative evaluation of accuracy of Fecal Calprotectin, Lactoferrin and Occult Blood test (FOBT) in predicting microbiological diagnosis for acute diarrhea: Prospective multicenter double blind randomized controlled trial.(*American Journal of Medicine*, Accepted)

Work Experience

All India Research Officer Department of Microbiology, Hindustan Lever Research Centre,
(15/01/2001-15/02/2004) Unilever India, Mumbai, India.

Microbiologist Nicolas Piramal India Limited, Pithampur, India.
(16/11/2000-
15/01/2001)

Lecturer Department of Microbiology, Vikram University, Ujjain, India.
(01/07/2000-
15/11/2000)

Microbiologist SGS India Pvt. Limited, Indore, India.
(01/04/2000-
01/07/2000)

Credentials

January 2003 'Quality award' for working on PURIT project at Unilever, India.

Oral Presentation

- Institute for chemistry and biochemistry, Free University, Berlin 2007
- 1st meeting of the Center for Biomolecular Magnetic Resonance, Frankfurt, 2007
- International Max Planck Research School excursion, Dresden 2006
- International Max Planck Research School excursion, Strasbourg 2005

Conferences

- 2008** · Joint Annual Conference of the Association for General and applied microbiology (VAAM) and the German Society for Biochemistry and Molecular Biology (GBM), Frankfurt am Main, 9th-11th March .
- 2007** · New NMR in Structural Biology, J.W. Goethe University Frankfurt am Main, 16th-17th November 2007.
- 6th European Biophysics Conference, Imperial College, London 14th-19th July 2007.
- International workshop on Structural Proteomics of membrane proteins 18th- 21st February 2007, Schloss Rauischhlozhausen, Marburg, Germany.

-
- 2006**
- 2006 September: International Max Planck Research School Retreat, Dresden, Germany.
 - 1st - 4th October 2006 Membrane Protein Meeting, Naurod/Wiesbaden, Germany.
- 2005**
- 2005 September: International Max Planck Research School Retreat, Strasbourg, Germany.
 - Poster presentation at BMBF Colloquium, Berlin, May 2005.
 - GDCh Magnetic Resonance Division 27th Discussion Meeting High-Field Bio-NMR Symposium, 26th-29th September 2005.

Workshops attended

- IMPRes /CMP- workshop on Protein Crystallography, May 2006.
- IMPRes /CMP- workshop on 2D Crystallography, May 2005.
- IMPRes /CMP- workshop on Solid State NMR, May 2004.